THREE-DIMENSIONAL HOLOGRAPHIC VIDEO DISPLAY SYSTEMS USING MULTIPLE SPATIAL LIGHT MODULATORS

A DISSERTATION

SUBMITTED TO THE DEPARTMENT OF ELECTRICAL AND ELECTRONICS ENGINEERING

AND THE GRADUATE SCHOOL OF ENGINEERING AND SCIENCE

OF BILKENT UNIVERSITY

IN PARTIAL FULFILLMENT OF THE REQUIREMENTS

FOR THE DEGREE OF

DOCTOR OF PHILOSOPHY

By

Fahri Yaraş

May 2011

I certify that I have read this thesis and that in my opinion it is fully adequate, in scope and in quality, as a thesis for the degree of Doctor of Philosophy.

Prof. Dr. Levent Onural (Supervisor)

I certify that I have read this thesis and that in my opinion it is fully adequate, in scope and in quality, as a thesis for the degree of Doctor of Philosophy.

Prof. Dr. Haldun M. Özaktaş

I certify that I have read this thesis and that in my opinion it is fully adequate, in scope and in quality, as a thesis for the degree of Doctor of Philosophy.

Prof. Dr. Hakan Ürey

I certify that I have read this thesis and that in my opinion it is fully adequate, in scope and in quality, as a thesis for the degree of Doctor of Philosophy.

Prof. Dr. Orhan Arıkan

I certify that I have read this thesis and that in my opinion it is fully adequate, in scope and in quality, as a thesis for the degree of Doctor of Philosophy.

Assoc. Prof. Dr. Uğur Güdükbay

Approved for the Graduate School of Engineering and Science:

Prof. Dr. Levent Onural
Director of Graduate School of Engineering and Science

ABSTRACT

THREE-DIMENSIONAL HOLOGRAPHIC VIDEO DISPLAY SYSTEMS USING MULTIPLE SPATIAL LIGHT MODULATORS

Fahri Yaraş
Ph.D. in Electrical and Electronics Engineering
Supervisor: Prof. Dr. Levent Onural
May 2011

Spatial light modulators (SLMs) are commonly used in electro-holographic display systems. Liquid crystal on silicon, liquid crystal, mirror-based, acousto-optic and optically addressed devices are some of the SLM types. Most of the SLMs are digitally driven and pixelated; therefore, they are easy to use. We use phase-only SLMs in our experiments. Resolution and size of currently available SLMs are inadequate for satisfactory holographic reconstructions. Space-bandwidth product (SBP) is a good metric for the quality assessments. High SBP is needed when lateral or rotational motion is allowed for the observer. In our experiments 2D images whose sizes are even larger than the SLM size are reconstructed using single SLM holographic displays. Volume reconstructions are also obtained by using such displays. Either LED or laser illumination is used in our experiments. After the experiments with the single SLM holographic displays, some laboratory prototypes of multiple SLM holographic systems are designed and implemented. In a real-time color holographic display system, three SLMs are used for red, blue and green channels. GPU acceleration is also used to achieve video rates. Beam-splitters and micro-stages are used for the alignments in all multiple SLM designs. In another multiple SLM configuration, SLMs are tiled side by side to form a three by two matrix to increase both vertical and horizontal field of view. Larger field of view gives flexibility to

the observer to move and rotate around the reconstructed images of objects. To further increase the field of view, SLMs are tiled in a circular configuration. A single large beam-splitter is used to tile the SLMs side by side without any gap. A cone mirror is used to direct incoming light toward all SLMs. Compared to planar configuration, circularly configured multiple SLMs increase the field of view, significantly. With the help of such configurations holographic videos of ghost-like 3D objects can be observed binocularly. Experimental results are satisfactory.

Keywords: Holographic Displays, Holographic Video, 3DTV, Digital Holography, Computer Generated Holography, Real-time Holography, Spatial Light Modulators, Phase Holograms

ÖZET

BİRDEN ÇOK UZAMSAL IŞIK MODÜLATÖRLÜ HOLOGRAFİK ÜÇ-BOYUTLU VİDEO GÖSTERİM SİSTEMLERİ

Fahri Yaraş
Elektrik ve Elektronik Mühendisliği Bölümü Doktora
Tez Yöneticisi: Prof. Dr. Levent Onural
Mayıs 2011

Uzamsal ışık modülatörleri, elektro-holografik gösterim sistemlerinde yaygın olarak kullanılmaktadır. Silikon üzerine sıvı kristal, sıvı kristal, mikro-aynalı, akusto-optik ve optik olarak adreslenebilir aygıtlar uzamsal ışık modülatörü çeşitlerinden bazılarıdır. Uzamsal ışık modülatörlerinin çoğu sayısal olarak kontrol edilebilir ve pikselli bir yapıya sahiptirler. Dolayısıyla kullanımları kolaydır. Deneylerimizde, ışığın sadece evresini modüle eden uzamsal ışık modülatörleri kullandık. Mevcut uzamsal ışık modülatörlerinin çözünürlüğü ve boyutları tatmin edici kalitede holografik geri çatımların elde edilmesinde yetersiz kalmaktadır. Uzam-bant genişliği çarpımı kalite değerlendirmesinde iyi bir ölçüttür. Gözlemciye yanal ve dönel hareket serbestisi verildiğinde yüksek uzam-bant genişliği çarpımına ihtiyaç duyulmaktadır. Deneylerimizde, tek uzamsal ışık modulatörlü holografik gösterim sistemleri ile, modülatörünün boyundan bile büyük iki-boyutlu görüntüler holografik olarak oluşturuldu. Bu gibi gösterim sistemleri ile hacimli görüntüler de holografik olarak oluşturuldu. Deneylerimizde LED ya da lazer aydınlatması kullanıldı. Tek uzamsal ışık modulatörlü holografik gösterim sistemleriyle yapılan deneylerden sonra birden çok uzamsal ışık modulatörlü holografik gösterim sistemleri tasarlandı ve gerçekleştirildi. Gerçek-zamanlı renkli bir holografik gösterim sisteminde kırmızı, yeşil ve mavi kanallar için üç adet uzamsal ışık modulatörü kullanıldı. Video hızlarına ulaşmak için ise grafik işleme ünitesi (GPU) kullanıldı. Bütün çok uzamsal ışık modülatörü kullanılan

sistemlerde hizalama işlemleri için hüzme-bölücüler ve mikro-konumlayıcılar kullanıldı. Diğer bir çok modülatörlü tasarımda, dikey ve düşey görüş alanını arttırmak için modulatörler üçe ikilik bir matris oluşturacak şekilde yan yana döşendi. Daha fazla görüş alanı, gözlemciye holografik olarak oluşturulmuş görüntülerin etrafında dolaşma esnekliği tanımaktadır. Bu görüş alanını daha da arttırmak için uzamsal ışık modülatörleri dairesel konumda yerleştirildi. Modülatörleri aralarında boşluk kalmayacak şekilde yerleştirmek için tek ve büyük bir hüzme-bölücü kullanıldı. Gelen ışığı tüm uzamsal ışık modülatörlerine yönlendirebilmek için ise koni şeklinde bir ayna kullanıldı. Düzlemsel olanlara kıyasla dairesel tasarımların görüş alanını belirli bir şekilde arttırdığı görüldü. Bu yapıdaki tasarımlar sonucunda, hayalete benzeyen üç-boyutlu nesnelerin holografik videoları iki gözle birden izlenebilmektedir. Deneysel sonuçlar tatmin edicidir.

Anahtar Kelimeler: Holografik Ekranlar, Holografik Video, 3-Boyutlu Televizyon, Sayısal Holografi, Bilgisayarla Üretilmiş Holografi, Gerçek Zamanlı Holografi, Uzamsal Işık Modülatörleri

ACKNOWLEDGMENTS

Foremost, I would like to gratefully and sincerely thank my supervisor, Prof. Dr. Levent Onural, whose guidance, encouragement, supervision and continuous support from the preliminary to the concluding level enabled me to develop an understanding of the subject.

Besides my advisor, I also would like to thank my thesis committee: Prof. Dr. Haldun M. Özaktaş, Prof. Dr. Hakan Ürey, Prof. Dr. Orhan Arıkan and Assoc. Prof. Dr. Uğur Güdükbay for their encouragement and insightful comments. I would like to thank the Department of Electrical and Electronics Engineering at Bilkent University for their support throughout my thesis study. This work is supported by EC within FP6 under Grant 511568 with acronym 3DTV and within FP7 under Grant 216105 with the acronym Real 3D. I also would like to thank to TÜBİTAK (The Scientific and Technological Research Council of Turkey) for financial support.

I thank my fellow friends and labmates, especially to Dr. Metodi Kovachev, Dr. Rossitza Ilieva, Dr. Hoonjong Kang and Dr. Elena Stoykova for all the discussions and their support. I also would like to thank Dr. Claas Falldorf for fruitful discussions.

Last but not the least, I would like to thank my wife, Ferda, for her support, encouragement and patience during the preparation of this thesis. I thank my parents, Necdet and Arife, for giving birth to me in the first place and supporting me spiritually throughout my life. Special thanks goes to my sister, Melike, for her endless joy and support.

Contents

1 Introduction **1**

1.1 Organization of the dissertation 3

2 Scalar Diffraction Theory **4**

2.1 A Historical Overview of Diffraction and Holography 4

2.2 Scalar Diffraction Theory 5

3 State-Of-The-Art In Holographic Displays **10**

3.1 Technical Issues in Electro-Holography 10

3.1.1 An Overview 10

3.1.2 Liquid Crystal Devices 13

3.1.3 LCoS Devices 15

3.1.4 Optically Addressed Liquid Crystal Devices 15

3.1.5 Mirror-based Devices 16

3.1.6 Acousto-Optic Modulators (AOMs) 16

3.2 Current Electro-holographic Display Systems 17

3.2.1 Holo-video 17

3.2.2 SeeReal 17

3.2.3 QinetiQ 18

3.2.4 Horn 20

3.2.5 Image Hologram 20

3.2.6 Coherent Stereogram 21

3.2.7 NICT 23

4 Design Parameters for Satisfactory Holographic Displays 26

4.1 Size and bandwidth specifications for a satisfactory electro-holographic display 27

4.1.1 Space-bandwidth product of electro-holographic displays 28

4.1.2 Pixel period 32

4.2 Space-bandwidth product as a quality metric for holographic reconstructions 38

4.3 Noise and Quantization 40

4.4 SLM tilting and polarization effect 42

4.5 Off-axis case 43

4.6 Cylindrically arranged electro-holographic display system 44

4.7 Extension to a spherical or other surface geometry designs 45

5 Experimental Setup And Results For The Holographic Displays Using Single Phase-only SLM 48

5.1 Phase-only Holograms 48

5.2 Setup and Results 51

6 Experimental Setup And Results For The Holographic Displays Using Multiple Phase-only SLMs 58

6.1 Color holographic reconstruction using multiple SLMs and LED illumination 58

6.2 Real-time multiple SLM color holographic display using multiple GPU acceleration and LED illumination 63

6.2.1 The Algorithm 64

6.2.2 The Client 66

6.2.3 The Server 66

6.2.4 Optics 67

6.2.5 Results 68

6.3 Multi-SLM holographic display system with a planar configuration 76

6.3.1 Advantages of using multiple SLMs 76
6.3.2 The Gap Problem 79
6.3.3 Setup and Hologram Generation 80
6.3.4 Experimental Results 80
6.4 Circular Holographic Video Display System 88
6.4.1 Field of View in Circular Holographic Displays 88
6.4.2 Some Laboratory Prototypes 89

7 Conclusions **106**

Bibliography **109**

List of Figures

2.1 Illustration of a planar surface and a point of interest. 9

3.1 Pictures of the dynamic holographic stereogram: (a) the curved array of SLMs mounted without upper arms and (b) whole system with electronic controllers. (J. Hahn, H. Kim, Y. Lim, G. Park, and B. Lee, "Wide viewing angle dynamic holographic stereogram with a curved array of spatial light modulators," Opt. Express 16, 12372-12386 (2008), ©2008 OSA. Reprinted with permission) 13

3.2 Illustration of one channel of the Active Tiling modulator concept of QinetiQ (Slinger, C., Cameron, C., Stanley, M., "Computer-Generated Holography as a Generic Display Technology," Computer , vol.38, no.8, pp. 46-53, Aug. 2005. ©2009 IEEE. Reprinted with permission) 14

3.3 Holographic display with a reconstructed 3D scene that is composed of object points. Each object point is encoded in a sub-hologram. The position and the size of a sub-hologram is determined by the object point position and the position of the virtual viewing window. The total hologram is generated by a summation of the sub-holograms. The 3D scene is visible through the virtual viewing window which is tracked to the eye position. The virtual viewing window contains the wavefront that would be generated by a real 3D scene at the eye position. (©2009 SeeReal. Reprinted with permission) 18

3.4 Illustration of SeeReal's holographic display prototype with a screen diagonal of 20 inch. (©2009 SeeReal. Reprinted with permission) 19

3.5 Replay of a spatial-multiplexed, 3 × 8 billion-pixel, full-parallax, full-color, 3D image. (Slinger, C., Cameron, C., Stanley, M., "Computer-Generated Holography as a Generic Display Technology," Computer , vol.38, no.8, pp. 46-53, Aug. 2005. ©2009 IEEE. Reprinted with permission) 20
3.6 Virtual window for image hologram calculation ("Real-time image plane full-color and full-parallax holographic video display system," T. Yamaguchi, G. Okabe, and H. Yoshikawa; Opt. Eng. 46, 125801 (2007). ©2009 SPIE. Reprinted with permission) 21
3.7 Reconstructed images of five letters from different viewpoints in depth: (a) focused on letters W and D, and (b) focused on R. ("Real-time image plane full-color and full-parallax holographic video display system," T. Yamaguchi, G. Okabe, and H. Yoshikawa; Opt. Eng. 46, 125801 (2007). ©2009 SPIE. Reprinted with permission) 22
3.8 A perspective image of the used 3D model and reconstructed images ("Quality improvements of the coherent holographic stereogram for natural 3D display and its applications," H. Kang, in PhD. Thesis, Nihon University, 2008. Reprinted with permission) 22
3.9 Real object and IP micro-lens array ©2009 NICT. Reprinted with permission. 23
3.10 Real object acquisition system by using integral photographic camera ©2009 NICT. Reprinted with permission. 24
3.11 Electro-holographic display system with three lasers and three LCoS ©2009 NICT. Reprinted with permission. 25
3.12 Reconstruction captured by a camcorder ©2009 NICT. Reprinted with permission. 25

4.1 Simple schematic for an electro-holographic display ("Digital holographic Three-dimensional video displays," L. Onural, F. Yaraş, and H. Kang, Proceedings of the IEEE, vol.99, no.4, pp.576-589, April 2011. ©2011 IEEE. Reprinted with permission.) 28

4.2 The "space" and "bandwidth" to compute the space-bandwidth product ("Digital holographic Three-dimensional video displays," L. Onural, F. Yaraş, and H. Kang, Proceedings of the IEEE, vol.99, no.4, pp.576-589, April 2011. ©2011 IEEE. Reprinted with permission.) 29

4.3 Hologram size for a stationary observer. (D_H: Distance between hologram and eye. S_{min}: Hologram extent) ("Digital holographic Three-dimensional video displays," L. Onural, F. Yaraş, and H. Kang, Proceedings of the IEEE, vol.99, no.4, pp.576-589, April 2011. ©2011 IEEE. Reprinted with permission.) 31

4.4 Hologram size and bandwidth modification for eye rotation. (D_H: Distance between hologram and eye. S_{min}: Hologram extent for a stationary observer. S_R: Additional hologram extent as a result of eye rotation. θ_R: Rotation angle in lateral direction.) ("Digital holographic Three-dimensional video displays," L. Onural, F. Yaraş, and H. Kang, Proceedings of the IEEE, vol.99, no.4, pp.576-589, April 2011. ©2011 IEEE. Reprinted with permission.) 32

4.5 (a) Minimum hologram size for a stationary observer. (b) Example for the allowed transverse motion range $A_O = S_{Ox} \times S_{Oy}$. (c) The shape of the minimum hologram is found as $A_H = A_{min} \oplus A_O$ where $\oplus$ denotes the morphological dilation ("Digital holographic Three-dimensional video displays," L. Onural, F. Yaraş, and H. Kang, Proceedings of the IEEE, vol.99, no.4, pp.576-589, April 2011. ©2011 IEEE. Reprinted with permission.) 33

4.6 Effect of pixel period on the angular distribution of diffracted light from a pixelated SLM and recovery by an optical low-pass filter. ("Digital holographic Three-dimensional video displays," L. Onural, F. Yaraş, and H. Kang, Proceedings of the IEEE, vol.99, no.4, pp.576-589, April 2011. ©2011 IEEE. Reprinted with permission.) 36
4.7 High diffraction orders in reconstruction field and their separation ("Digital holographic Three-dimensional video displays," L. Onural, F. Yaraş, and H. Kang, Proceedings of the IEEE, vol.99, no.4, pp.576-589, April 2011. ©2011 IEEE. Reprinted with permission.) 37
4.8 (a) Orthographic illumination (b) Tilted illumination ("Digital holographic Three-dimensional video displays," L. Onural, F. Yaraş, and H. Kang, Proceedings of the IEEE, vol.99, no.4, pp.576-589, April 2011. ©2011 IEEE. Reprinted with permission.) 38
4.9 Quality metric of reconstruction by the hologram on the SLM as a function of distance of the reconstructed image (white: high quality, black: low quality) ("Digital holographic Three-dimensional video displays," L. Onural, F. Yaraş, and H. Kang, Proceedings of the IEEE, vol.99, no.4, pp.576-589, April 2011. ©2011 IEEE. Reprinted with permission.) . . . 39
4.10 Variation of "space" and "bandwidth" with respect to reconstruction distance z. (a) When z is small, "space" is also small and the "band" is limited by the maximum band supported by the SLM. (b) As z moderately increases, "space" also increases and "band" is still limited by the maximum band supported by the SLM. (c) Transition (d) For larger z, "space" does not change anymore, but "band" decreases since the supported diffraction angle (and therefore the spatial frequency) decreases. (e) For very large z, "space" does not change, but "band" decreases even further ("Digital holographic Three-dimensional video displays," L. Onural, F. Yaraş, and H. Kang, Proceedings of the IEEE, vol.99, no.4, pp.576-589, April 2011. ©2011 IEEE. Reprinted with permission.) 40

4.11 Variation of normalized quality metric for a reconstructed image from a finite size SLM along the optical axis ("Digital holographic Three-dimensional video displays," L. Onural, F. Yaraş, and H. Kang, Proceedings of the IEEE, vol.99, no.4, pp.576-589, April 2011. ©2011 IEEE. Reprinted with permission.) 41
4.12 Vertically tilted SLM. 42
4.13 Effect of polarization on tilting. Red arrows denote the modulated light. 43
4.14 Reconstructions by tilted SLM. 46
4.15 Space variation of the quality metric for piecewise planar circular SLM configuration with multiple planar SLMs. The bright region at the center is the highest quality reconstruction zone. SLMs are at the left end of bright bands. Observer is at the right hand side. (white: high quality, black: low quality) ("Digital holographic Three-dimensional video displays," L. Onural, F. Yaraş and H. Kang, Proceedings of the IEEE, vol.99, no.4, pp.576-589, April 2011. ©2011 IEEE. Reprinted with permission.) 47
4.16 Spherically arranged electro-holographic display design ("Current research activities on holographic video displays," L. Onural, F. Yaraş and H. Kang, Proc. SPIE 7690, 769002, (2010). ©2010 SPIE. Reprinted with permission.) 47

5.1 Hologram and Object planes ("Holographic reconstructions using phase-only spatial light modulators," F. Yaraş, M. Kovachev, R. Ilieva, M. Agour and L. Onural, in 3DTV Conference: The True Vision - Capture, Transmission and Display of 3D Video, IEEE, 2008. ©2008 IEEE. Reprinted with permission.) 49

5.2 Block diagram of the Gerchberg-Saxton algorithm for calculating phase holograms ("Holographic reconstructions using phase-only spatial light modulators," F. Yaraş, M. Kovachev, R. Ilieva, M. Agour and L. Onural, in 3DTV Conference: The True Vision - Capture, Transmission and Display of 3D Video, IEEE, 2008. ©2008 IEEE. Reprinted with permission.) . . 50
5.3 Photograph of a Holoeye HEO-1080P phase-only spatial light modulator. (courtesy of www.holoeye.com) 51
5.4 Illustration of the optical setup for single SLM holographic display experiments. 52
5.5 (a) 2D picture of a die, (b) phase hologram, computed in 10 iterations, (c) optical reconstruction from the phase hologram ("Holographic reconstructions using phase-only spatial light modulators," F. Yaraş, M. Kovachev, R. Ilieva, M. Agour and L. Onural, in 3DTV Conference: The True Vision - Capture, Transmission and Display of 3D Video, IEEE, 2008. ©2008 IEEE. Reprinted with permission.) 54
5.6 (a) 3DTV Lab photograph as a 2D grayscale object, (b) numerical and (c) optical reconstructions from the phase hologram computed in 20 iterations ("Holographic reconstructions using phase-only spatial light modulators," F. Yaraş, M. Kovachev, R. Ilieva, M. Agour and L. Onural, in 3DTV Conference: The True Vision - Capture, Transmission and Display of 3D Video, IEEE, 2008. ©2008 IEEE. Reprinted with permission.) 55
5.7 Optical reconstruction of the 1920×2160 size object from a 1920x1080 phase-only hologram computed in 200 iterations. The SLM size is visible due to diffraction from its edges ("Holographic reconstructions using phase-only spatial light modulators," F. Yaraş, M. Kovachev, R. Ilieva, M. Agour and L. Onural, in 3DTV Conference: The True Vision - Capture, Transmission and Display of 3D Video, IEEE, 2008. ©2008 IEEE. Reprinted with permission.) 56

5.8 Optical reconstruction of the three objects at different depths (450mm, 500mm and 500mm from the SLM) ("Holographic reconstructions using phase-only spatial light modulators," F. Yaraş, M. Kovachev, R. Ilieva, M. Agour and L. Onural, in 3DTV Conference: The True Vision - Capture, Transmission and Display of 3D Video, IEEE, 2008. ©2008 IEEE. Reprinted with permission.) 57

6.1 Optical setup. (BE: Beam Expander, BS: Beam Splitter, D: Driver Module.) 59
6.2 2D picture of 3DTV logo (courtesy of www.3dtv-research.org). 60
6.3 Color phase hologram ("Color holographic reconstruction using multiple SLMs and LED illumination," F. Yaraş and L. Onural, Proc. SPIE 7237, 72370O, (2009). ©2009 SPIE. Reprinted with permission.) 61
6.4 Computer reconstruction from color phase hologram ("Color holographic reconstruction using multiple SLMs and LED illumination," F. Yaraş and L. Onural, Proc. SPIE 7237, 72370O, (2009). ©2009 SPIE. Reprinted with permission.) 62
6.5 Optical reconstruction from color phase hologram ("Color holographic reconstruction using multiple SLMs and LED illumination," F. Yaraş and L. Onural, Proc. SPIE 7237, 72370O, (2009). ©2009 SPIE. Reprinted with permission.) 62
6.6 Overall setup (BE: Beam expander, R: Red SLM, B: Blue SLM, G: Green SLM, D: Driver unit of SLMs, N: Network, BS: Non-polarized beam splitter.) ("Real-time phase-only color holographic video display system using LED illumination," F. Yaraş, H. Kang and L. Onural, Appl. Opt. 48, H48-H53 (2009). ©2009 OSA. Reprinted with permission.) 70
6.7 Hologram calculation algorithm. ("Real-time phase-only color holographic video display system using LED illumination," F. Yaraş, H. Kang and L. Onural, Appl. Opt. 48, H48-H53 (2009). ©2009 OSA. Reprinted with permission.) 71

6.8 Illustration of N-point DFT as a weighted sum of complex sinusoids. ("Real-time phase-only color holographic video display system using LED illumination," F. Yaraş, H. Kang and L. Onural, Appl. Opt. 48, H48-H53 (2009). ©2009 OSA. Reprinted with permission.) 71
6.9 Pipelined computation using GPUs ("Real-time color holographic video display system," F. Yaraş, H. Kang and L. Onural, in 3DTV Conference: The True Vision - Capture, Transmission and Display of 3D Video, IEEE, 2009. ©2009 IEEE. Reprinted with permission.) 72
6.10 The end-to-end system ("Real-time color holographic video display system," F. Yaraş, H. Kang and L. Onural, in 3DTV Conference: The True Vision - Capture, Transmission and Display of 3D Video, IEEE, 2009. ©2009 IEEE. Reprinted with permission.) 72
6.11 A rigid color 3D object ("Real-time phase-only color holographic video display system using LED illumination," F. Yaraş, H. Kang and L. Onural, Appl. Opt. 48, H48-H53 (2009). ©2009 OSA. Reprinted with permission.) 73
6.12 Computer reconstruction using the ACPAS algorithm ("Real-time phase-only color holographic video display system using LED illumination," F. Yaraş, H. Kang and L. Onural, Appl. Opt. 48, H48-H53 (2009). ©2009 OSA. Reprinted with permission.) 73
6.13 Single color reconstruction (a) by green laser (b) by green LED ("Real-time phase-only color holographic video display system using LED illumination," F. Yaraş, H. Kang and L. Onural, Appl. Opt. 48, H48-H53 (2009). ©2009 OSA. Reprinted with permission.) 74
6.14 Optical reconstruction of a single frame of the 3D object ("Real-time phase-only color holographic video display system using LED illumination," F. Yaraş, H. Kang and L. Onural, Appl. Opt. 48, H48-H53 (2009). ©2009 OSA. Reprinted with permission.) 75

6.15 Increase in the field of view when multiple SLMs are used ("Multi-SLM holographic display system with planar configuration," F. Yaraş, H. Kang and L. Onural, in 3DTV Conference: The True Vision - Capture, Transmission and Display of 3D Video, IEEE, 2010. ©2010 IEEE. Reprinted with permission.) 77
6.16 Increase in the reconstruction space when multiple SLMs are used ("Multi-SLM holographic display system with planar configuration," F. Yaraş, H. Kang and L. Onural, in 3DTV Conference: The True Vision - Capture, Transmission and Display of 3D Video, IEEE, 2010. ©2010 IEEE. Reprinted with permission.) 78
6.17 Increase in the quality when multiple SLMs are used. Only those SLM pixels within the dotted cone contributed to the image ("Multi-SLM holographic display system with planar configuration," F. Yaraş, H. Kang and L. Onural, in 3DTV Conference: The True Vision - Capture, Transmission and Display of 3D Video, IEEE, 2010. ©2010 IEEE. Reprinted with permission.) 82
6.18 Illustration of larger object reconstruction with a single SLM ("Circularly configured multi-SLM holographic display system," F. Yaraş, H. Kang and L. Onural, in 3DTV Conference: The True Vision - Capture, Transmission and Display of 3D Video, IEEE, 2011. ©2011 IEEE. Reprinted with permission.) 83
6.19 Illustration of larger object reconstruction with multiple SLMs ("Circularly configured multi-SLM holographic display system," F. Yaraş, H. Kang and L. Onural, in 3DTV Conference: The True Vision - Capture, Transmission and Display of 3D Video, IEEE, 2011. ©2011 IEEE. Reprinted with permission.) 83
6.20 Discontinuous field of view due the mount of the SLM. 84

6.21 Removing the gaps by using a beam-splitter ("Circularly configured multi-SLM holographic display system," F. Yaraş, H. Kang and L. Onural, in 3DTV Conference: The True Vision - Capture, Transmission and Display of 3D Video, IEEE, 2011. ©2011 IEEE. Reprinted with permission.) . . 84
6.22 Field of view increases when object gets closer to the SLM ("Multi-SLM holographic display system with planar configuration," F. Yaraş, H. Kang and L. Onural, in 3DTV Conference: The True Vision - Capture, Transmission and Display of 3D Video, IEEE, 2010. ©2010 IEEE. Reprinted with permission.) 85
6.23 (a) Top view of the setup, (b) front view of the tiled SLMs ("Multi-SLM holographic display system with planar configuration," F. Yaraş, H. Kang and L. Onural, in 3DTV Conference: The True Vision - Capture, Transmission and Display of 3D Video, IEEE, 2010. ©2010 IEEE. Reprinted with permission.) 86
6.24 Rigid 3D model of a square pyramid ("Multi-SLM holographic display system with planar configuration," F. Yaraş, H. Kang and L. Onural, in 3DTV Conference: The True Vision - Capture, Transmission and Display of 3D Video, IEEE, 2010. ©2010 IEEE. Reprinted with permission.) . . 86
6.25 Optical reconstructions: (a) left, (b) front and (c) right view ("Multi-SLM holographic display system with planar configuration," F. Yaraş, H. Kang and L. Onural, in 3DTV Conference: The True Vision - Capture, Transmission and Display of 3D Video, IEEE, 2010. ©2010 IEEE. Reprinted with permission.) 87
6.26 Field of view for (a) single SLM, (b) multiple SLMs in planar configuration, (c) multiple SLMs in circular configuration. ("Circular Holographic Video Display System," F. Yaraş, H. Kang and L. Onural, Optics Express vol. 19, no. 10, pp.9147-9156, 2011. ©2011 OSA. Reprinted with permission.) 95

6.27 Schematic of the setup ("Circularly configured multi-SLM holographic display system," F. Yaraş, H. Kang and L. Onural, in 3DTV Conference: The True Vision - Capture, Transmission and Display of 3D Video, IEEE, 2011. ©2011 IEEE. Reprinted with permission.) 96
6.28 Front view of the display ("Circularly configured multi-SLM holographic display system," F. Yaraş, H. Kang and L. Onural, in 3DTV Conference: The True Vision - Capture, Transmission and Display of 3D Video, IEEE, 2011. ©2011 IEEE. Reprinted with permission.) 97
6.29 Top view of the display ("Circularly configured multi-SLM holographic display system," F. Yaraş, H. Kang and L. Onural, in 3DTV Conference: The True Vision - Capture, Transmission and Display of 3D Video, IEEE, 2011. ©2011 IEEE. Reprinted with permission.) 98
6.30 Computer generated wire-frame 3D model of a cube ("Circularly configured multi-SLM holographic display system," F. Yaraş, H. Kang and L. Onural, in 3DTV Conference: The True Vision - Capture, Transmission and Display of 3D Video, IEEE, 2011. ©2011 IEEE. Reprinted with permission.) 99
6.31 Optical reconstruction of 3D wire-frame model of a cube. (a) Left, (b) center, and (c) right views ("Circularly configured multi-SLM holographic display system," F. Yaraş, H. Kang and L. Onural, in 3DTV Conference: The True Vision - Capture, Transmission and Display of 3D Video, IEEE, 2011. ©2011 IEEE. Reprinted with permission.) 99
6.32 Optical reconstructions from a curved array of SLMs: (a) left, (b) front and (c) right view ("Digital holographic Three-dimensional video displays," L. Onural, F. Yaraş and H. Kang, Proceedings of the IEEE , vol.99, no.4, pp.576-589, April 2011. ©2011 IEEE. Reprinted with permission.) 100

6.33 Discontinuous field of view due the frame of the SLMs. (“Circular Holographic Video Display System,” F. Yaraş, H. Kang and L. Onural, Optics Express vol. 19, no. 10, pp.9147-9156, 2011. ©2011 OSA. Reprinted with permission.) 101
6.34 Top view of the laboratory prototype (“Circular Holographic Video Display System,” F. Yaraş, H. Kang and L. Onural, Optics Express vol. 19, no. 10, pp.9147-9156, 2011. ©2011 OSA. Reprinted with permission.) 101
6.35 (a) Side view of the experimental setup. (b) Vertical and horizontal illumination (“Circular Holographic Video Display System,” F. Yaraş, H. Kang and L. Onural, Optics Express vol. 19, no. 10, pp.9147-9156, 2011. ©2011 OSA. Reprinted with permission.) 102
6.36 Pictures of (a) SLMs and SLM Modules, (b) side view of the setup, (c) cone mirror and (d) SLMs and beam splitter (“Circular Holographic Video Display System,” F. Yaraş, H. Kang and L. Onural, Optics Express vol. 19, no. 10, pp.9147-9156, 2011. ©2011 OSA. Reprinted with permission.) 103
6.37 Single frame of the video of the 3D horse model (“Circular Holographic Video Display System,” F. Yaraş, H. Kang and L. Onural, Optics Express vol. 19, no. 10, pp.9147-9156, 2011. ©2011 OSA. Reprinted with permission.) 103
6.38 Writing nine holograms on a single bitmap image (“Circular Holographic Video Display System,” F. Yaraş, H. Kang and L. Onural, Optics Express vol. 19, no. 10, pp.9147-9156, 2011. ©2011 OSA. Reprinted with permission.) 104
6.39 Optical reconstructions for a single frame for (a) 0 degree, (b) 12 degrees and (c) 24 degrees. (The business card with the rectangular aperture is placed both as a size reference and to block distracting optical component views.) (“Circular Holographic Video Display System,” F. Yaraş, H. Kang and L. Onural, Optics Express vol. 19, no. 10, pp.9147-9156, 2011. ©2011 OSA. Reprinted with permission.) 105

List of Tables

6.1 **Overall System Specifications ("Real-time phase-only color holographic video display system using LED illumination," F. Yaraş, H. Kang and L. Onural, Appl. Opt. 48, H48-H53 (2009). ©2009 OSA. Reprinted with permission.)** 67

6.2 **Characteristics of LEDs** 68

6.3 **Performance analysis of the system for two Megapixel hologram output ("Real-time color holographic video display system," F. Yaraş, H. Kang and L. Onural, in 3DTV Conference: The True Vision - Capture, Transmission and Display of 3D Video, IEEE, 2009. ©2009 IEEE. Reprinted with permission.)** 69

List of Publications

This dissertation is based on the following publications.

[Publication-I] F. Yaraş, H. Kang, and L. Onural, "*Circular Holographic Video Display System,*" Optics Express, Vol. 19, No. 10, pp.9147-9156, 2011.

[Publication-II] L. Onural, F. Yaraş, and H. Kang, "*Digital Holographic Three-dimensional Video Displays,*" Proceedings of the IEEE , vol.99, no.4, pp.576-589, April 2011 (3D Media and Displays Special Issue - Invited Paper).

[Publication-III] F. Yaraş, H. Kang, and L. Onural, "*State of the Art in Holographic Displays: A Survey,*" IEEE/OSA Display Technology, Journal of, 3-D Displays and Visualization (Special Issue) vol.6, no.10, pp.443-454, Oct. 2010.

[Publication-IV] F. Yaraş, H. Kang, and L. Onural, "*Real-time phase-only color holographic video display system using LED illumination,*" Appl. Opt. 48, H48-H53 (2009).

[Publication-V] H. Kang, F. Yaraş, and L. Onural, "*Graphics processing unit accelerated computation of digital holograms,*" Appl. Opt. 48 , H137-H143 (2009).

[Publication-VI] F. Yaraş, H. Kang, and L. Onural, "*Circularly configured multi-SLM holographic display system,*" in Proceedings of 3D TV Conference: The True Vision– Capture, Transmission and Display of 3D Video (IEEE, 2011).

[Publication-VII] F. Yaraş, H. Kang, and L. Onural, "*Multi-SLM holographic display system with planar configuration,*" in Proceedings of 3D TV Conference: The True Vision– Capture, Transmission and Display of 3D Video (IEEE, 2010).

[Publication-VIII] F. Yaraş, H. Kang, and L. Onural, "*Real-time color holographic video display system,*" in Proceedings of 3D TV Conference: The True Vision–Capture, Transmission and Display of 3D Video (IEEE, 2009).

[Publication-IX] H. Kang, F. Yaraş, and L. Onural, "*Quality comparison and acceleration for digital hologram generation method based on segmentation,*" in Proceedings of 3DTV Conference: The True Vision–Capture, Transmission and Display of 3D Video, (IEEE, 2009).

[Publication-X] F. Yaraş, H. Kang, and L. Onural, "*Real-time multiple SLM color holographic display using multiple GPU acceleration,*" in Digital Holography and Three-Dimensional Imaging (Optical Society of America, 2009), paper DWA4.

[Publication-XI] H. Kang, F. Yaraş, L. Onural, and H. Yoshikawa, "*Real-time fringe pattern generation with high quality,*" in Digital Holography and Three-Dimensional Imaging (Optical Society of America, 2009), paper DTuB7.

[Publication-XII] F. Yaraş and L. Onural, "*Color holographic reconstruction using multiple SLMs and LED illumination,*" Proc. SPIE 7237, 72370O (2009).

[Publication-XIII] F. Yaraş, M. Kovachev, R. Ilieva, M. Agour, and L. Onural, "*Holographic reconstructions using phase-only spatial light modulators,*" in Proceedings of 3DTV Conference: The True Vision-Capture, Transmission and Display of 3D Video (2008), paper PD-1-PD-4.

The contributions of the author to publications are as follows. As the first author in Publication-I, -IV, -VI, -VII, -VIII, -X, -XII and -XIII, the author designed and implemented the optical setups, performed experiments and prepared the manuscript. The author designed and implemented the optical systems and performed the experiments in

Publication-V, -IX and -XI. In Publication-II, the author performed the derivations and experiments and prepared the related manuscript. The author performed the literature survey for the Publication-III and prepared the manuscript for Sections-I, -II and -IV.

Dedicated to My Beloved Wife and Family ...

Chapter 1

Introduction

Holographic three-dimensional display is one of the exciting technologies that attract public attention. What makes people curious about this technology is the imagination of the ghost-like motion pictures. When holographic displays were shown in science-fiction movies, they were perceived just as an impossible dream. However, as a consequence of the developments in display technologies, electronics, signal processing, optics, nano-technology, computer science and other related fields, commercial three-dimensional displays that produce ghost-like images may be available within a decade. When a method is able to reproduce all relevant physical properties of the volume filling light, it is called a "True-3D" technique. Holography is one of the sophisticated true-3D techniques. Using holographic techniques, we can record and then replay a 3D-scene with all relevant physical properties. Since holographic reconstructions aim the physical duplication of light, such displays can provide 3D content independent of the observer properties'. Not only humans but also animals or 2D camcorders can see the same scene as if it is really there. The 3D televisions or 3D movie theaters that operate based on stereoscopic techniques cannot provide such true-3D content. Stereoscopic techniques are dependent on the human-visual system, and since they cannot duplicate the physical light, the resultant 3D images are highly artificial and disturbing. A 3D scene is recorded by a stereoscopic camcorder (i.e. two side by side conventional 2D video recorders); and then, the recorded videos are projected to the corresponding eyes. The 3D scene is formed

by the brain. For example, the 3D images that are formed by stereoscopic techniques can not be seen or captured by the camcorders or cameras as 3D. Volumetric displays also provide good-looking 3D experience. However, they usually have moving parts and form transparent objects. Even though the state of the holographic displays are not yet mature as the stereoscopic technologies, holographic displays are superior and desirable; however the technology is more challenging. More research on holographic displays are needed. This dissertation is dedicated to overcome such challenges and to contribute to the development of future holographic display systems.

In order to develop such holographic displays, we first need to understand the relevant physical properties of the light. When we look at a physical 3D object, what we actually see is the light that scatters from the object. The light that is reflected from the objects carries the geometry and optical information of the objects and fills the 3D space. Then, such volume filling light field enters through our eye pupils and we see the objects. The quality of the 3D experience is related to the closeness of the generated light field to the original. We can extent our 3D object to the entire room that we are in, or to any other setting. The key issue is to know all relevant physical properties of the volume filling light field, and to regenerate the same volume filling light field at another place and maybe at another time; therefore the same light field will enter through our pupils. Since the same light field will enter through our pupils, we will see the same scene as if it is real. Although the idea is simple, there are severe problems and bottlenecks in both recording and displaying of the volume filling light field. Even though recording of the holograms is also an important task for the holographic systems, we deal only with the display part in this work. In this thesis the problems and bottlenecks for the holographic displays are first examined and then possible solutions are given together with the experiments and the laboratory prototypes.

In this thesis, we deal with display of dynamic holograms to display holographic 3D videos. The display of dynamic holograms is usually called “electro-holography”. In electro-holography, mostly electrically controlled pixelated spatial light modulators (SLMs) are used. SLMs modulate the light by changing the magnitude and/or the phase

of it at each pixel. They are quite convenient for electro-holography. Although, the SLMs are good candidates for holographic displays, they currently have many bottlenecks, related to their size, pixel number and geometry. Thus, a single SLM can not provide an adequate 3D experience. Therefore, a need for multiple SLM designs is obvious. In addition, the geometry of multiple SLM designs is also crucial for quality of the resultant holographic display system. This thesis is devoted to novel designs of multiple SLM 3D holographic video displays. The conducted work covers different holographic video display system designs using multiple SLMs. The designed and implemented holographic display systems generate ghost-like 3D reconstructions of physical and synthetically generated 3D content.

We believe that the developments in technology and scientific research will increase the demand for the holographic display systems in the future. Developments in the size, resolution and geometry of the SLMs are expected and we believe that such improvements will boost the subsequent research. In the future, the holographic images of the Jedi's may not be just as a dream; however, it may turn out to be a reality.

1.1 Organization of the dissertation

The organization of the dissertation is as follows. In the following chapter, after the historical overview of diffraction and holography, a synopsis of the scalar diffraction theory is given. In Chapter 3, a survey of holographic displays is presented. In addition, some technical issues of the electro-holography and some examples of electro-holographic displays are given. In Chapter 4, design parameters for satisfactory holographic displays are presented. In Chapter 5, an experimental setup and the results for the holographic displays using single phase-only spatial light modulator are given. Multiple spatial light modulator holographic display systems are presented in Chapter 6. Conclusions are drawn in Chapter 7.

Chapter 2

Scalar Diffraction Theory

2.1 A Historical Overview of Diffraction and Holography

Diffraction was first mentioned by Francesco Maria Grimaldi (1618–1663) in his posthumous work in 1665 [1]. Robert Hooke (1635–1703) experienced the interference and reported it in his book also in 1665 [2]. In 1666 Isaac Newton (1642–1727) conducted experiments about composition of light and published a letter in 1672 by stating that the white light can be split into different colors as in the rainbow [3]. Christian Huygens (1629–1695) formulates the wave theory of light in 1678 and published his work in 1690 [4]. He also discovered the polarization of light. Thomas Young (1773–1829) reported the interference principle in 1801 [5] and revived the wave theory of light again. Augustin Jean Fresnel (1788–1827) used the Huygens principle and calculated diffraction patterns for different objects. Michael Faraday (1791–1867) studied the relationship between magnetism and electricity [6]. Then, James Clark Maxwell (1831–1879) gathered together all research results in this field into a set of equations [7]. Albert Abraham Michelson (1852–1931) proved that the waves do not need ether to propagate [8]. Albert Einstein's special theory of relativity also supported Michelson's work [9]. Gustav Kirchhoff (1824–1887)

was the first person who put the Huygen's and Fresnel's ideas into a mathematical foundation and showed that the amplitude and the phase are properties of the wave nature of the light [10]. Kirchhoff used two assumptions about the boundary conditions and those were proved by Henri Poincare (1854–1912) and Arnold Sommerfeld (1868–1951) independently from each other. Later Sommerfeld modified the Kirchhoff's formulation and waived one of his assumptions by using Green's functions [10]. The new theory of wave propagation is called Rayleigh-Sommerfeld diffraction theory.

Holography was first presented by Dennis Gabor (1900–1979) in 1948 [11–13]. Although the ideas of Gabor was supported by many scientists [14–16], interest in holography faded later because of the low quality holographic reconstructions. Together with the invention of the laser, holography started to attain its popularity again. Emmett N. Leith (1927–2005) and Juris Upatnieks (1936–) introduced the off-axis reference beam method by using the idea of Gabor's holography [17–19]. Yuri Nikolaevich Denisyuk (1927–2006) invented the thick reflection hologram in 1962 [20].

Digital holography first appeared in 1960s. Goodman and Lawrence proposed the basic idea of digital holography in 1967 [21]. However the fundamental theory was developed by Yaroslavsky and Merzlyakov in 1980 [22]. Computer generated holography for electro-holographic applications are reported by Onural [23, 24]. Digital recording of the holograms by CCD were discussed by Schnars and Jüptner [25]. The detailed history of the digital holography can be found in the book by T. Kreis [26] and more extensive history of the optics can be found in [27].

2.2 Scalar Diffraction Theory

In this thesis, we use propagating optical waves to compute holograms and to perform numerical reconstructions from the holograms. Although the scalar diffraction theory is well discussed in the literature [10, 27–30], it is beneficial to revisit the subject and clarify the notation for the sake of completeness. In the literature, scalar optical diffraction theory deals with diffraction field relation between a planar surface and a point in

space. Such relation is depicted in Fig. 2.1, where S_O defines a planar surface, P_O is the observation point in space, $\mathbf{r}_O$ is the position vector of the observation point, $\mathbf{r}_S$ is the position vector of a point on the planar surface S_O and $\mathbf{r}_{OS}$ is the difference vector defined by $\mathbf{r}_O - \mathbf{r}_S$. The planar surface S_O is placed at $z = 0$ plane. By definition, the diffraction field on S_O is known. The light disturbance at position P_O, i.e. $\psi(\mathbf{r}_O)$, due to the contributions of all the points on surface S_O is expressed as [10, 27]:

$$\psi(\mathbf{r}_O) = -\frac{1}{2\pi}\int_{S_O} \psi(\mathbf{r}_S)(jk - \frac{1}{|\mathbf{r}_{OS}|})\frac{\exp(jk|\mathbf{r}_{OS}|)}{|\mathbf{r}_{OS}|}\cos\theta dS \quad , \tag{2.1}$$

where, $\cos\theta = z/|\mathbf{r}_{OS}|$, $k = 2\pi/\lambda$ (monochromatic propagating plane waves), $dS = dx_S dy_S$ and,

$$|\mathbf{r}_{os}| = [(x_O - x_S)^2 + (y_O - y_S)^2 + z_O^2]^{1/2} \quad . \tag{2.2}$$

Here the "disturbance at position P_O" should be interpreted as the light amplitude at the point P_O on an infinitesimal planar patch parallel to input plane. If we write an impulse response $h(\mathbf{r})$ as:

$$h(\mathbf{r}) = -\frac{1}{2\pi}(jk - \frac{1}{|\mathbf{r}|})\frac{\exp(jk|\mathbf{r}|)}{|\mathbf{r}|}\cos\theta \quad , \tag{2.3}$$

then we can write the Eq. 2.1 in the form of a convolution integral as:

$$\psi(\mathbf{r}_O) = \int_{S_O} \psi(\mathbf{r}_S)h(\mathbf{r}_O - \mathbf{r}_S)dS \quad . \tag{2.4}$$

Please note that, we can write the term $\exp(jk|\mathbf{r}|)/|\mathbf{r}|$ as:

$$\frac{\exp(jk|\mathbf{r}|)}{|\mathbf{r}|} = \frac{j}{2\pi}\int_{-\infty}^{+\infty} \frac{\exp[j(k_x x + k_y y + k_z z)]}{k_z} dk_x dk_y \quad for \quad z \geq 0 \tag{2.5}$$

as expressed in [27,31]. Here k_x and k_y represent the spatial frequencies of the propagating plane wave along x and y axes, respectively. Due to the monochromatic propagating wave constraint, $k_z = (k - k_x^2 + k_y^2)^{1/2}$. Positive values of k_z denotes propagation in positive z direction and negative values of it denotes propagation in negative z direction. Then if we take the derivative of the expression in Eq.2.5, we obtain:

$$\begin{aligned} \frac{\partial\left\{\frac{\exp(jk|\mathbf{r}|)}{|\mathbf{r}|}\right\}}{\partial z} &= (jk - \frac{1}{|\mathbf{r}|})\frac{\exp(jk|\mathbf{r}|)}{|\mathbf{r}|}\cos\theta \\ &= -\frac{1}{2\pi}\int_{-\infty}^{+\infty} \exp[j(k_x x + k_y y + k_z z)]dk_x dk_y \quad for \quad z \geq 0 \quad . \end{aligned} \tag{2.6}$$

Please note that, Eq. 2.6 can be written as an inverse Fourier transform,

$$\begin{aligned}\frac{\partial\left\{\frac{\exp(jk|\mathbf{r}|)}{|\mathbf{r}|}\right\}}{\partial z} &= -\frac{1}{2\pi}\int_{-\infty}^{+\infty}\exp(jk_z z)\exp[j(k_x x+k_y y)]dk_x dk_y \quad for \quad z\geq 0 \\ &= -2\pi\mathcal{F}_{2D}^{-1}\left\{\exp(jk_z z)\right\} \quad .\end{aligned} \tag{2.7}$$

Note that $\mathcal{F}_{2D}$, which denotes the $2D$ Fourier transform from the domain (x,y) to the domain (k_x,k_y), is defined as:

$$\mathcal{F}_{2D}\{f(x,y)\} = \int_{-\infty}^{+\infty} f(x,y)\exp[-j(k_x x+k_y y)]dxdy \quad , \tag{2.8}$$

and, $\mathcal{F}_{2D}^{-1}$ is the inverse Fourier transform. If we substitute Eq. 2.6 into Eq. 2.1, we get:

$$\begin{aligned}\psi(\mathbf{r}_O) &= \frac{1}{(2\pi)^2}\int_{S_O}\psi(\mathbf{r}_S)\int_{-\infty}^{+\infty}\exp\{j[k_x(x_O-x_S)+k_y(y_O-y_S)+k_z z_O]\}dk_x dk_y dS \quad , \\ &= \frac{1}{(2\pi)^2}\int_{-\infty}^{+\infty}\Psi(k_x,k_y)\exp[j(k_x x_O+k_y y_O+k_z z_O)]dk_x dk_y \quad .\end{aligned} \tag{2.9}$$

Please note that $\Psi(k_x,k_y)$ is the Fourier transform of $\psi(\mathbf{r}_S)$ over the surface S_O at $z=0$. The Fourier transform relation is denoted as:

$$\Psi(k_x,k_y) = \int_{S_O}\psi(\mathbf{r}_S)\exp[-j(k_x x_S+k_y y_S)]dS \quad . \tag{2.10}$$

The expression in Eq. 2.9 is called plane wave decomposition (PWD). Note that the solution is valid for parallel planes and can also be written as [27, 31]:

$$\psi(x,y,z) = \mathcal{F}_{2D}^{-1}\{\mathcal{F}_{2D}[\psi(x,y,0)]\exp[j(k^2-k_x^2-k_y^2)^{1/2}z]\} \quad . \tag{2.11}$$

Here $\psi(x,y,0)$ denotes the field on the planar surface at $z=0$. If we take the Fourier transform of the input field (i.e. $\psi(x,y,0)$), we obtain the complex coefficients of the plane waves that form the entire complex field as [28, 30]:

$$(2\pi)^2 A(k_x,k_y) = \mathcal{F}_{2D}[\psi(x,y,0)] \quad ; \tag{2.12}$$

and thus the PWD is expressed as:

$$\psi(x,y,z) = \int_{-\infty}^{+\infty}A(k_x,k_y)\exp[j(k_x x+k_y y+k_z z)]dk_x dk_y \quad . \tag{2.13}$$

Please note that, PWD and Rayleigh-Sommerfeld diffraction integral gives the same result if the condition $r \gg \lambda$ is satisfied [30,31]. This condition eliminates the evanescent modes; and thus, only propagating waves exists. As a result, the impulse response of the RS diffraction integral becomes [30, 31]:

$$h_z(x,y) = \frac{1}{j\lambda} \frac{\exp[jk(x^2+y^2+z^2)^{1/2}]}{(x^2+y^2+z^2)^{1/2}} \cos\theta \quad , \tag{2.14}$$

and the frequency response is [30, 31]:

$$h_z(x,y) = \mathcal{F}_{2D}^{-1}\{\exp[jz(k^2-k_x^2-k_y^2)^{1/2}]\} \quad , \quad k_x^2+k_y^2 \leq k^2. \tag{2.15}$$

Furthermore, if we take the inverse Fourier transform of the evanescent part of the diffraction field, we get [30, 31]:

$$\frac{1}{2\pi} \frac{\exp[jk(x^2+y^2+z^2)^{1/2}]}{(x^2+y^2+z^2)} \cos\theta = \mathcal{F}_{2D}^{-1}\{\exp[jz(k^2-k_x^2-k_y^2)^{1/2}]\} \quad , \quad k_x^2+k_y^2 \geq k^2. \tag{2.16}$$

As mentioned in this section, however, we are dealing with propagating waves; therefore, evanescent part of the diffraction field is eliminated.

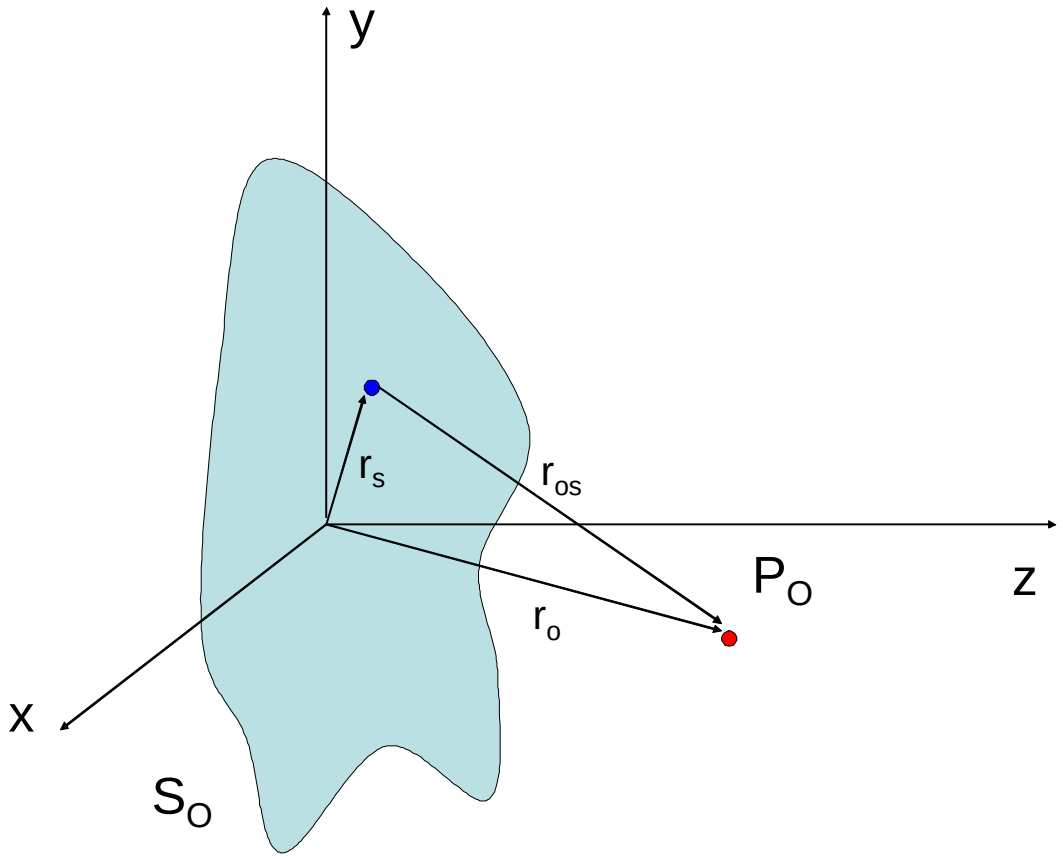

Figure 2.1: Illustration of a planar surface and a point of interest.

Chapter 3

State-Of-The-Art In Holographic Displays

3.1 Technical Issues in Electro-Holography

This chapter is mainly based on our publication in Journal of Display Technology, titled as *State of the Art in Holographic Displays: A Survey.*

3.1.1 An Overview

Several electro-holographic reconstruction approaches are reported in the literature. Liquid crystal devices are commonly used in electro-holography. Advances in liquid crystal SLMs are reported by Bauchert *et al.* [32]. In their study, these advances are summarized as smaller pixel periods, improved optical efficiency, higher pixel density and higher speed operation. Frauel *et al.* also reviewed digital holography applications [33]. Holographic reconstructions by using SLMs and three-dimensional (3D) imaging are some of the reported applications. Several problems associated with 3D imaging are also discussed in their study. Yet in another review was published by Michalkiewicz *et al.* [34]. In their report, advances in liquid crystal on silicon (LCoS) SLMs, their applications to digital holography and several issues related to electro-holographic reconstructions by using LCoS devices are discussed. Ito *et al.* reported holographic reconstructions by

using reflective type liquid crystal devices and light-emitting diode (LED) illumination in [35]. Setup and results for electo-holographic reconstructions by using LED illumination are reported in their paper. Temporal and spatial multiplexing of spatial light modulators are important approaches for electro-holography applications. An electro-holographic reconstruction method using time multiplexed illumination is discussed by Shimobaba *et al.* A color 3D object first divided into red, green and blue components then three computer generated holograms (CGHs) are computed from those color components. Calculated holograms are then written sequentially on a LCD at 100 Hz. Yet in another study, a different time multiplexing method is proposed by Ohmura *et al.* [36]. In this method a single spatial light modulator is driven by a mirror module to increase the viewing angle of the holographic reconstruction. Mirror module is used to divide the SLM into two horizontal parts and to tile them side by side. Since the resolution along the horizontal direction is doubled, the horizontal viewing angle is also approximately doubled. A color holographic display system is developed by Takano, Minami and Sato [37–40]. In their system, three SLMs and a metal halide lamp illumination is used. Their system is compared with systems that use laser illumination. In their subsequent papers, Sato and Takano presented a full-color electro-holographic 3D display system that uses LED illumination [41, 42]. In addition, they reported the ease of LED illumination while adjusting the white balance. Also in their study, a virtual image reconstruction is discussed. Tudela *et al.* combined two LCDs and used them to display full complex Fresnel holograms [43–45]. Ito and Okano reported another color holographic display system in [46]. Different from systems mentioned above, they use three color illumination and a single SLM and control the illumination by using an electronic shutter. Another color holographic display system is proposed by Sato *et al.* [47–49]. In their system, a time-multiplexed method is carried out by using a high-resolution reflective type LCD display that consists of 1920×1080 square pixels with the pixel period of $8.1\mu m$. Red, green and blue lasers are used in their prototype. Yamaguchi *et al.* reported a full-color holographic projection system [50, 51]. They used original parts of a commercially available projector to have a holographic display system. Fresnel holograms are used to speed

up their system. Yet in another color holographic system, proposed by Moon and Kim, full color holographic reconstructions are achieved by using three reflective type LCoS SLMs and a color wheel [52, 53]. We also used LCoS technology and LED illumination in our holographic display systems [54–59]. Phase-only spatial light modulators are used in our holographic display systems. Real-time holographic displays, circularly configured holographic displays and color holographic displays are some of the research topics of our group. In a recent prototype, we developed a curved holographic display with a viewing angle of 24°. Those systems will be discussed in the following chapters.

A method of enlarging the viewing angle is reported by Mishina *et al.* [60]. In their study, they combined the high diffraction orders to enlarge the viewing zone. Furthermore, in another work, they reported a single-sideband holography method by using a half-zone plate [61]. With the help of this method they managed to eliminate the conjugate beams in the Fresnel region. In holographic reconstructions, undiffracted beam may disturb the resultant image. Palima *et al.* established a method to suppress the undiffracted beam. In their proposed method, they performed some adjustments to the phase-only computer generated holograms. One of the adjustments is using a correction beam that destructively interferes with the undiffracted beam. A group from Korea reported full-parallax holographic display system [62]. The group is specialized for integral imaging and they combine a micro-lens array and phase-only spatial light modulators. The proposed system has a full-parallax viewing angle of about ±6°. The same research group proposed another horizontal-parallax-only holographic display system [63]. The system works with holographic stereograms and contains curved array of spatial light modulators (Fig.3.1). In their system, they used a mirror-module to divide the image of the SLM surface into three equal horizontal regions and tile them side by side. As a result, the resolution in horizontal direction is tripled. The total viewing angle of this system is about 22.8°. However, since they used a horizontal parallax only (HPO) holographic diffuser the system can not provide vertical parallax.

QinetiQ project developed a holographic display system by using so called "Active Tiling" system [64]. As shown in Fig.3.2, a high speed electrically addressed SLM

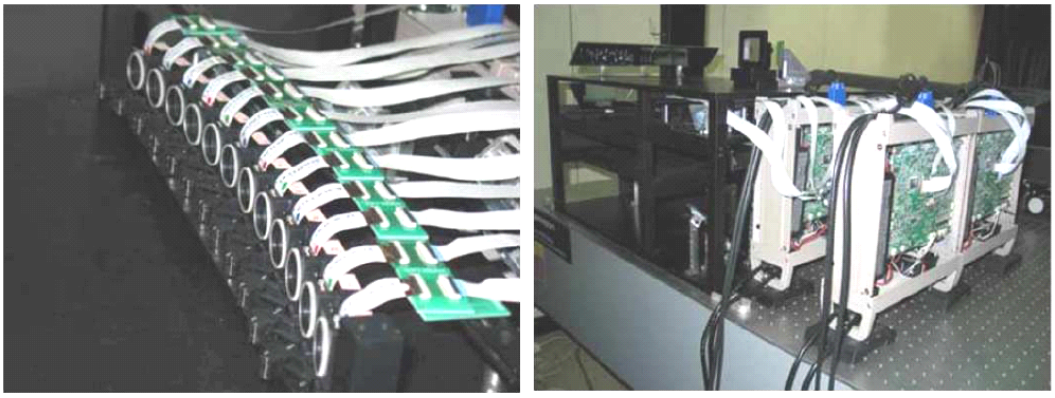

Figure 3.1: Pictures of the dynamic holographic stereogram: (a) the curved array of SLMs mounted without upper arms and (b) whole system with electronic controllers. (J. Hahn, H. Kim, Y. Lim, G. Park, and B. Lee, "Wide viewing angle dynamic holographic stereogram with a curved array of spatial light modulators," Opt. Express 16, 12372-12386 (2008), ©2008 OSA. Reprinted with permission)

(EASLM) projects the tiles of a hologram on an optically addressed SLM (OASLM). The size of the proposed system in horizontal direction is about 14cm.

Kohler *et al.* reported the SLM properties and their settings [65]. In their paper, they stated that the reconstruction quality depends on the SLM's properties such as flatness of the reflective surfaces. They showed that those deviations may degrade the quality of the holographic reconstructions. Putten *et al.* presented another development related to spatial light modulators [66]. They combined four neighboring pixels to form a superpixel. With the help of the superpixel, any complex amplitude can be generated. They presented that the proposed system can modulate the phase in 2π range while keeping the magnitude constant. Otón *et al.* developed another calibration technique for spatial light modulators [67]. In order to compensate the thickness variations of the SLM surfaces, they presented a multi-point calibration technique by using a look-up table.

3.1.2 Liquid Crystal Devices

The liquid crystal first discovered by an Austrian botanist Friedrich Reinitzer in 1888 [68]. Due to the unique characteristics of the liquid crystal, it is very suitable for display applications. The properties of the liquid crystal may change under electric or magnetic

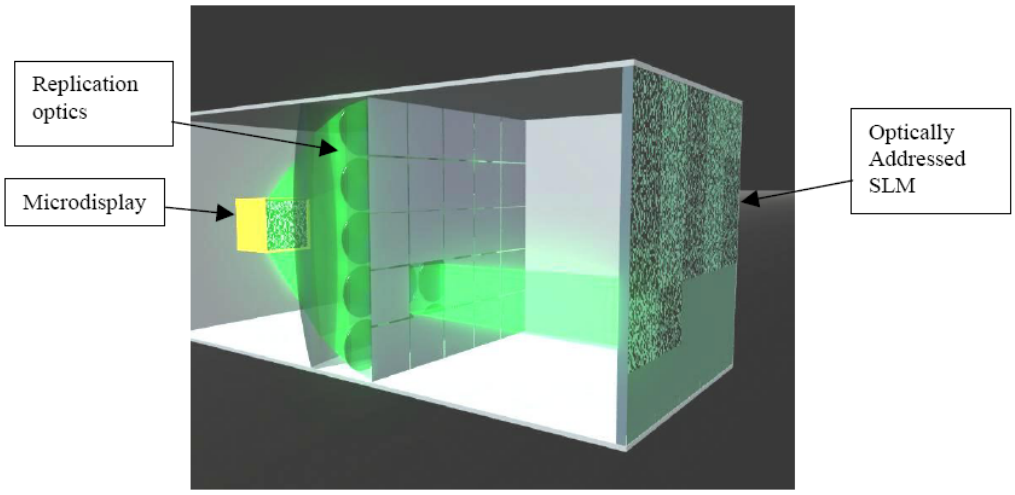

Figure 3.2: Illustration of one channel of the Active Tiling modulator concept of QinetiQ (Slinger, C., Cameron, C., Stanley, M., "Computer-Generated Holography as a Generic Display Technology," Computer , vol.38, no.8, pp. 46-53, Aug. 2005. ©2009 IEEE. Reprinted with permission)

field; and therefore, by applying proper time varying electric/magnetic field dynamic interference patterns can be displayed by LC SLMs. Twisted nematic and ferroelectric versions are two of the main types of LC SLMs. LC SLMs modulate the amplitude or the phase of the incoming light. Type of modulation is chosen according to the application. Since the diffraction efficiency is higher in phase-only SLMs, often they are prefered over amplitude-only SLMs.

Twisted nematic cells in LC SLMs that are formed in a matrix structure can be individually addressed. Orientation of the liquid crystal molecules, which are sandwiched between two glass substrates, gradually twisted to 90° [69]. Polarization of the outgoing beam is controlled by the electric field applied to the cells. If the resultant polarization of the outgoing light is perpendicular to the transmission axis of the output polarizer, no light emanates from the cell. On the other hand, all light emanates from the cell if the polarization of the outgoing light is parallel to the transmission axis of the polarizer. By controlling the polarization of the light inside the cell, amplitude modulation is achieved. The liquid crystal molecules can also be used for phase modulation. When molecules are not twisted, LC cell modulates the phase. Each pixel in the LC SLM consists of an

active and a passive area. In the passive area, there is a transistor to control the pixel. Therefore, due to the physical limitations (e.g. limitation of the transistor size) pixel size can not be reduced indefinitely. When the pixel size is reduced, the fill factor (ratio of the active area to the passive area) may degrade.

3.1.3 LCoS Devices

Liquid crystal on silicon devices (LCoS) use liquid crystal molecules and a mirror to modulate light. The mirror at the end of the liquid crystal layer controls the electric field. Therefore there is no transistor beside each pixel, and this yields a higher fill factor (up to 93 percent) [70, 71]. As in the transmissive LC SLMs, light passes through the liquid crystal molecules. However in LCoS SLMs, light passes through it twice. Some commercially available LCoS SLMs have 1920×1080 pixels and pixel size is about $8\mu m$ [71]. Optical efficiency of the LCoS SLMs are better than the transmissive type LC SLMs. Moreover, the pixel size is smaller. Therefore, for holography applications, LCoS SLMs have advantages over transmissive type SLMs.

3.1.4 Optically Addressed Liquid Crystal Devices

Optically addressed liquid crystal devices (OALCDs) modulate the phase or the amplitude of light. There are two sides of the SLM; the writing side and the reading side. When the writing side is illuminated by an intensity pattern, refractive index in the liquid crystal changes [72]. As a result, the reading side modulates the light corresponding to the refractive index change. One of the important advantages of the OALCDs is the absence of pixels. Thus, higher efficiency is achieved and high diffraction orders does not exist. However due to the physical limitations of the photo-conductors, the resolution of the displays is rather low (50 $lines/mm$) [73].

3.1.5 Mirror-based Devices

Compared to devices above, digital micro-mirror device (DMD) is a different type of spatial light modulator. DMDs consist of a 2D array of micro-mirrors which are individually controllable [74]. An electro-mechanical technique is used to control each micro-mirror. Two types of DMDs are commonly used: first one is a binary modulator; therefore, the pixels are either "on" or "off". Grayscaling is achieved by a time-averaging technique. A pixel stays "on" for a longer period relative to "off" position, to achieve brighter intensity and vice versa. The other one modulates the phase of the light by performing an out-of-plane linear translation. High optical efficiency is one of the advantages of the DMDs. In liquid crystal devices, some of the light power is lost while passing through the substrate by absorption. Furthermore, since the absorption of the light is low, DMDs can operate under high intensity light without running into thermal problems.

3.1.6 Acousto-Optic Modulators (AOMs)

Acousto-optic (AO) SLMs have been used for real time holography since 1989 [75–77]. Benton used an acousto-optic (AO) device as an SLM in computer generated holography. To modulate the light, AO SLMs use the interaction of traveling acoustic waves and a coherent light source. The acoustic wave acts like a "phase grating" when a RF signal is applied to the medium. The wave travels through the cell at the acoustic velocity. This phase grating diffracts the incident coherent light. However, AO SLMs operate in one-dimension. To generate 2D modulation a scan mechanism is required.

An acousto-optical holographic display device is proposed by Onural *et al.* [78]. Traveling surface acoustic waves (SAW) are used to produce a hologram as a surface pattern. An acoustical wave is generated on the surface of the crystal by applying an electric signal to the electrodes of the surface acoustic wave device. If the electric signal is applied to all electrodes simultaneously, a time-varying SAW pattern can be achieved.

3.2 Current Electro-holographic Display Systems

3.2.1 Holo-video

The Spatial Imaging Group at MIT Media Lab developed the first practical electro-holographic display in 1989 and named it as Mark-I [79–86]. The system is capable of rendering $25 \times 25 \times 25mm^3$ color images at a rate of 20 frames per second. The total viewing angle of the Mark-I is 15 degrees. An acousto-optic modulator (AOM) is used for the holographic reconstructions. To generate color reconstructions, a three-channel AOM is used. The second Mark system, Mark-II, was developed by the same group in 1992. The second prototype was capable of rendering $150 \times 75 \times 150mm^3$ images at rates of around 2.5 frames per second with a 36 degrees of viewing angle. In Mark-II, 18-channel AOM and bank of scanning mirrors are used instead of a three-channel AOM. The latest version of the Mark series (Mark-III) was reported in 2007 [87]. In this prototype, they used a surface acoustic wave (SAW) device. The SAW device, so called guided-wave optical scanner, uses acoustic waves traveling along the surface of the crystal. Instead of horizontal bank of scanning mirrors a holographic optical element (HOE) is used for horizontal scanning. Mark-III is capable of rendering $80 \times 60 \times 80mm^3$ images at rates of around 30 frames per second with a 24 degrees of viewing angle.

3.2.2 SeeReal

A new approach for the holographic displays was developed by SeeReal Technologies. The main idea of the system is to reconstruct only a part of the light field originating from the object that actually enters from the eye pupils of the observer [88–92]. A wavefront in this small region is called the observer window. Separate observer windows are generated for each eye of the observer. If the observer moves, the observer window is shifted to the actual position of the eye by moving the light source. The system tracks the position of the eyes and calculates only the so called “subhologram”. Two object points at different locations and corresponding subholograms in different sizes are shown in Fig. 3.3. The

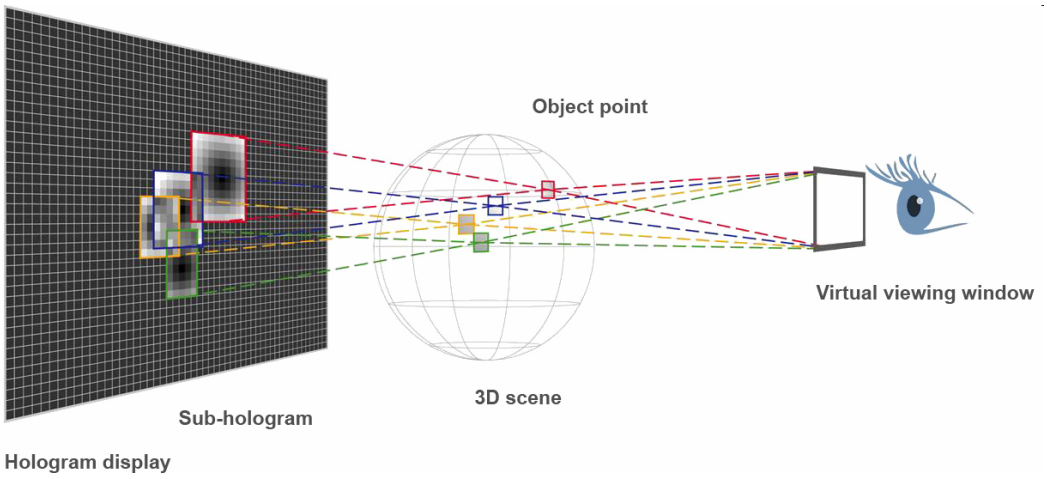

Figure 3.3: Holographic display with a reconstructed 3D scene that is composed of object points. Each object point is encoded in a sub-hologram. The position and the size of a sub-hologram is determined by the object point position and the position of the virtual viewing window. The total hologram is generated by a summation of the sub-holograms. The 3D scene is visible through the virtual viewing window which is tracked to the eye position. The virtual viewing window contains the wavefront that would be generated by a real 3D scene at the eye position. (©2009 SeeReal. Reprinted with permission)

volume of the reconstruction region is quite large. The reconstructions can be located between the display and the observer, and also fully or partially behind the display.

Fig. 3.4 shows a monochrome prototype that was demonstrated in 2007. Although the illustrated system is monochrome, a color version is also available. As mentioned above, the holographic reconstruction is formed only at the observer's eye position. With the help of this configuration, relatively large pixel periods are sufficient for a satisfactory holographic reconstruction. A state-of-the-art high-resolution LCD display is used for the 20 inch prototype. Although the pixel periods of the LCD panel is quite large, since the size of the LCD panel is large and an eye-tracking method is used, a clear large holographic reconstruction can be observed with a large depth of field (approximately 4 meters). All adjustments and calculations are done in real-time.

3.2.3 QinetiQ

QinetiQ group developed a system, so called "Active Tiling" [64] in 2003. The system uses a high speed electrically addressed spatial light modulator (EASLM) and a comparatively

Figure 3.4: Illustration of SeeReal's holographic display prototype with a screen diagonal of 20 inch. (©2009 SeeReal. Reprinted with permission)

large optically addressed spatial light modulator (OASLM) [93]. With the help of the developed system, large size holograms are generated at video rates. The EASLM acts as a "image engine". It can display images or fringe patterns quite fast. However the size of the SLM is small. After a large hologram is calculated, it is divided into 5×5 tiles. Those tiles are then projected onto the OASLM one-by-one using a replication optics (Fig. 3.2). The OASLM stores those projected tiles of the computer generated hologram. A readout optics is used to reconstruct the 3D objects. The described system forms a single channel. Multiple channels are used to increase the size of the display.

A single Active Tiling channel consists of a ferroelectric crystal on silicon (FLCoS) EASLM which has 1024×1024 binary pixels refreshed at 2.5 kHz frame rate, refractive optics with a binary-phase diffractive optical element to perform 5×5 replication, an optically addressed SLM, a dielectric mirror, a ferroelectric liquid crystal (FLC) output layer and light blocking layers [94]. Each channel has 26 million pixels. The pixel density of the Active Tiling system is about 2.2×10^6 pixels per cm^2. Pixel period of the FLCoS is about $6.6\mu m$. The overall system has 1×4 channels (5120×20480 pixels = 104 megapixels). A color full-parallax holographic reconstruction is shown in Figure 3.5.

Figure 3.5: Replay of a spatial-multiplexed, 3 × 8 billion-pixel, full-parallax, full-color, 3D image. (Slinger, C., Cameron, C., Stanley, M., "Computer-Generated Holography as a Generic Display Technology," Computer , vol.38, no.8, pp. 46-53, Aug. 2005. ©2009 IEEE. Reprinted with permission)

3.2.4 Horn

Ito *et al.* developed a system, so called Horn (HOlographic ReconstructioN), that calculates computer generated holograms at high speeds using field programmable gate arrays (FPGAs) [95–101]. The first system named as HORN-1 and was developed in 1993. The latest version is called HORN-6 and has four FPGA chips on it and DDR-SDRAM to increase the computation performance. In addition, an approximated Fresnel hologram generation algorithm is utilized by using a look-up table. As a result, objects that have around 10000 object points can be reconstructed in real-time.

3.2.5 Image Hologram

As the name implies, it is a method to record the image of the object instead of the object itself [50, 102, 103]. The method is realized by using a large lens to project the image of the object on a photographic plate. A color holographic display by using an image-type digital hologram was reported in 2007.

The object point, calculated fringe area and the viewing zone are shown in Figure 3.6. If the distance between the object point and the hologram plane is decreased and the distance between the virtual plane and hologram plane is increased, the calculation time

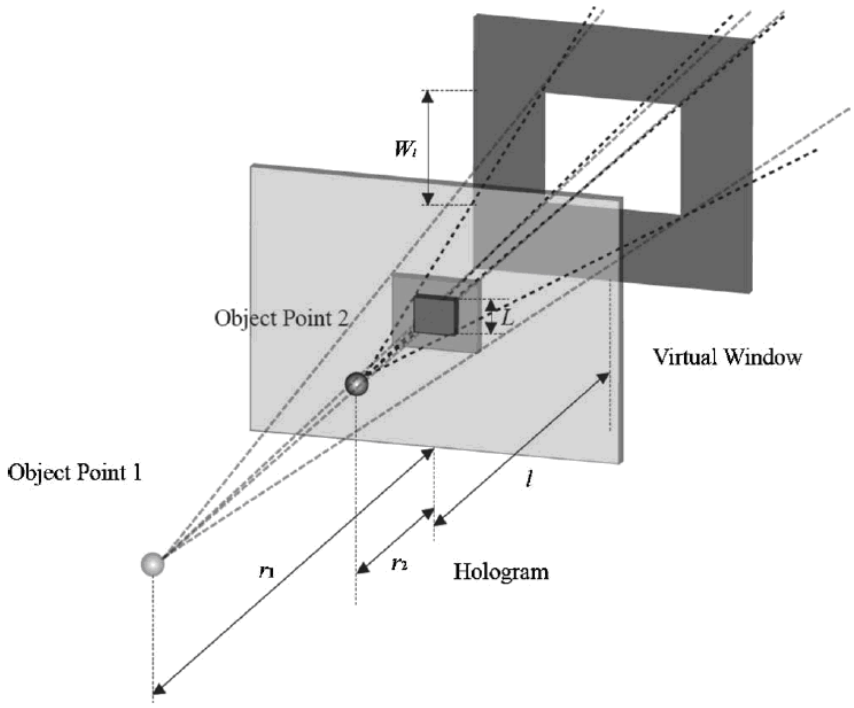

Figure 3.6: Virtual window for image hologram calculation ("Real-time image plane full-color and full-parallax holographic video display system," T. Yamaguchi, G. Okabe, and H. Yoshikawa; Opt. Eng. 46, 125801 (2007). ©2009 SPIE. Reprinted with permission)

decreases. The developed system has $1408 \times 1058 \times 3(RGB)$ pixels with a pixel period of 10.4 μm. For an object which has 3000 object points, the computing time is about 60 msec. Fig. 3.7 shows the optically reconstructed images.

3.2.6 Coherent Stereogram

Coherent stereogram (CS) technique yields fast calculation of holograms [104]. The speed up stems from the segmentation of the fringe patterns and approximating the effect of the object points as a single 2D complex sinusoid to the hologram plane over one segment. Such complex sinusoids in a segment are superposed in the Fourier domain and an inverse fast Fourier transform completes the fringe pattern generation. The same procedure is repeated for all segments. Some improved versions of the coherent stereogram are reported in [105–110].

The accurate compensated phase-added stereogram (ACPAS) is one of those improved

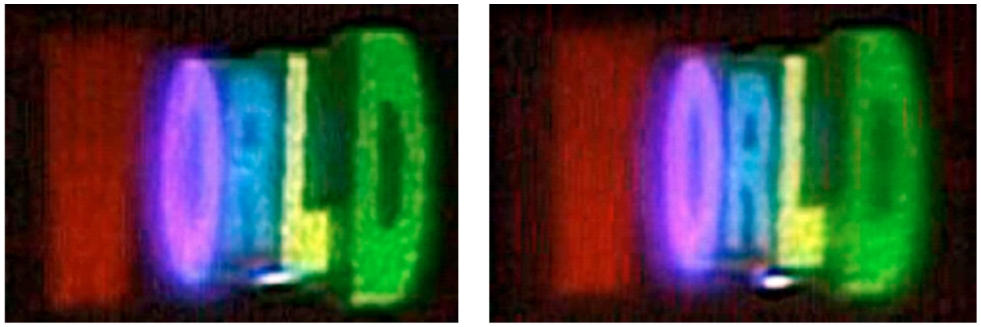

Figure 3.7: Reconstructed images of five letters from different viewpoints in depth: (a) focused on letters W and D, and (b) focused on R. ("Real-time image plane full-color and full-parallax holographic video display system," T. Yamaguchi, G. Okabe, and H. Yoshikawa; Opt. Eng. 46, 125801 (2007). ©2009 SPIE. Reprinted with permission)

versions of the coherent stereogram. ACPAS is a combination of compensated phase-added stereogram (CPAS) and accurate phase-added stereogram (APAS). The ACPAS generates more accurate results which are close to the Fresnel hologram. Fig. 3.8 shows the 3D model and the reconstructed images.

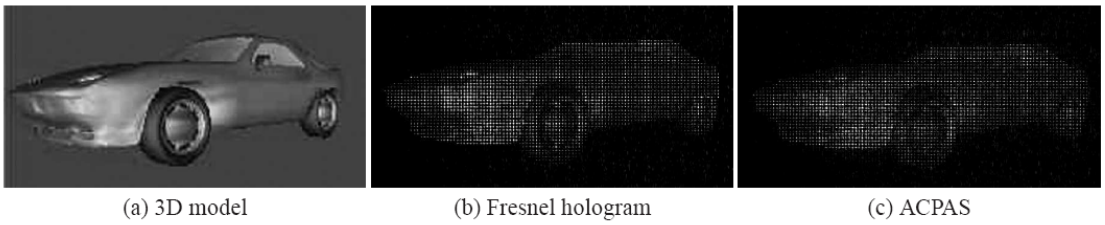

Figure 3.8: A perspective image of the used 3D model and reconstructed images ("Quality improvements of the coherent holographic stereogram for natural 3D display and its applications," H. Kang, in PhD. Thesis, Nihon University, 2008. Reprinted with permission)

Since the CS algorithm uses segments, it is suitable for parallel computing. Thus, ACPAS can significantly benefit from GPU based programming. The applications of the ACPAS in real-time holographic reconstructions by using GPUs are reported in [56–58, 111–113].

3.2.7 NICT

Japan's National Institute of Information and Communications Technologies (NICT) demonstrated an electro-holographic display system [114]. The system has three parts, a capturing system, a computing system and an electro-holographic display system. The capturing system uses integral imaging methods to capture 3D scene. It has an ultra-high-definition integral photography camera ($8K \times 4K$). The captured image processed by the computing system to calculate a digital hologram. Then the resultant hologram is displayed by three spatial light modulators ($4K \times 2K$). Three color lasers (red, green and blue) are used to illuminate those SLMs. All operations are done in real-time. Since the SLMs are small in size, holographic reconstructions are also small. However, end-to-end system operates successfully. Fig. 3.9 shows the developed system.

Figure 3.9: Real object and IP micro-lens array ©2009 NICT. Reprinted with permission.

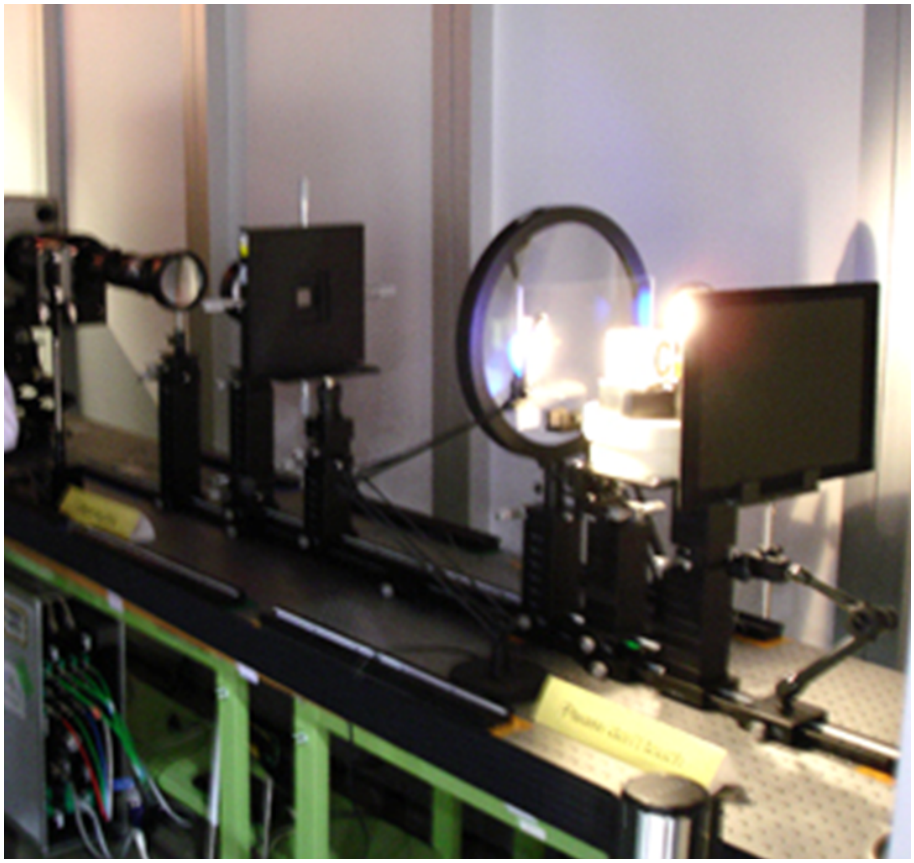

Figure 3.10: Real object acquisition system by using integral photographic camera ©2009 NICT. Reprinted with permission.

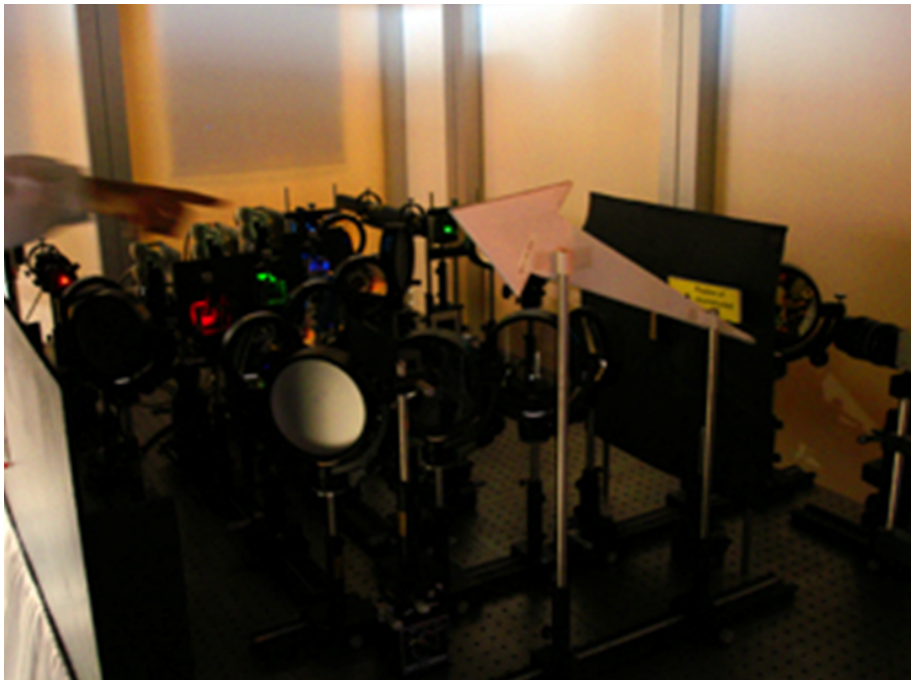

Figure 3.11: Electro-holographic display system with three lasers and three LCoS ©2009 NICT. Reprinted with permission.

Figure 3.12: Reconstruction captured by a camcorder ©2009 NICT. Reprinted with permission.

Chapter 4

Design Parameters for Satisfactory Holographic Displays

This chapter is mainly based on our publication in Proceedings of the IEEE, titled as *Digital Holographic Three-dimensional Video Displays*.

The design and implementation of electronically controllable dynamic displays to support holographic video are significant topics for the accomplishment of the true 3D displays. Since currently available devices have quite limited capabilities, they have not provided satisfactory performance, yet. However, those features are expected to be significantly improved in the future. In order to achieve satisfactory quality 3D reconstructions from digital holographic display systems, one should find the requirement related to various physical parameters. Electronically controlled pixelated spatial light modulators are potential candidates and thus form the basis for such systems. Here in this chapter, we present various specifications with the help of associated analysis and experiments. As a result, we use those specifications to understand and design multiple SLM holographic display systems. Our analysis is based on human visual system properties and limitations. They are then used to final the features of satisfactory 3D reconstructions. Finally subsequent association of these reconstructed image properties to the SLM parameters completes the analysis.

It is informative to look at some relevant features of classical analog photographic

films to facilitate the discussions about satisfactory still holographic displays. In order to have a satisfactory reproduction of the 3D image of a physical object, the holographic recording material is required to be highly sensitive and high in resolution. The spatial resolution of the finest hologram material goes up to many thousands of lines per millimeter. The diffraction efficiency of such photographic materials is approximately 98%. Still holograms may go up to many tens of centimeters in size, or even larger. In order to reproduce high quality 3D images of physical objects in natural color and texture such size and resolution properties are sufficient.

4.1 Size and bandwidth specifications for a satisfactory electro-holographic display

For the rest of the chapter our discussion will be based on the space-bandwidth product that should be supported by a holographic display device and by propagating optical waves that emanate from such a device. The capabilities of the human visual system will be our starting point in our analysis. The physical parameters of the human visual system are naturally limited. Field of view, visible spectrum, spatial resolution, temporal resolution are some of these limitations. Therefore, an electro-holographic device may also be limited in terms of spatial bandwidth because of the corresponding limitations of the human visual system. Fig. 4.1 shows a simple schematic for an electro-holographic display system. The hologram is illuminated by a plane wave. The area of the hologram is denoted by S_H. The incident beam is diffracted by the SLM. The outgoing beam diffracted towards multiple directions within an angle $2\theta_{max}$. D_H denotes the distance between the observer and the hologram. The angular field of view of the observer is $2\phi_v$.

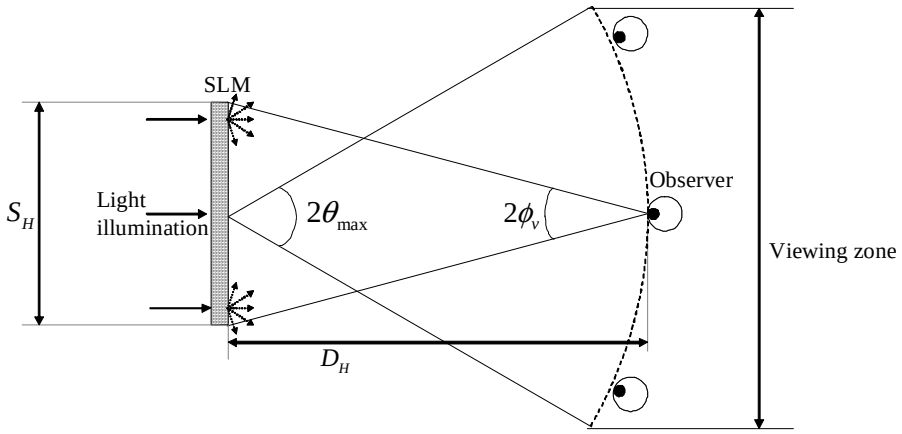

Figure 4.1: Simple schematic for an electro-holographic display ("Digital holographic Three-dimensional video displays," L. Onural, F. Yaraş, and H. Kang, Proceedings of the IEEE, vol.99, no.4, pp.576-589, April 2011. ©2011 IEEE. Reprinted with permission.)

4.1.1 Space-bandwidth product of electro-holographic displays

We start with the discussion of the *space-bandwidth product (SBP)*. For the quality assessment of the holographic displays SBP may be a good metric [63, 115]. As shown in Fig. 4.2, at each point of the hologram plane we assume a local frequency bandwidth, yet it is an idealization. Furthermore, we assume a constant local frequency band throughout the SLM surface [63]. Higher SBP provides higher reconstruction quality. The analysis and the figures are in 1D for convenience and final results are for 2D holograms. The limitations on the bandwidth and the size of the holographic displays should be investigated. Bandwidth restriction results in propagation angle restriction of the plane waves that are emerging from the hologram. Higher bandwidth means higher propagation angles of the plane waves. Since high propagation angles carry the high frequency contents of the reconstructions, they affect the "sharpness" of the reconstructed object. This restriction is equivalent to low-pass filtering the reconstructed image. If we assume that the pixel periods of the SLMs are not the limiting factor for the bandwidth of the hologram and thus the high propagation angles, then the human visual system restricts the bandwidth. According to studies, the field of view, $2\phi_v$, is between 2° and 5° [116–118]. In our analysis we choose the field of view in which the maximum resolution on the retina as 3° and circularly symmetric. The resolution of the image degrades away from the maximum

resolution field of view. However this does not mean that we can not see if the incoming light is outside of this region. Up to 100 - 140 degrees, a low resolution image can be seen and it is called the peripheral vision [116, 118]. Therefore, in order to have realistic holographic reconstructions we still need high propagation angles (i.e. larger bandwidth) in our electro-holography display systems. Being aware of this fact, we still start with a stationary observer whose field of view is restricted by 3°. This restriction is similar to tunnel-vision. However we will loosen our restriction when we deal with moving and rotating observers.

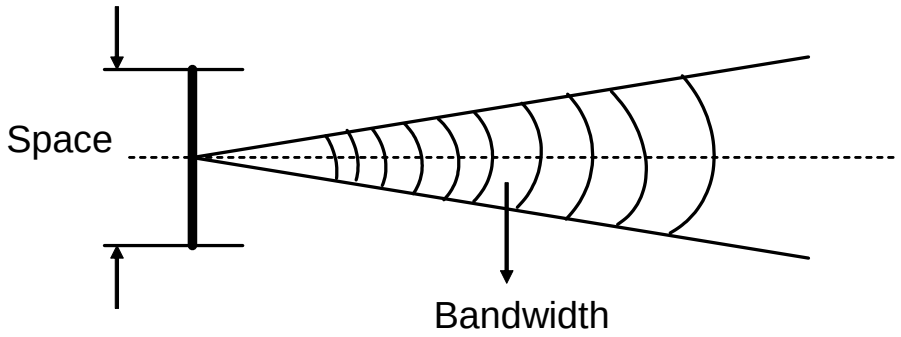

Figure 4.2: The "space" and "bandwidth" to compute the space-bandwidth product ("Digital holographic Three-dimensional video displays," L. Onural, F. Yaraş, and H. Kang, Proceedings of the IEEE, vol.99, no.4, pp.576-589, April 2011. ©2011 IEEE. Reprinted with permission.)

To start our analysis we first assume that the observer is stationary and the the viewing angle of the observer is restricted to 3°. This restriction is equivalent to low-pass filtering of the 2D cross section of any transversal image along the propagation direction, since the wave propagation between parallel 2D planes is a linear shift invariant operation [119]. The hologram and reconstruction planes are also subsets of those transversal images. Therefore, for a stationary observer propagation angles higher than the limit supported by the field of view are not needed and thus, the maximum local diffraction angle of the electro-holographic display system should be chosen as equal to the field of view ($\theta_{max} = \phi_v$). Then the maximum spatial frequency of the hologram can be calculated as:

$$f_{max} = sin(\theta_{max})/\lambda. \tag{4.1}$$

The needed hologram size for a stationary observer can be calculated by using the distance between the eye and the hologram. The relation between the maximum local diffraction angle and the hologram size is shown in Fig. 4.3. The size of the hologram in one dimension is:

$$S_{min} = 2\tan(\theta_{max})D_H. \tag{4.2}$$

Therefore for the stationary observer, the required space-bandwidth product of a 1D SLM is $2f_{max}S_{min}$, where, f_{max} and S_{min} are as given by Eq. 4.1 and Eq. 4.2. If we have a holographic display system with the specified size and the bandwidth we obtain the highest resolution for holographically reconstructed 3D image for a stationary observer.

For the next step we will analyze the space bandwidth product of the holographic display system that supports lateral movement of the observer. Let us assume that the observer is free to move along the lateral direction by S_O. Then the needed hologram size to support such a movement will be:

$$S_H = S_{min} + S_O. \tag{4.3}$$

Furthermore, if the observer is free to rotate around the holographically reconstructed 3D object by θ_R, we need to modify the hologram size together with the bandwidth of the hologram (See Fig. 4.4). The resultant hologram size should be $S_H = S_{min} + 2S_R$ where $S_R = \tan(\theta_R + \theta_{max})D_H - S_{min}/2$. The new maximum frequency is then calculated as $f_{max} = \sin(\theta_R + \theta_{max})/\lambda$. To sum up, for free movement along the lateral direction by S_O and rotation up to an angle of $\pm\theta_R$, the final hologram size should be $S_H = S_{min} + S_O + 2S_R$ and the maximum frequency will be $f_{max} = \sin(\theta_R + \theta_{max})/\lambda$. Therefore the resultant bandwidth will be $2f_{max}$. Then the needed space-bandwidth product will be $\{(S_{min} + S_O + 2S_R)[2\sin(\theta_R + \theta_{max})/\lambda]\}$. As a conclusion, if we insist on using a planar holographic display we will need significantly higher bandwidth to support eye rotations. However we do not need to use planar holograms. High diffraction angles can be supported by using curved holograms or circularly/spherically configured planar holograms or oblique incident light sources. The detailed analysis of curved holographic displays will be given in Section 4.6. When we are able to support higher propagation

angles, a more realistic 3D vision will be achieved for a stationary observer due to the support also in peripheral view.

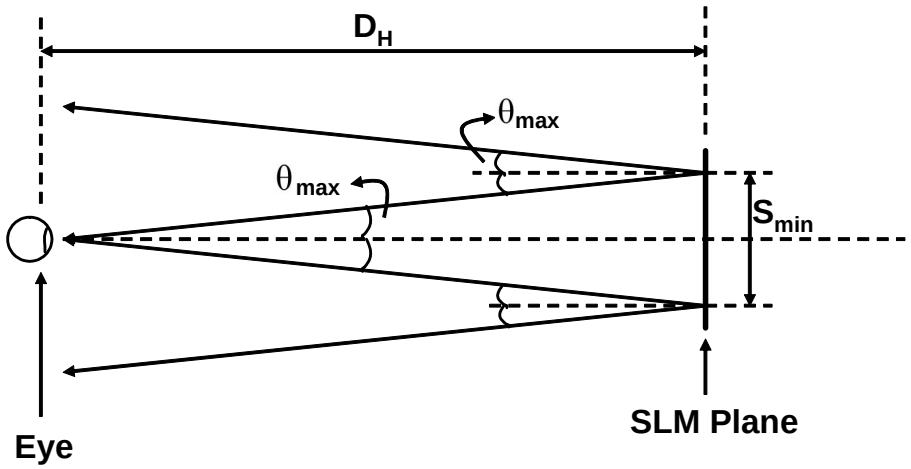

Figure 4.3: Hologram size for a stationary observer. (D_H: Distance between hologram and eye. S_{min}: Hologram extent) ("Digital holographic Three-dimensional video displays," L. Onural, F. Yaraş, and H. Kang, Proceedings of the IEEE, vol.99, no.4, pp.576-589, April 2011. ©2011 IEEE. Reprinted with permission.)

2D hologram 3D image reconstruction case

In the previous section the discussion is for the 1D hologram case. However, 2D holograms are used for our multiple SLM holographic display system. Therefore, extension of the analysis to the 2D hologram case (3D reconstruction) is needed. For a circularly symmetric resolution property of the human eye (stationary), a circular hologram with a shape A_{min} is sufficient. (See Fig. 4.5 (a)) Furthermore, if the observer has a freedom to move with a 2D transversal motion in a parallel plane within an area of shape A_O (Fig. 4.5 (b)), the minimum hologram shape and the size can be calculated by using morphological dilation of A_{min} with A_O: $A_H = A_{min} \oplus A_O$ as shown in Fig. 4.5(c). (Please see [120] for the morphological dilation.) For the observer with a freedom of 2D rotation, the sufficient spatial extent and the maximum frequency along the rotation direction can be calculated as in the 1D case. The space-bandwidth product can be found by multiplying the area and the resultant 2D bandwidth.

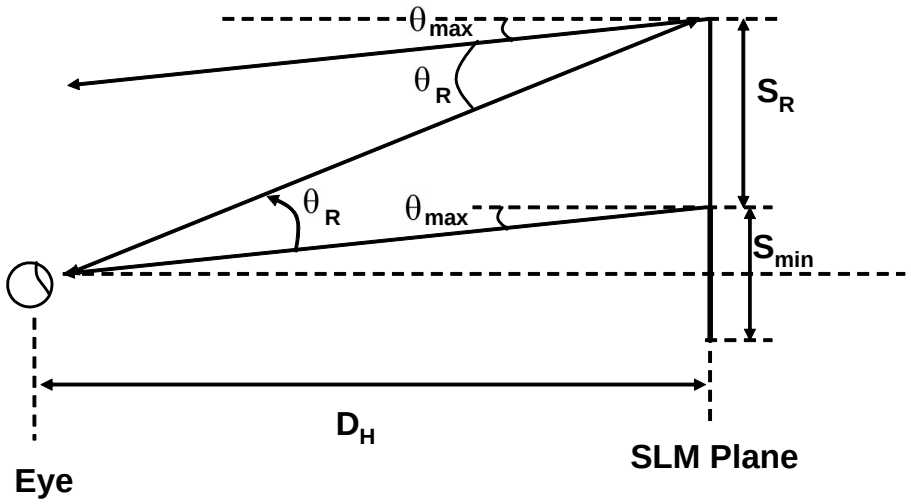

Figure 4.4: Hologram size and bandwidth modification for eye rotation. (D_H: Distance between hologram and eye. S_{min}: Hologram extent for a stationary observer. S_R: Additional hologram extent as a result of eye rotation. θ_R: Rotation angle in lateral direction.) ("Digital holographic Three-dimensional video displays," L. Onural, F. Yaraş, and H. Kang, Proceedings of the IEEE, vol.99, no.4, pp.576-589, April 2011. ©2011 IEEE. Reprinted with permission.)

4.1.2 Pixel period

Commonly used spatial light modulators consist of pixels. Liquid crystal (LC) devices, liquid crystal on silicon (LCoS) devices, digital micro-mirror devices (DMDs) are some of them. The pixelated function $g_p(x,y)$ of the bandlimited 2D signal, $g(x,y)$, on a SLM with $2N \times 2M$ pixels can be expressed as:

$$\begin{aligned} g_p(x,y) &= \left(\sum_{n=-N}^{N-1} \sum_{m=-M}^{M-1} g(x,y)\delta(x - n\Delta p_x, y - m\Delta p_y) \right) \\ &\quad ** \left[\mathrm{rect}\left(\frac{x}{\Delta p_{ax}} \right) \mathrm{rect}\left(\frac{y}{\Delta p_{ay}} \right) \right] \\ &= \left(\sum_{n=-N}^{N-1} \sum_{m=-M}^{M-1} g(n\Delta p_x, m\Delta p_y) \right. \\ &\quad \left. \times \left[\mathrm{rect}\left(\frac{x - n\Delta p_x}{\Delta p_{ax}} \right) \mathrm{rect}\left(\frac{y - m\Delta p_y}{\Delta p_{ay}} \right) \right] \right), \end{aligned} \tag{4.4}$$

where Δp_x and Δp_y are the pixel periods on the SLM at the (x,y) plane, and Δp_{ax} and Δp_{ay} are the active pixel sizes along x and y, respectively [121]. The 2D convolution is represented by $**$ and $\delta(\cdot,\cdot)$ is the 2D impulse function. Rectangular function, $\mathrm{rect}(\cdot)$ is

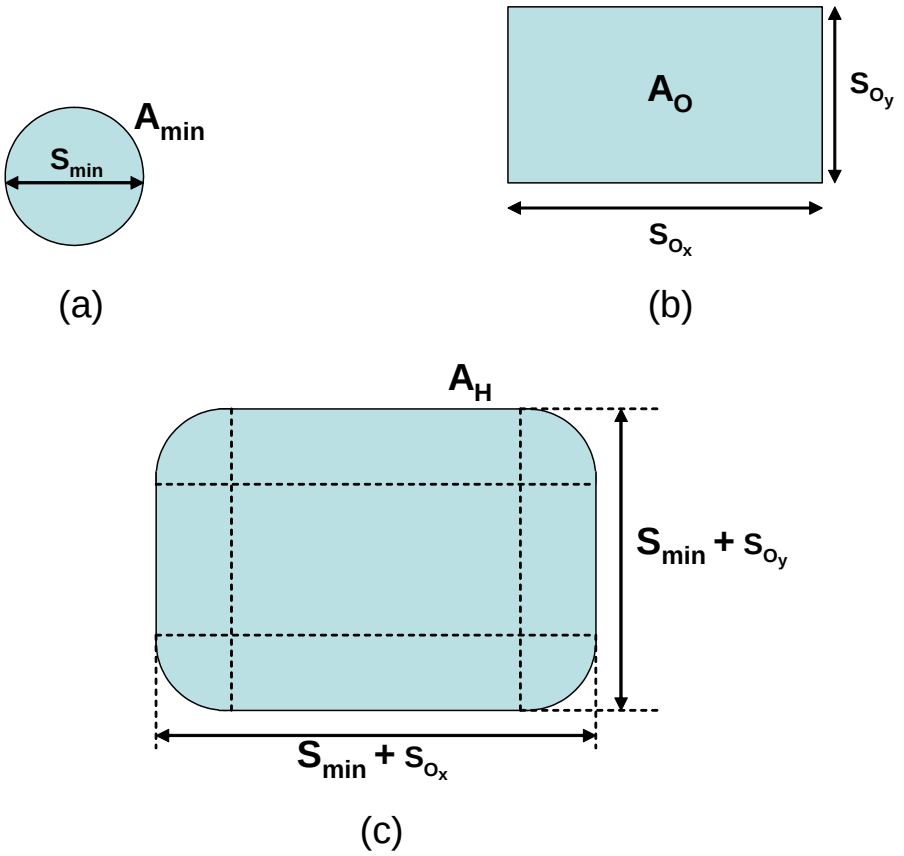

Figure 4.5: (a) Minimum hologram size for a stationary observer. (b) Example for the allowed transverse motion range $A_O = S_{Ox} \times S_{Oy}$. (c) The shape of the minimum hologram is found as $A_H = A_{min} \oplus A_O$ where $\oplus$ denotes the morphological dilation ("Digital holographic Three-dimensional video displays," L. Onural, F. Yaraş, and H. Kang, Proceedings of the IEEE, vol.99, no.4, pp.576-589, April 2011. ©2011 IEEE. Reprinted with permission.)

defined as:

$$rect\,(x) = \begin{cases} 0 \;\text{ for } |x| > 1/2 \\ 1/2 \;\text{ for } |x| = 1/2 \\ 1 \;\text{ for } |x| < 1/2 \end{cases} \tag{4.5}$$

To avoid aliasing during the recovery of the original image by simple low-pass filtering, samples have to be chosen dense enough. With the help of dense sampling, overlapping replicas in the spectral regions of $G_p(k_x, k_y)$ (it is the Fourier transform of $g_p(x, y)$) are

separated. To find how dense we should take those samples, we first assume that the rectangular frequency band is centered around the origin and the maximum frequencies along the x and y directions are $k_{x_{\max}}$ and $k_{y_{\max}}$, respectively. The centers of the replicas in the Fourier domain, i.e. $G_p(k_x, k_y)$ are separated by $2\pi/\Delta p_x$ and $2\pi/\Delta p_y$ along the k_x and k_y directions, respectively. Therefore in order to avoid aliasing the pixel periods have to be chosen as:

$$\Delta p_x \leq \frac{2\pi}{2k_{x_{\max}}} \qquad \text{and} \qquad \Delta p_y \leq \frac{2\pi}{2k_{y_{\max}}}. \tag{4.6}$$

For an infinite extent pixelated band limited function $g_p(x, y)$, to recover the original function by low-pass filtering, the maximum spacings of the sampling lattice are $(\pi/k_{x_{\max}})$ and $(\pi/k_{y_{\max}})$. These are the maximum sampling intervals according to the Nyquist criteria. Fig 4.6 shows the effect of sampling to the waves propagating away from the SLM.

Recovering the original function by low-pass filtering (i.e. Shannon recovery) is only one of the possible techniques. Other recovery techniques may relieve the Nyquist rate requirement and we may not need that much dense sampling. Full recovery of the severely undersampled (undersampled below the Nyquist rate) Fresnel diffraction patterns is reported by Onural [122]. The full recovery condition for undersampled diffraction patterns is different than the band-limitedness, like the space-limitedness of the original function. Therefore, when the diffraction pattern of a finite size object is sampled, higher diffraction orders (replicas of the original image) will also fall onto the reconstruction. If we increase the sampling rate, those image replicas will further separate from each other. Therefore we start with a higher sampling rate and we decrease it until the image replicas just overlap [28, 122, 123]. Then just by filtering out the replicas by windowing in the space domain we obtain the original function. In real-life applications, space-limitedness is more common rather than band-limitedness. Therefore, we can conclude that full recovery from samples that are below the Nyquist rate is possible.

If we go back to Shannon recovery case, we can use the Nyquist criteria to find out the maximum pixel period. For example, for a observer (stationary) looking directly to the

hologram from a distance $D_H = 1m$ ($\lambda = 633nm$ and $\theta_{max} = \phi_v = 1.5°$), the maximum pixel period is $\Delta_p = \frac{\lambda}{2\sin(\theta_{max})} \approx 12\mu m$ and $S_{min} = 5cm$ from Eq. 4.1, Eq. 4.2 and Eq. 4.6.

As mentioned in the previous section, when the observer is allowed to move along the lateral direction and rotate around the reconstruction the required bandwidth and size of the hologram should be modified. For example, if the distance between the observer and the holographic display is one meter ($D_H = 1m$), and the observer is free to move $20cm$ ($S_O = 20cm$) along the lateral direction and free to rotate $\pm 15°$ ($\theta_R = 15°$) around the reconstruction, the diffraction angle is $\theta_R + \theta_{max} = 17°$ (where $\theta_{max} = 2°$) and the display size is $0.80m$ ($S_H = S_O + 2\tan(\theta_R + \theta_{max})D_H$). For the holographic display whose size and pixel period are $0.80m$ and $1.1\mu m$, respectively, the total number of pixels along one direction will be more than 860000.

In addition to the sampling of the hologram due to the pixelated structure of the SLMs, recovery of the original 3D object from the sampled hologram is also an issue. For this purpose, as mentioned before, full recovery of the original signal can be obtained by low-pass filtering. Since the wave propagation between two parallel planes is a linear shift invariant operation, low-pass filtering can be performed at any transversal plane along the propagation direction. Thus, we can perform it also at the reconstruction plane. We can use an optical low-pass filter which blocks the high-order diffractions and moves along the transversal direction together with the observer (See Fig. 4.6(d)). However the filter imposes a key-hole effect due to the associated narrow viewing angle.

As an alternative way to avoid overlapping of the higher diffraction orders, sampling density can be increased and this yields smaller pixel periods. High diffraction orders at the reconstruction plane are shown in Fig. 4.7. D_R is the distance between the hologram plane and the reconstruction plane, and S_{Rec} is the reconstruction size ($S_{Rec} = S_H + 2\tan(\theta_{max})D_R$ from the previous discussions). The angle of the m^{th} high diffraction order is $\theta_{Om} = \sin^{-1}(m\lambda/\Lambda)$, where λ is wavelength Λ is period of the diffraction grating and m is the index of the diffraction order [124]. As shown in Fig. 4.7, to avoid overlapping of the high diffraction orders $\tan(\gamma)$ should be larger than S_{Rec}/D_R, where $\gamma = \theta_{O1} - \theta_{max}$.

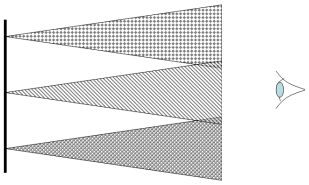

(a) Local bandwidth (propagation angle) associated with a hypothetical continuous (non-pixelated) SLM. Diffracted light propagates within a cone from each location on the SLM.

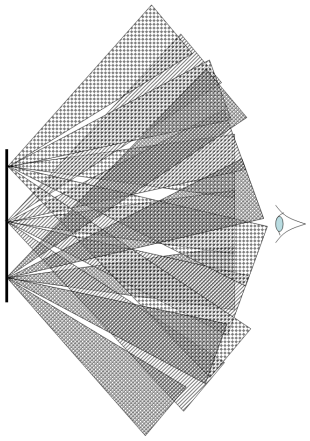

(b) Consequence of the pixelated structure (sampling) to the propagation angle distribution (no aliasing case). Many well separated cones of light propagate from each SLM location.

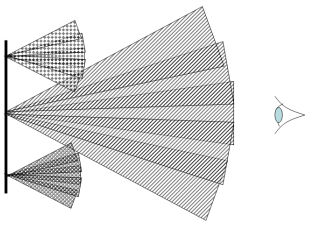

(c) Aliasing due to larger pixel size (coarse sampling). Propagating cones from each SLM location overlap. (Please note that cones propagate along the horizontal axis, indefinitely; only a portion is shown not to clutter the drawings. The extent of the cones has no relevance.)

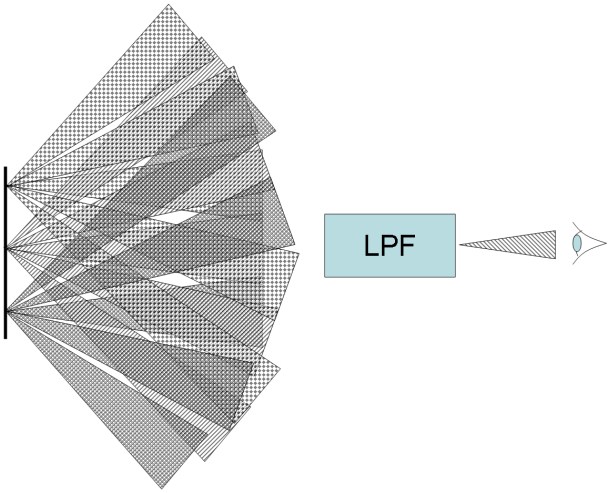

(d) Optical low-pass filter to recover the original image observed in (a). Only low angle propagation passes through the filter at each SLM point (and low-pass filter) location.

Figure 4.6: Effect of pixel period on the angular distribution of diffracted light from a pixelated SLM and recovery by an optical low-pass filter. ("Digital holographic Three-dimensional video displays," L. Onural, F. Yaraş, and H. Kang, Proceedings of the IEEE, vol.99, no.4, pp.576-589, April 2011. ©2011 IEEE. Reprinted with permission.)

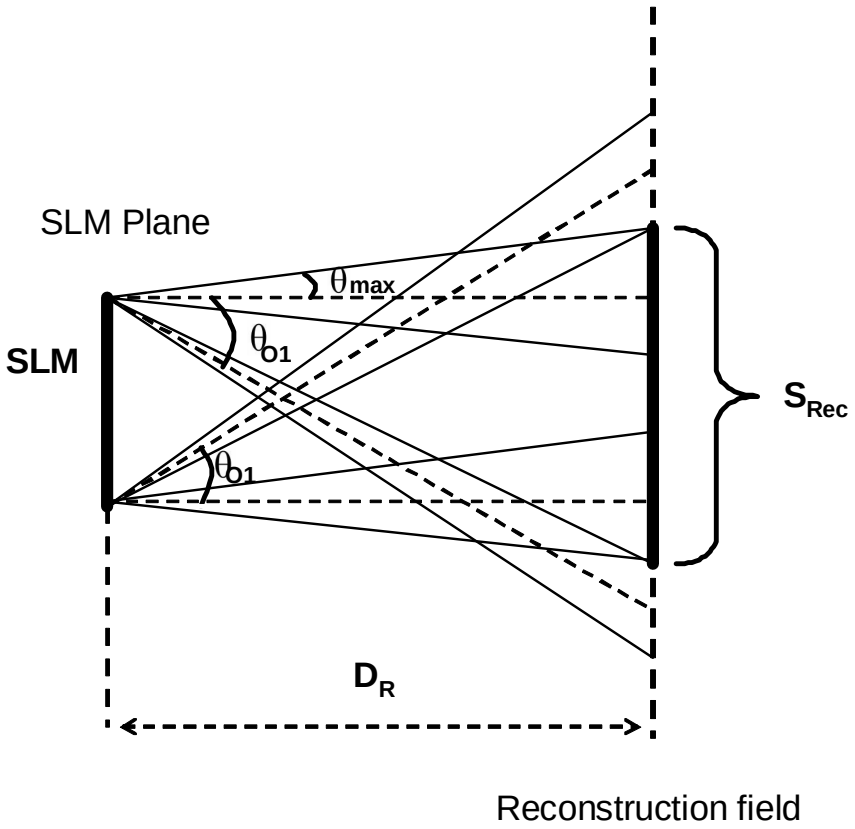

Figure 4.7: High diffraction orders in reconstruction field and their separation ("Digital holographic Three-dimensional video displays," L. Onural, F. Yaraş, and H. Kang, Proceedings of the IEEE, vol.99, no.4, pp.576-589, April 2011. ©2011 IEEE. Reprinted with permission.)

As an example, if the observer is free to move along lateral direction by $15cm$ ($S_O = 15cm$) and the distance between the observer and the hologram is $1m$ ($D_H = 1m$), the required hologram size is $20.2cm$ ($S_H = 20.2cm$ and $\theta_{max} = 1.5°$). For $D_R = 0.5m$ (the distance between the reconstruction and the SLM), the maximum reconstruction size will be $22.8cm$ ($S_{Rec} = 22.8cm$). To avoid overlapping of the high diffraction orders for the hologram whose frequency content is fixed, γ should be larger than $\tan^{-1}(S_{Rec}/D_R) \approx 24.5°$, which gives $\theta_{O1} = 26°$. Since $\theta_{O1} = \sin^{-1}(\lambda/2\Delta p)$, the pixel period Δp should be smaller than $0.72\mu m$ (for $\lambda = 633nm$).

This example shows that even without the eye rotation (i.e. $\theta_R = 0$), the required pixel period may be less than the wavelength of the light. If the observer can rotate around the reconstruction, pixel periods will decrease rapidly. Such pixel periods may not be feasible

due to physical constraints. As a result, we may conclude that planar configurations may not be the ultimate solution for the satisfactory holographic display systems. With the help of the analysis in this section we understand that other geometrical configurations (i.e. non-planar cases) or adaptive systems may relieve the large space-bandwidth product (see Fig. 4.8). Therefore the narrower bandwidth can be used as shifted around the center frequency imposed by the oblique illumination. As a result, instead of a space-bandwidth of $BW \times S_{max}$, a space-bandwidth product of $BW \times S_H$ at a time may still be sufficient.

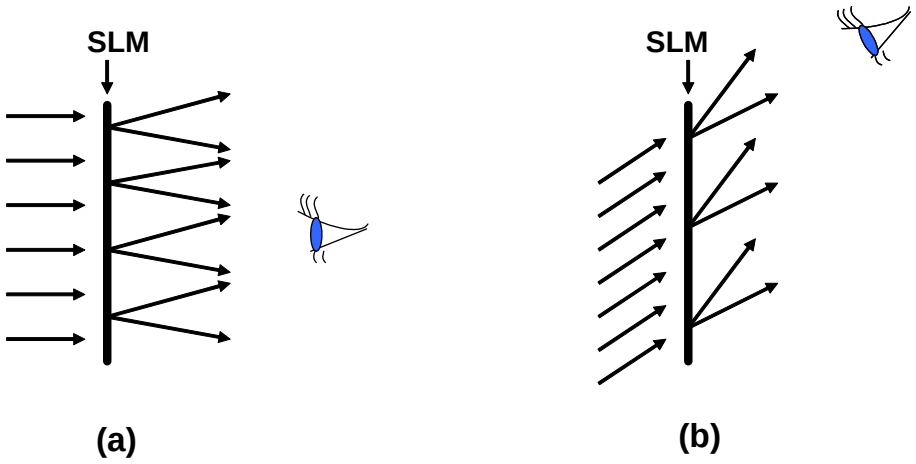

Figure 4.8: (a) Orthographic illumination (b) Tilted illumination ("Digital holographic Three-dimensional video displays," L. Onural, F. Yaraş, and H. Kang, Proceedings of the IEEE, vol.99, no.4, pp.576-589, April 2011. ©2011 IEEE. Reprinted with permission.)

4.2 Space-bandwidth product as a quality metric for holographic reconstructions

The discussion until this point is about space-bandwidth product of the SLMs to have satisfactory quality holographic reconstructions. In this section we want to find out how the information is distributed in space during the reconstruction. First we start with the single planar SLM case.

When a plane wave is modulated by a planar SLM, it is diffracted depending on the pattern written on the SLM. This propagation after the diffraction is in a limited angle and the limit is related to the bandwidth of the pattern written on the SLM. For

a given SLM, the quality metric can be illustrated as a function of distance with respect to the SLM. Fig. 4.9 is an illustration of the variation of the profile of such a quality metric. Note that the figure does not show the diffraction pattern. Quality metric is used to determine the optimum location for a holographic reconstruction in terms of quality. The solid angle in which the diffracted light propagates is equal to the frequency band of the system. We first set a variable z, denoting the distance of a focused point on the optical axis. When we move away from the SLM, as shown in Fig. 4.10 (a) and (b) the bandwidth of the system is restricted by the capabilities of the SLM until $z = z_0$. Up to this point the bandlimited quadratic phase pattern (i.e. the Fresnel lens) remains entirely in the SLM, thus the bandwidth is constant. However in this region the area that the bandlimited quadratic phase pattern sits increases with z^2. As a result, quality metric increases proportional to z^2 in $0 < z < z_0$.

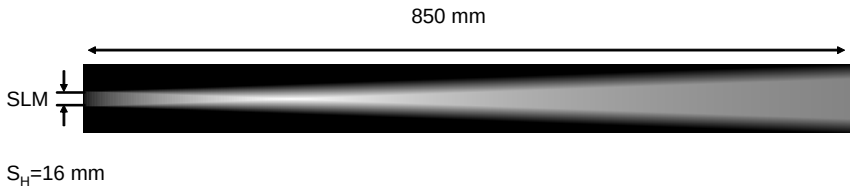

Figure 4.9: Quality metric of reconstruction by the hologram on the SLM as a function of distance of the reconstructed image (white: high quality, black: low quality) ("Digital holographic Three-dimensional video displays," L. Onural, F. Yaraş, and H. Kang, Proceedings of the IEEE, vol.99, no.4, pp.576-589, April 2011. ©2011 IEEE. Reprinted with permission.)

After a certain distance (i.e. $z = z_1$), the quadratic phase pattern covers the entire SLM and the 2D frequency band, so the quality metric, will decrease with z^2. Between those two points, $z_0 < z < z_1$ is the transition region.

Fig. 4.11 shows the variation of the quality metric along the optical axis. For example, if we have a SLM with a size of $16mm$ and pixel period $9\mu m$ (i.e. $\theta_{max} = 2°$) and for the wavelength $\lambda = 633nm$, optimum distance corresponding to the highest quality metric, D_R, is approximately $228mm$ (Fig. 4.11). The extension of this analysis to a circularly configured planar SLMs will be presented in Sec. 4.6.

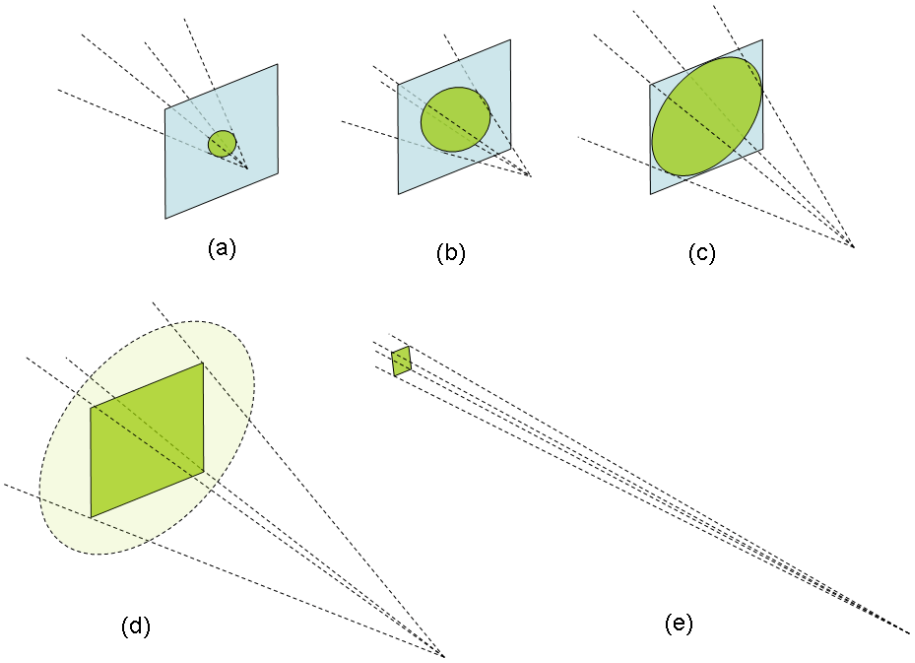

Figure 4.10: Variation of "space" and "bandwidth" with respect to reconstruction distance z. (a) When z is small, "space" is also small and the "band" is limited by the maximum band supported by the SLM. (b) As z moderately increases, "space" also increases and "band" is still limited by the maximum band supported by the SLM. (c) Transition (d) For larger z, "space" does not change anymore, but "band" decreases since the supported diffraction angle (and therefore the spatial frequency) decreases. (e) For very large z, "space" does not change, but "band" decreases even further ("Digital holographic Three-dimensional video displays," L. Onural, F. Yaraş, and H. Kang, Proceedings of the IEEE, vol.99, no.4, pp.576-589, April 2011. ©2011 IEEE. Reprinted with permission.)

4.3 Noise and Quantization

Information about a 3D object is carried and distributed to the space via diffraction. For common objects, this information is well spread all over the holographic pattern. Therefore, such holograms are immune to quantization noise to some extent. In this section, noise sources and the effect of the quantization to holograms will be investigated. Common spatial light modulators and other display devices usually have 256 quantization levels. For example, most of the commercially available phase-only spatial light modulators quantize the phase interval $(0 - 2\pi)$ to 256 levels. According to Mills and Yamaguchi, even 4-bit quantization is enough for phase hologram quantization and the difference between 6-bit and 8-bit quantization is unnoticeable [125]. Since commercially

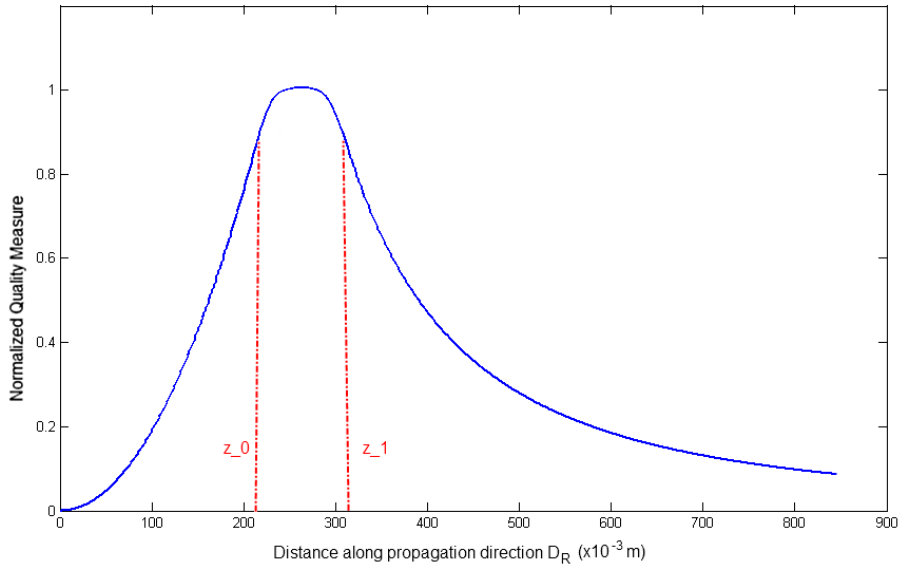

Figure 4.11: Variation of normalized quality metric for a reconstructed image from a finite size SLM along the optical axis ("Digital holographic Three-dimensional video displays," L. Onural, F. Yaraş, and H. Kang, Proceedings of the IEEE, vol.99, no.4, pp.576-589, April 2011. ©2011 IEEE. Reprinted with permission.)

available SLMs have usually 8-bit quantization, they are adequate, in terms of quantization properties, for holographic display systems. Moreover, optical elements such as prisms, beam-splitters and lenses may also introduce some distortion to the holographic reconstructions.

Yet another noise source is the speckle. If coherent light passes through or reflected from an optically rough surface, its phase is randomized. Superposition of random phase light contributions result in the speckle [126]. There are several methods to eliminate the speckle noise [127–131]. Using LED illumination is an alternative way of reducing speckle. Although LEDs have some degree of temporal and spatial coherence, since they are not perfectly coherent speckle may not exist in the reconstruction. Furthermore, LED illumination is not harmful to human eye, if it is not too bright [132]. Thus, holographic reconstructions obtained by LED illumination can be observed by naked eye [55–59]. In addition, LEDs are low-cost and easy-to-use devices. However, since they exhibit low coherence, the reconstructions may be somewhat blurred.

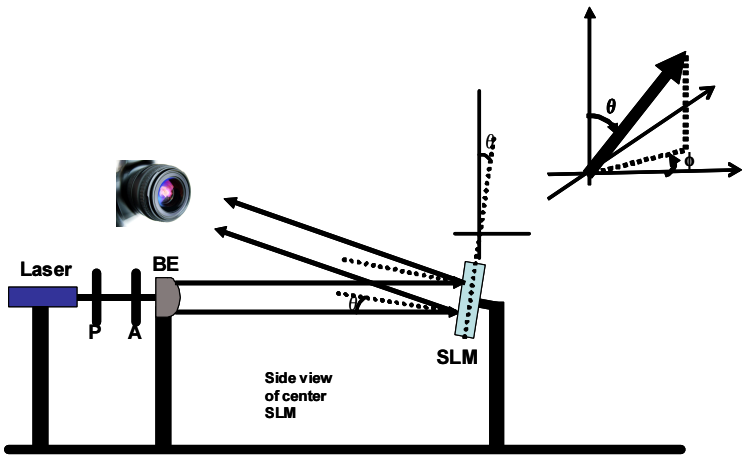

Figure 4.12: Vertically tilted SLM.

4.4 SLM tilting and polarization effect

In our multiple SLM holographic display systems, we usually tilt the SLMs vertically to move the holographic reconstructions above the setup. With the help of this technique, observers have a clear sight without any obstacles. Therefore, in this section we examined the reconstruction quality when the SLM is illuminated by an oblique incident light. First of all, based on our experiments and subjective evaluations, 10 degrees of tilt along the vertical direction allows the observer to see the reconstructions without any obstacles such as beam expanders, beam splitters and so on. Fig. 4.12 shows that the optical setup of the vertically tilted SLM.

The quality of the reconstructions from a commercially available SLM under oblique illumination was not known. Therefore we conducted some experiments and recorded the reconstructions for 0, 10, 25 and 33 degrees of tilted illumination as shown in Figs. 4.14 (a) - (j). Figures indicate that up to 25 degrees of tilting, the results are satisfactory. However at 33 degrees the reconstructions significantly degrade.

There are also polarization issues for tilted reconstructions. In the manual of the HoloEye 1080 P, it is shown that SLM modulates best when polarization of the incident light is along the vertical direction. We used such a vertical polarization for our experiment. Since the polarization of the incident light is 90 degrees (perpendicular to the

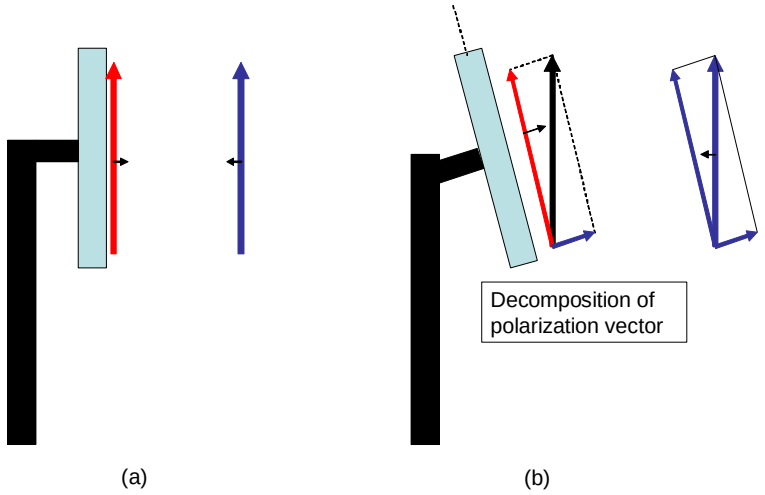

Figure 4.13: Effect of polarization on tilting. Red arrows denote the modulated light.

ground), more degradation is observed when there is a vertical tilt (Fig. 4.13) compared to horizontal tilt. For larger tilt angles if the tilting direction and the polarization is in the same direction (e.g. vertical tilt - vertical polarization), scalar diffraction calculations fail. Based on our reconstructions we can conclude that up to 25 degrees of tilting the reconstructions are still satisfactory and thus we can use this result during the design of a cylindrical holographic display.

4.5 Off-axis case

Since we use off-axis holography in our circular holographic displays, the related design parameters should also be investigated. Holographic reconstructions from inline holograms may suffer from the undiffracted beam. When the object beam and the undiffracted beam overlap the observer may not see the reconstructed image. In order to separate the object beam and the undiffracted beam, a tilted reference beam may be used. However this procedure may increase the maximum spatial frequency of the holographic pattern since it is equivalent to a modulation of a signal by a carrier frequency which is determined by the direction of the reference wave. If the tilt of the reference wave is θ_T along the vertical direction, the maximum spatial frequency will increase by an additional $\sin(\theta_T)/\lambda$. For a stationary observer, as in the example given in Section 4.1.2, if the angle between the

object beam and the undiffracted beam is chosen as 2° along the vertical direction, the resultant spatial frequency will be $f_{max} = sin(1.5°)/\lambda + sin(2°)/\lambda = 96 cycles/mm$, the maximum diffraction angle, θ_{max}, will be approximately 3.5°, and finally the pixel period will be $\Delta_p \approx 5\mu m$, instead of $12\mu m$ (as given in Section 4.1.2). Therefore we can conclude that off-axis holography affects the pixel period, significantly.

4.6 Cylindrically arranged electro-holographic display system

Commercially available spatial light modulators are generally planar. In the literature, planar holographic display systems consist of multiple SLMs are reported [59, 64, 88, 103, 133]. However, as presented in Section 4.1.1 a problem related to the planar configuration is the necessary high space-bandwidth product to support rotational movements. Therefore, as also discussed in Section 4.1.2 the need for circular configuration of planar SLMs is obvious. Some of the circularly configured holographic display systems will be discussed in the following sections and this thesis mainly focuses on such configurations. With the help of such designs, the necessity for too small pixel periods is relieved. Fig. 4.15 shows the space variation of the quality metric when multiple planar SLMs are configured circularly. The bright region shows the highest quality region of the holographic reconstruction. By increasing the total number of SLMs higher propagation angles are supported and, thus the space-bandwidth product increases. The gaps between the SLMs yield discontinuous regions at the observer side. However solutions for this problem will also be presented in the following chapters.

4.7 Extension to a spherical or other surface geometry designs

In the previous sections we dealt with circularly configured holographic display arrangements. However, extensions to spherical or other more general configurations are rather straightforward. Instead of tiling the SLMs on a cylindrical surface, planar SLMs should be tiled on a spherical surface. Such a configuration will also increase the vertical parallax. A spherical electro-holographic display design is shown in Fig. 4.16.

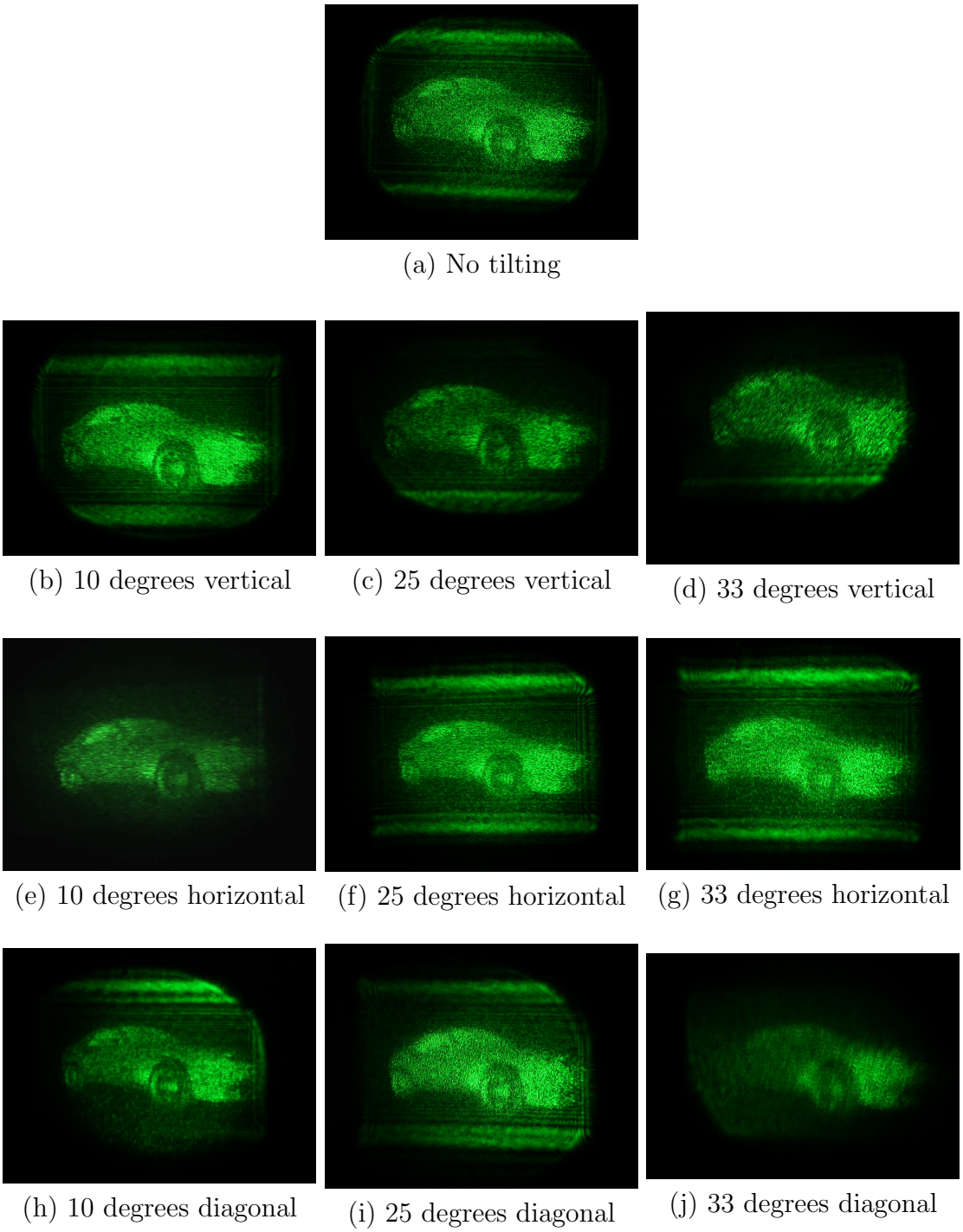

(a) No tilting

(b) 10 degrees vertical

(c) 25 degrees vertical

(d) 33 degrees vertical

(e) 10 degrees horizontal

(f) 25 degrees horizontal

(g) 33 degrees horizontal

(h) 10 degrees diagonal

(i) 25 degrees diagonal

(j) 33 degrees diagonal

Figure 4.14: Reconstructions by tilted SLM.

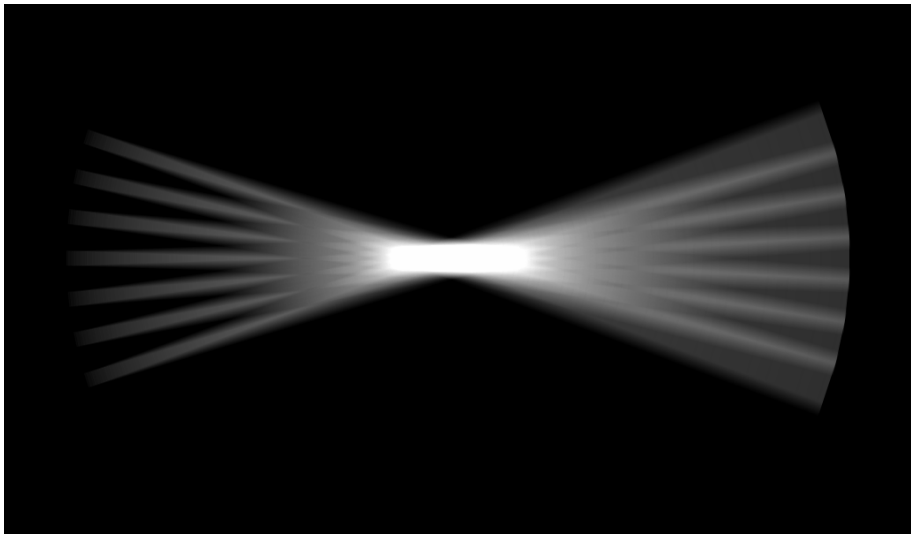

Figure 4.15: Space variation of the quality metric for piecewise planar circular SLM configuration with multiple planar SLMs. The bright region at the center is the highest quality reconstruction zone. SLMs are at the left end of bright bands. Observer is at the right hand side. (white: high quality, black: low quality) ("Digital holographic Three-dimensional video displays," L. Onural, F. Yaraş and H. Kang, Proceedings of the IEEE, vol.99, no.4, pp.576-589, April 2011. ©2011 IEEE. Reprinted with permission.)

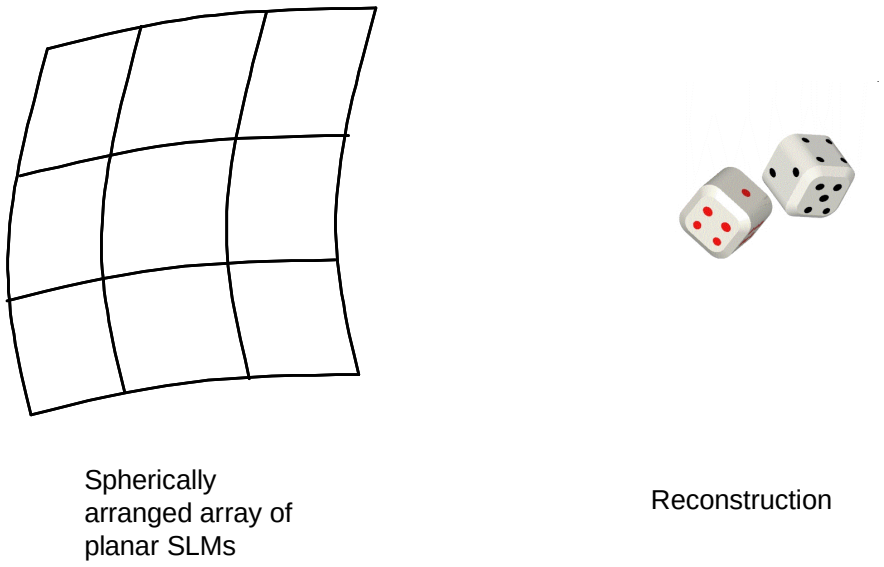

Figure 4.16: Spherically arranged electro-holographic display design ("Current research activities on holographic video displays," L. Onural, F. Yaraş and H. Kang, Proc. SPIE 7690, 769002, (2010). ©2010 SPIE. Reprinted with permission.)

Chapter 5

Experimental Setup And Results For The Holographic Displays Using Single Phase-only SLM

In order to design and implement multiple SLM holographic displays, first we need to investigate the single SLM holographic reconstructions. Therefore in this chapter, we present the properties of phase holograms and some single SLM holographic display examples. Some parts of this chapter is based on our publication in 2008 3DTV Conference, titled as *Holographic reconstructions using phase-only spatial light modulators* [54] . In Chapter 6, we will extent our discussion and analysis to multiple SLM configurations.

5.1 Phase-only Holograms

As discussed in Chapter 3, phase-only spatial light modulators (SLMs) have some advantage over amplitude-only SLMs. One of the most important properties is the high diffraction efficiency. Theoretically phase-only holograms may have up to %100 diffraction efficiency. Phase-only holograms modulate the phase of the incident wave either by changing the path length of the incident wave or changing the refractive index of the medium. Phase-only SLMs perform phase variations by altering the refractive index.

Uniaxial birefringent liquid crystal layer has an extraordinary refractive index, n_e, and an ordinary refractive index, n_o [134]. When an alternating electric-field is applied to the birefringent liquid crystal layer, LC molecules tend to align with the electric field and thus, the extraordinary refractive index decreases.

To define the phase hologram, we first start with a 2D complex distribution $f(x, y) = a(x, y) \exp[j\phi(x, y)]$. Then we assume that $\psi_z(x, y) = A(x, y) \exp[jp(x, y)]$ is the diffraction pattern of the given 2D complex function, $f(x, y)$, under the coherent illumination at a distance z. If the hologram has the form $\psi_z(x, y) = A \exp[jp(x, y)]$ (i.e. constant amplitude) then $\exp[jp(x, y)]$ is called the phase hologram. For common objects (i.e. for most $f(x, y)$), the phase hologram can only be obtained as an approximation since $A(x, y)$ is not a constant.

Throwing away the magnitude of a complex field is a non-linear operation and such process degrades the quality of the reconstruction by enhancing the edges and suppressing the intensity in smooth areas. However based on our subjective test, the quality of the optical reconstructions from such phase holograms are satisfactory for casual observers. Furthermore, we can increase the quality if we perform some iterative processes to the phase holograms.

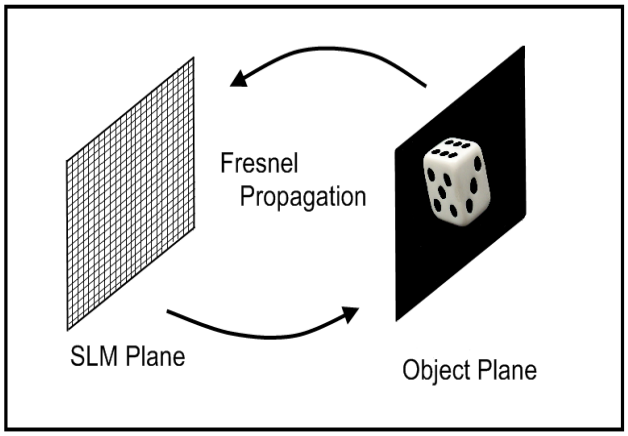

Figure 5.1: Hologram and Object planes ("Holographic reconstructions using phase-only spatial light modulators," F. Yaraş, M. Kovachev, R. Ilieva, M. Agour and L. Onural, in 3DTV Conference: The True Vision - Capture, Transmission and Display of 3D Video, IEEE, 2008. ©2008 IEEE. Reprinted with permission.)

One of the iterative algorithms is the Gerchberg-Saxton algorithm [54,55,135,136]. 2D phase holograms of 2D objects are computed with the help of this algorithm (See Fig. 5.1). We first start with the object plane where the initial phase distribution, $\phi_{initial}(x, y)$, is chosen randomly and the magnitude, $a(x, y)$ is the real valued 2D target image. Then the complex distribution at the object plane is propagated to the hologram plane by using the Fresnel wave propagation kernel. Let us denote the resultant complex field at the hologram plane as $A_1(x, y) \exp(j\psi_1(x, y))$, where subscript 1 denotes the first iteration step. Then, the magnitude, $A_1(x, y)$ is replaced by 1 assuming that the hologram will be illuminated by a plane wave parallel to the hologram plane. The resultant complex distribution is back-propagated to the object plane, again by using the Fresnel propagation. Here, the magnitude of the resultant field, say $a_1(x, y)$, is replaced by the target object, i.e. $a(x, y)$. If the desired iteration number is reached or the error between the target and the resultant intensity distribution drops below a certain point, the iteration is stopped and the phase distribution at the hologram plane, $\psi_{final}(x, y)$, become our phase hologram. Fig. 5.2 shows the block diagram of the Gerchberg-Saxton algorithm.

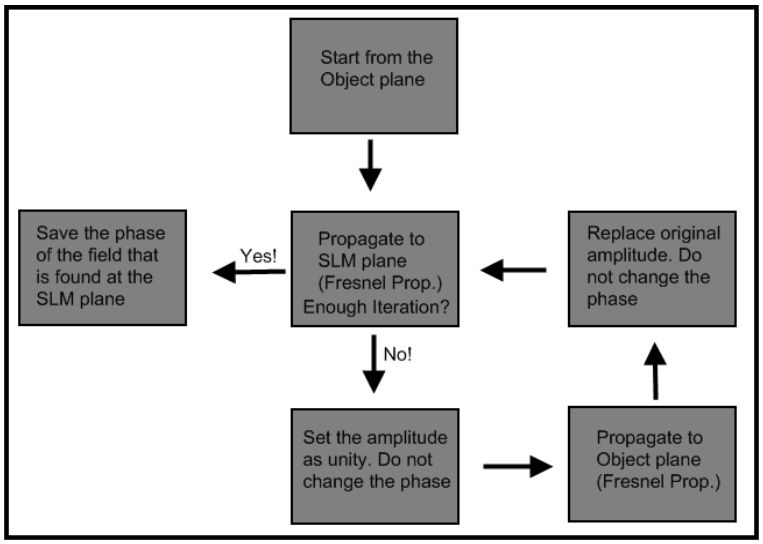

Figure 5.2: Block diagram of the Gerchberg-Saxton algorithm for calculating phase holograms ("Holographic reconstructions using phase-only spatial light modulators," F. Yaraş, M. Kovachev, R. Ilieva, M. Agour and L. Onural, in 3DTV Conference: The True Vision - Capture, Transmission and Display of 3D Video, IEEE, 2008. ©2008 IEEE. Reprinted with permission.)

5.2 Setup and Results

In our both single and multiple SLM experiments, we used Holoeye phase-only SLMs [71]. It has 1920×1080 pixels and the pixels are square with a period of $8\mu m$ in both directions. The panel size of the spatial light modulator is about $16mm \times 8mm$. The fill factor of the SLM is reported as %87. Refresh rate is 60 Hz and an 8-bit quantization is used. Picture of the Holoeye HEO-1080P is shown in Fig. 5.3.

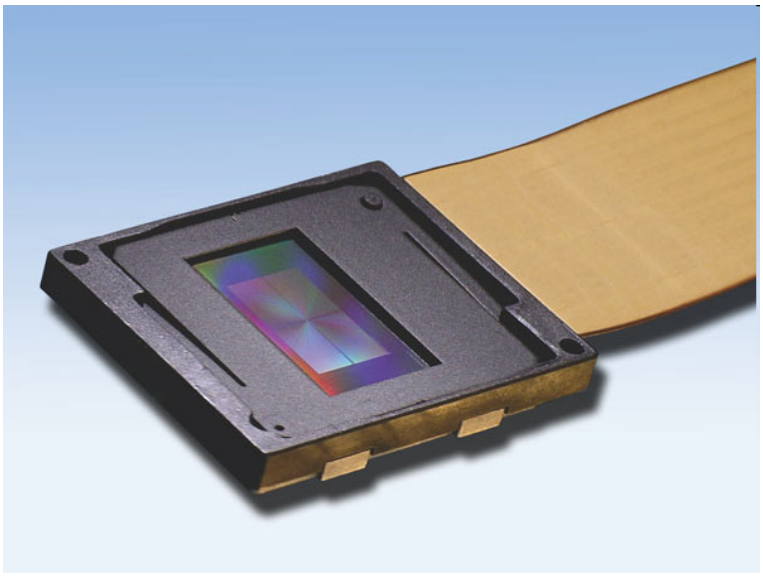

Figure 5.3: Photograph of a Holoeye HEO-1080P phase-only spatial light modulator. (courtesy of www.holoeye.com)

Illustration of the optical setup for the single SLM experiments is shown in Fig. 5.3. Laser light is first passed through a spatial filter to clean up the beam, since there may exist abberations due to dust or imperfection in optics, or even defects in the laser medium. The filtered light is then re-shaped by the lenses (grouped under the name of "beam expender" in the figure) to have a plane wave illumination. The generated plane wave illumination is passed directly across the beam-splitter and illuminates the phase hologram on the spatial light modulator. The modulated light from the SLM is reflected by the beam-splitter to the observation region. Without the beam-splitter it would be difficult to observe the reconstruction. With the help of a camera, a focused reconstruction is captured at the reconstruction plane.

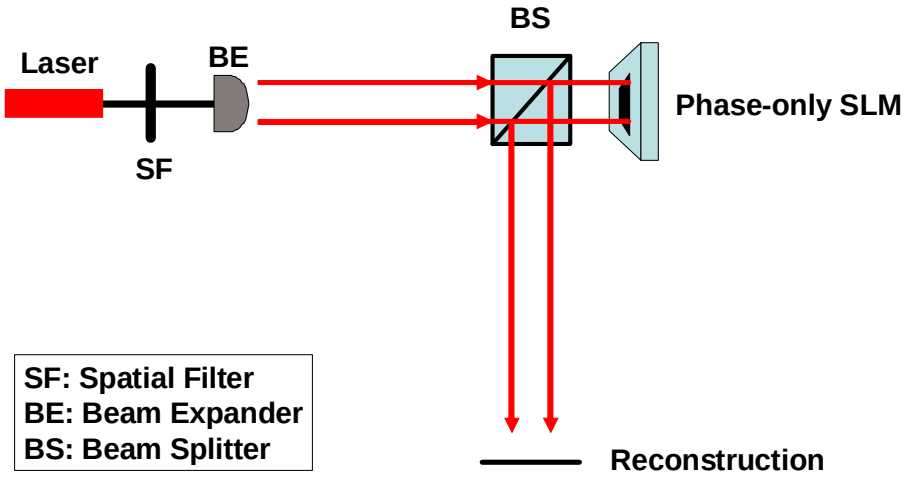

Figure 5.4: Illustration of the optical setup for single SLM holographic display experiments.

Although iterative algorithms are quite slow due to demanding computational complexity, we obtained successful results even after a low number of iterations. Fig. 5.5(a) shows the 2D intensity distribution of the target image. Since our phase-only SLM is designed for monochromatic applications, we use a grayscale image. The phase hologram of the target image is shown in Fig. 5.5(b). Hologram is calculated by using the Gerchberg-Saxton algorithm and only 10 iterations are performed. The optical reconstruction from the phase hologram under coherent plane wave illumination is illustrated in Fig. 5.5(c). The wavelength of the illuminating light source is $633nm$.

Phase holograms of more complicated 2D intensity distributions are also calculated. Fig. 5.6(a) shows the photograph of the Bilkent 3DTV Laboratory. Phase hologram of the image (the 2D gray level photograph) is calculated by performing 20 iterations. The numerical and optical reconstructions from the resultant phase hologram is shown in Fig. 5.6(b) and Fig. 5.6(c), respectively.

Above reconstructions have the same size as the SLM. However, larger holographic reconstructions compared to SLM size is possible. As illustrated in Figure 4.7, the maximum reconstruction size is defined as $S_{Rec} = S_H + 2\tan(\theta_{max})D_R$, where S_H is the SLM size in this case. (Note that, higher diffraction orders are eliminated by windowing at the reconstruction plane and size of the reconstructions can be increased until the higher

diffraction orders overlap. See Section 4.1.2.) In order to reconstruct larger size images, the same Gerchberg-Saxton algorithm is used. Now we take a larger window size to propagate back and forth. At the hologram plane, the amplitude should be replaced by zeros except within the SLM window. The amplitude at the SLM window is replaced by the magnitude of the illuminating wave. Figure 5.7 shows the optical reconstruction of a $16mm \times 16mm$ size object from a $16mm \times 8mm$ size phase-only hologram. The hologram is computed by 200 iterations. The size of the hologram, i.e. SLM, is visible in the figure due to the diffraction from edges of the SLM and can be used as a size reference.

Up until here in this chapter, we dealt with 2D single plane holographic reconstructions. However, to understand the potentials of phase holograms in future 3D holographic display systems, we also performed 3D display experiments using a single phase-only SLM. We generated phase holograms of three planar objects ("3DTV", "BILKENT" and "BIAS" words) at different depths. First, three separate phase-only holograms are generated by using the Gerchberg-Saxton algorithm for each object. Then all three complex fields at the hologram plane are superposed as:

$$\exp(j\psi_{3DTV}(x,y))+\exp(j\psi_{Bilkent}(x,y))+\exp(j\psi_{Bias}(x,y)) = A(x,y)\exp(j\psi_{Final}(x,y)) \quad . \tag{5.1}$$

The resultant phase, $\psi_{Final}(x,y)$ is written onto the SLM and the same setup is used for the optical reconstructions. Figure 5.8 shows the optical reconstruction of three objects that are captured at $450mm$, $500mm$ and $550mm$. Note that there is no occlusions or overlaps since the objects are separate enough. Therefore the effect of mutual interactions of the objects to the hologram is negligible.

Several holographic display experiments for a single phase-only spatial light modulators are conducted. We saw that even for a low number of iterations, satisfactory holographic reconstructions are possible. Although the iterative algorithms are slow due to demanding computational complexity, results indicate that phase-only holograms are strong candidates for future 3DTV applications. This concludes our discussion on single SLM holographic reconstructions and phase holograms and leads us to multiple SLM holographic display systems.

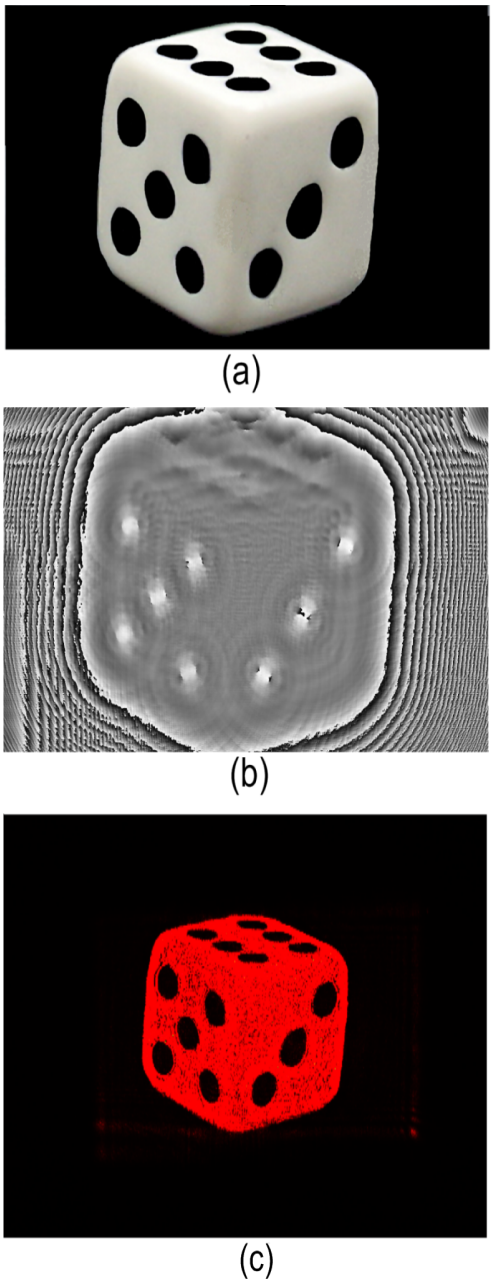

Figure 5.5: (a) 2D picture of a die, (b) phase hologram, computed in 10 iterations, (c) optical reconstruction from the phase hologram ("Holographic reconstructions using phase-only spatial light modulators," F. Yaraş, M. Kovachev, R. Ilieva, M. Agour and L. Onural, in 3DTV Conference: The True Vision - Capture, Transmission and Display of 3D Video, IEEE, 2008. ©2008 IEEE. Reprinted with permission.)

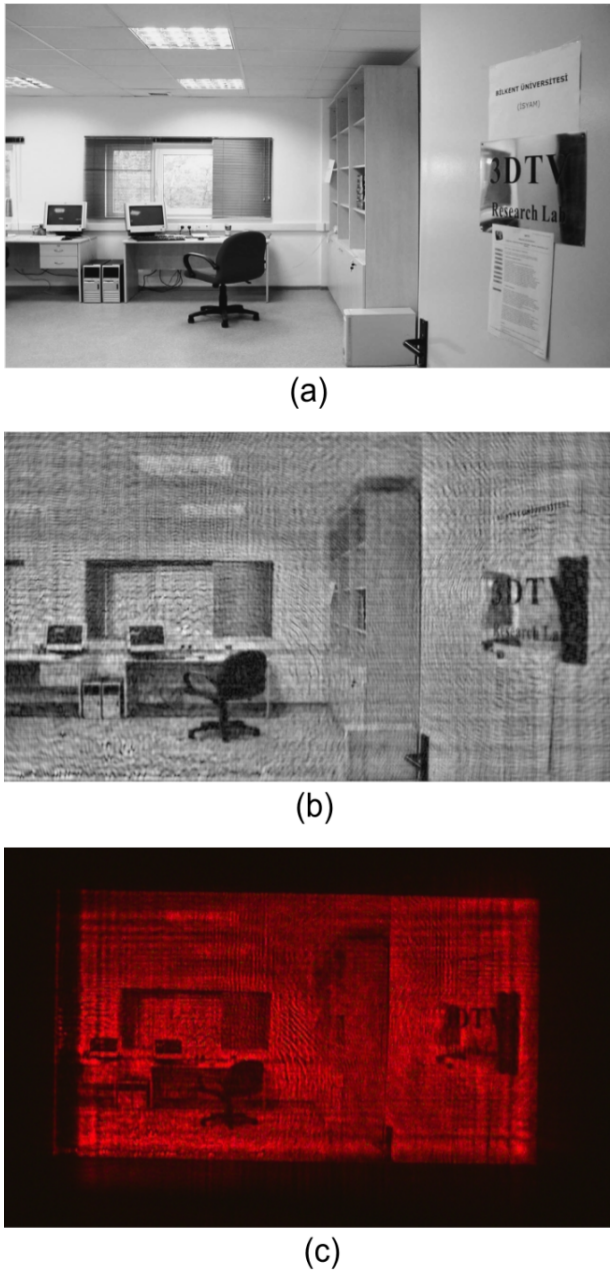

Figure 5.6: (a) 3DTV Lab photograph as a 2D grayscale object, (b) numerical and (c) optical reconstructions from the phase hologram computed in 20 iterations ("Holographic reconstructions using phase-only spatial light modulators," F. Yaraş, M. Kovachev, R. Ilieva, M. Agour and L. Onural, in 3DTV Conference: The True Vision - Capture, Transmission and Display of 3D Video, IEEE, 2008. ©2008 IEEE. Reprinted with permission.)

Figure 5.7: Optical reconstruction of the 1920×2160 size object from a 1920x1080 phase-only hologram computed in 200 iterations. The SLM size is visible due to diffraction from its edges ("Holographic reconstructions using phase-only spatial light modulators," F. Yaraş, M. Kovachev, R. Ilieva, M. Agour and L. Onural, in 3DTV Conference: The True Vision - Capture, Transmission and Display of 3D Video, IEEE, 2008. ©2008 IEEE. Reprinted with permission.)

Figure 5.8: Optical reconstruction of the three objects at different depths (450mm, 500mm and 500mm from the SLM) ("Holographic reconstructions using phase-only spatial light modulators," F. Yaraş, M. Kovachev, R. Ilieva, M. Agour and L. Onural, in 3DTV Conference: The True Vision - Capture, Transmission and Display of 3D Video, IEEE, 2008. ©2008 IEEE. Reprinted with permission.)

Chapter 6

Experimental Setup And Results For The Holographic Displays Using Multiple Phase-only SLMs

In this chapter, we present the experimental setups and results for the multiple SLM holographic display systems. All those experiments and designs serve for the sake of designing the satisfactory quality holographic display system. For this purpose, we present several multi-SLM configurations including color holographic display, real-time holographic display, planar and circularly configured holographic displays. This chapter is mainly based on our publications [55, 56, 58, 59, 115, 137, 138].

6.1 Color holographic reconstruction using multiple SLMs and LED illumination

As discussed in Chapter 5, phase-only holograms have advantageous properties for holographic display systems. High diffraction efficiency, low-power higher diffraction orders and low-power undiffracted-beam are some of these advantageous properties [139]. Here in this section, experimental color holographic reconstruction results using multiple SLMs and LED illumination are reported. In the experiments in this section, phase holograms

were calculated by using the Gerchberg-Saxton algorithm. The iterative algorithm is described in Section 5.1. In addition, LED illumination is used instead of laser illumination. For the laboratory prototype, we used three monochromatic phase-only spatial light modulators and three color LEDs (red, green and blue). Those separate phase-only SLMs are synchronized by the SLM driver module and also each SLM is connected to a color channel (red, green and blue) in the driver module. The driver module is connected to the graphics card of a computer by a digital visual interface (DVI) cable. For example, if a signal of a RGB color image is sent to the SLM driver module by the computer graphics card, the driver module first separates the red, green and blue components of the RGB image and sends each color component to the corresponding color channel and, then to the associated SLM.

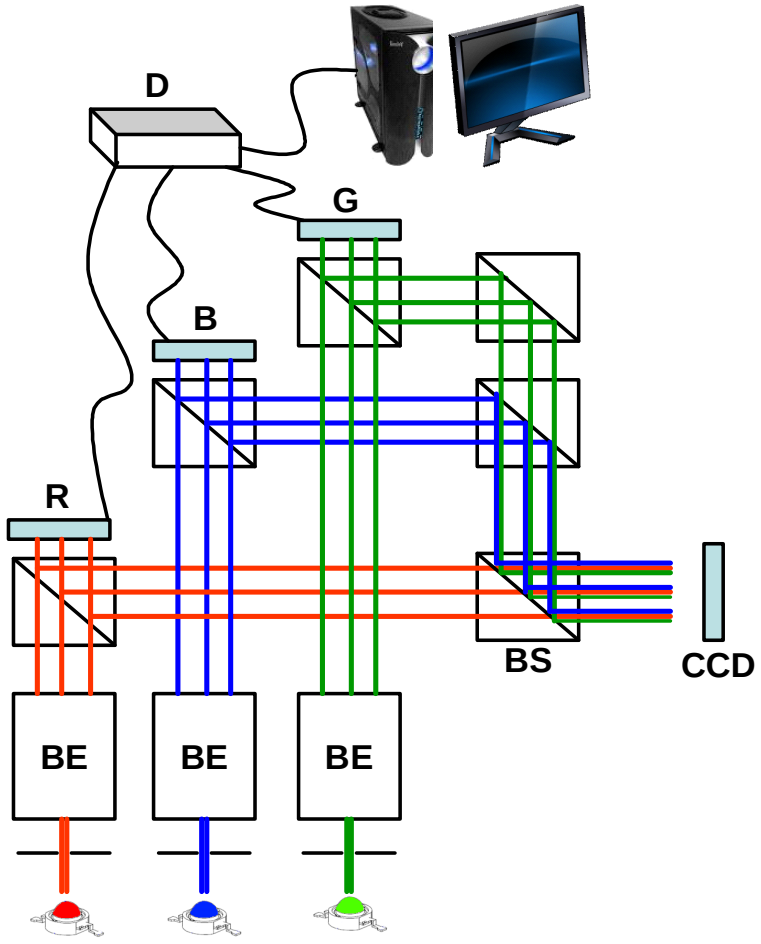

Figure 6.1: Optical setup. (BE: Beam Expander, BS: Beam Splitter, D: Driver Module.)

For the color holographic reconstruction experiment, we first calculate the phase hologram of a color 2D object. For this purpose, we first separate the color components of the color image. For each color, a phase hologram is separately calculated by using the Gerchberg-Saxton algorithm. Reconstruction distances are chosen equal for all color components. Note that, wavelength of each color is different. After calculating all three phase holograms, they are then saved in a RGB image to obtain a color hologram. The resultant color phase hologram is then sent to the SLM driver module by the computer graphics card. As described above, the color components of the color phase hologram is separated by the SLM diver module and sent to the associated SLM. Then those SLMs are illuminated by a plane wave generated by LED illumination setup. Optical reconstructions from each phase hologram is aligned to obtain the final optical color holographic reconstruction.

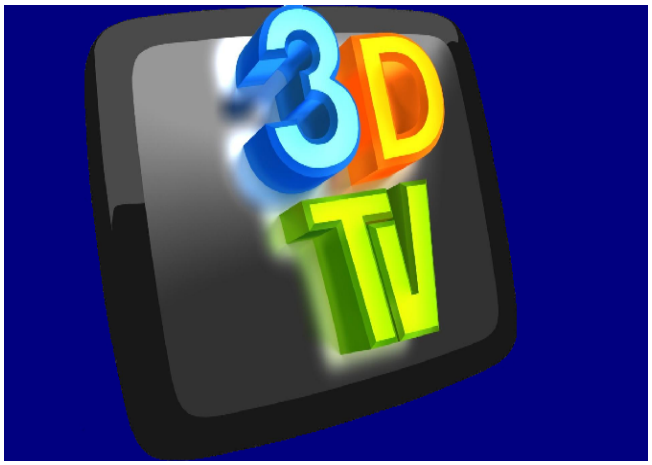

Figure 6.2: 2D picture of 3DTV logo (courtesy of www.3dtv-research.org).

The diagram of the optical setup is shown in Fig. 6.1. The wavelengths of the LEDs are around $625nm$, $520nm$ and $460nm$ for red, green and blue, respectively. The emitted light from the LED first passes through a spatial filter to increase the spatial coherence by cleaning up the beam. Beam expenders (BEs) that are used to obtain the plane wave and the optical reconstructions for each color are combined with the help of beam splitters (BS). The original 2D color object and the resultant color phase hologram are shown in Figs. 6.2 and 6.3, respectively. We used a lensless CCD array to capture the optical

reconstructions. The reconstructed image size is about $16mm \times 10mm$ and the reconstruction distance is $60cm$. 250 iterations are performed to obtain the phase holograms. The digital (computer based) and the optical color holographic reconstructions are shown in Figs. 6.4 and 6.5, respectively.

The results show that the color holographic reconstructions are possible by using multiple SLMs. However, the reconstruction sizes and the angle of view are quite small. Therefore, observers can not see the reconstructions with both eyes. In addition, since the iterative algorithms are rather slow due to demanding computational complexity, such a procedure may not be suitable for future 3DTV applications. We present a real-time multiple SLM holographic display system, which solves this problem, in the next section.

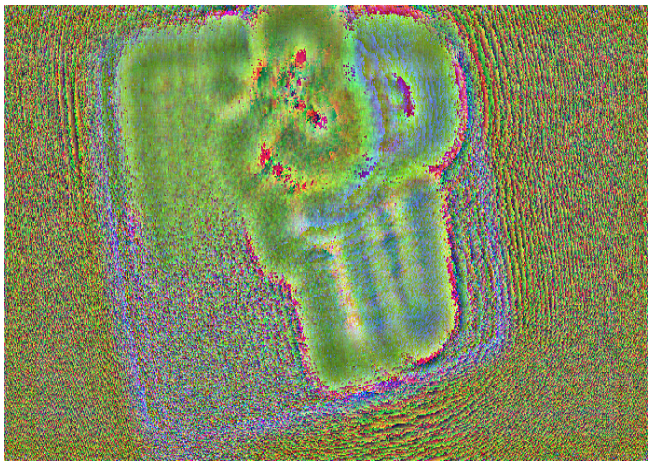

Figure 6.3: Color phase hologram ("Color holographic reconstruction using multiple SLMs and LED illumination," F. Yaraş and L. Onural, Proc. SPIE 7237, 72370O, (2009). ©2009 SPIE. Reprinted with permission.)

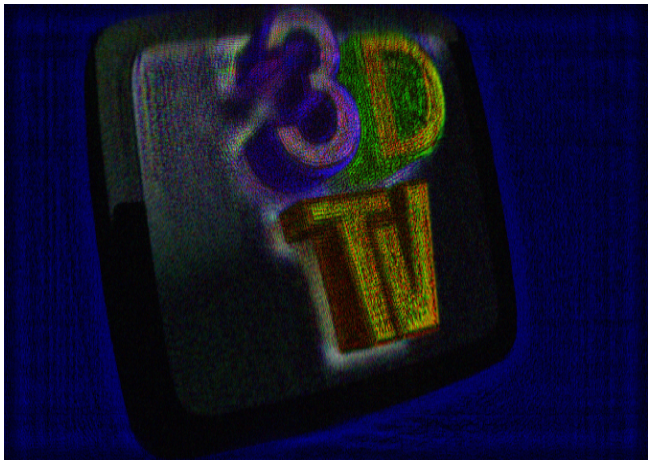

Figure 6.4: Computer reconstruction from color phase hologram ("Color holographic reconstruction using multiple SLMs and LED illumination," F. Yaraş and L. Onural, Proc. SPIE 7237, 72370O, (2009). ©2009 SPIE. Reprinted with permission.)

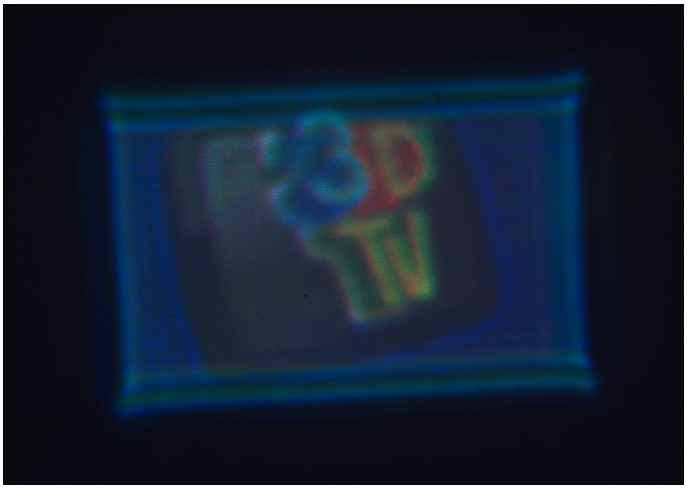

Figure 6.5: Optical reconstruction from color phase hologram ("Color holographic reconstruction using multiple SLMs and LED illumination," F. Yaraş and L. Onural, Proc. SPIE 7237, 72370O, (2009). ©2009 SPIE. Reprinted with permission.)

6.2 Real-time multiple SLM color holographic display using multiple GPU acceleration and LED illumination

Real-time holographic display systems are being investigating for future 3DTV applications. Real-time holographic fringe pattern generation is an important issue for 3D display technologies and will have a significant impact. However there are some severe problems in fast calculation of the computer generated holograms. There are several methods for fast computation of holograms [140–142]. Some prototypes of the real-time holographic display systems are already demonstrated. SeeReal, QinetiQ and MIT's Holo-video are some of the examples of real-time holographic display systems [64, 79, 87, 88] (See Chapter 3). Some parts of this section is based on our publications [56] and [58].

In our real-time holographic video display system we used Accurate Compensated Phase-Added Stereogram (ACPAS) [110]. This algorithm is proposed by Kang in his thesis and can be used as a real-time color holographic fringe generation method. ACPAS is an improved version of Compensated Phase-Added Stereogram (CPAS) [106]. ACPAS is a slightly slower algorithm than CPAS algorithm but resultant holograms from the ACPAS algorithm produce better reconstructions which are similar to that of Fresnel holograms. Here we again used phase-only spatial light modulators (SLMs) to display holograms and we benefited from the desirable properties of phase holograms. These properties are listed in previous sections. We used light emitting diodes (LEDs) to illuminate those SLMs. By the help of LED illumination, unwanted properties of laser illumination, such as speckle noise and eye hazard, is eliminated. As mentioned in the previous sections, LEDs are somewhat coherent. They have some degree of both time and space coherence. However, since they are not fully coherent, the reconstructions might be somewhat blurred.

We used multiple graphics processing units (GPUs) to increase the hologram generation speed and to achieve real-time hologram generation. GPUs are commonly used as

parallel processing devices [143–145] and they are quite powerful. ACPAS algorithm is suitable for parallel processing and when multiple GPUs are used the overall performance of the hologram generation increased significantly. The designed system has three major parts. These are the client, server and the optics. The client stores a video of a rigid 3D object. The object consists of a point cloud. Each point in the point cloud has 3D coordinate and color information. Coordinate and the color information of all points in the 3D scene are sent to the server by the TCP/IP protocol in real-time. Upon receiving the data, server calculates three holograms associated with red, green and blue components of the 3D scene by using a multi-GPU architecture. Resultant holograms are merged into a single RGB image and sent to the driver module of the phase-only spatial light modulators. As mentioned in the previous section, the driver module splits and directs the red, green and the blue channel holograms to associated SLMs. After the holograms are loaded to the SLMs, they are illuminated by plane waves obtained from red, green and blue LEDs (See Fig. 6.6). The propagated light that hits on the surface of the SLMs is modulated and reflects back. Holographic reconstructions from each SLM are overlapped by the help of beam splitters and micro-stages. The resultant reconstructions are captured by a lensless CCD array.

6.2.1 The Algorithm

For a real-time holographic display system, we need a fast algorithm to generate the holograms. The so called, coherent stereogram generation method (CS) is one of the fast algorithms [106]. An improved version of the coherent stereogram algorithm which is called "accurate compensated phase-added stereogram (ACPAS)" method, is proposed by Kang [56–58,110,112,113]. The reconstruction from the holograms that are calculated by ACPAS algorithm closely resembles the reconstructions from the Fresnel hologram. The computation time for ACPAS is much faster than that of the Fresnel hologram. As a result, the ACPAS algorithm is suitable for real-time hologram generation.

Fig. 6.7 shows the geometry of coherent stereogram calculation. The ACPAS algorithm first takes a blank 2D plane and partitions it into suitable square size segments.

Contribution of each point in the point cloud is approximated as a weighted single complex sinusoid within a segment. The weights are calculated by $(a_i/r_i)\exp(jkr_i)\exp(j\phi_c)$. For a single segment in (ξ, η) plane, the holographic fringe pattern of a point cloud in (x, y, z) volume is found as [110],

$$\mathbf{I}_{ACPAS}(\xi,\eta) = \sum_{i=1}^{N} \frac{a_i}{r_i} \exp\{j2\pi[(\xi-\xi_c)f_{i\xi\text{cint}} + (\eta-\eta_c)f_{i\eta\text{cint}}] + jkr_i + j\phi_c\}, \tag{6.1}$$

where a_i is the intensity of an object point, N is the number of object points, k is the wave number and defined as $2\pi/\lambda$, where λ is the wavelength of the coherent light. The distance r_i between the *i-th* object point and the point on the hologram (ξ_c, η_c) is $[(\xi_c - x_i)^2 + (\eta_c - y_i)^2 + z_i^2]^{1/2}$, where (ξ_c, η_c) is the center of each segment on the hologram plane. The spatial phase error compensation ϕ_c is then expressed as [110]:

$$\phi_c = 2\pi\{(f_{i\xi c} - f_{i\xi\text{cint}})(\xi_c - x_i) + (f_{i\eta c} - f_{i\eta\text{cint}})(\eta_c - y_i)\}, \tag{6.2}$$

where $f_{i\xi\text{cint}}$ and $f_{i\eta\text{cint}}$ are discrete spatial frequencies and $f_{i\xi c}$ and $f_{i\eta c}$ are the continuous spatial frequencies in cycles per unit length on ξ and η axes, respectively. We can simplify Eq. 6.1 for a given segment as:

$$\mathbf{I}_{ACPAS}(\xi,\eta) = \sum_{i=1}^{N} A_i(\xi,\eta)\exp(j2\pi\Phi_i(\xi,\eta)), \tag{6.3}$$

where,

$$A_i(\xi,\eta) = \frac{a_i}{r_i}\exp(jkr_i)\exp(j\phi_c), \tag{6.4}$$

and,

$$\Phi_i(\xi,\eta) = (\xi-\xi_c)f_{i\xi\text{cint}} + (\eta-\eta_c)f_{i\eta\text{cint}}. \tag{6.5}$$

After this simplification, we observe that Eqn. 6.3 is an N-point inverse discrete Fourier transform (IDFT). For the computation part we use inverse fast Fourier transform (IFFT). There are some computer program libraries that calculate FFT, such as "fftw". FFTW is a free subroutine library for C. Each segment is processed independently and after that they are combined to have the resultant fringe pattern. Since the calculation of each segment is independent of others, they can be handled in parallel. Therefore the algorithm is suitable for parallel processing. The hologram computation algorithm is shown

in Figs. 6.7 and 6.8. The resultant fringe pattern is a 2D complex field. Since we use phase-only spatial light modulators, we extract the phase and discard the amplitude.

6.2.2 The Client

The client computer stores a movie of the 3D model (see Fig. 6.6). The rigid model consists of a point cloud (discrete points floating in space). In the movie, our model moves and rotates within a volume. Its track and rotation direction is random and determined at real-time. To display the model in the client computer we use OpenGL. The coordinates of the points in the point cloud is being updated at real-time while the object moves and/or rotates. Then the updated information (3D coordinates and color information associated with each point) is sent to the server through the internet. There is not any computational processes running on the client, therefore an average PC is adequate for this stage.

6.2.3 The Server

The server computer calculates the computer generated holograms (CGHs) in real-time (see Fig. 6.6). Server receives the 3D coordinate and the color information that is sent by the client. After the data is received, the holographic fringe pattern for each segment is calculated as described in Section 6.2.1. GPU architecture is used to take the Inverse Fast Fourier Transform for each segment in parallel. By this method the calculation time decreases significantly. In addition, we use multiple GPUs to increase the overall frame rate of the system. A pipelined real-time computation is achieved by using three GPU boards. Fig. 6.9 shows the pipelined computation using three GPU boards. As a consequence of this scheme, while the first GPU calculates the n^{th} frame of the scene, $(n+1)^{st}$ and $(n+2)^{nd}$ frames are calculated by the second and third GPUs, respectively. As a result, the frame rate is tripled. The entire hologram generation process is the same for each color. Holograms for red, green and blue components of the 3D model is calculated separately and then the phase holograms are extracted from the resultant

complex fringe patterns. Then for each frame, three phase holograms (red, green and blue) are merged into a single RGB bitmap image at real-time and the phase values (0 to 2π radians) are mapped to grayscale (0 to 255). Then the resultant RGB image is sent to the driver module of the SLMs. The overall system specifications are shown in Table 6.1.

Table 6.1: **Overall System Specifications ("Real-time phase-only color holographic video display system using LED illumination," F. Yaraş, H. Kang and L. Onural, Appl. Opt. 48, H48-H53 (2009). ©2009 OSA. Reprinted with permission.)**

Computing system	CPU	Two Intel(R) Xeon(R) CPU 2GHz
	Main memory	8 GByte
	GPU	Three NVIDIA GeForce GTX 280
Programming environment	Operating system	Linux 64 bit (Ubuntu 8.10)
	Programming language	Standard C and CUDA
	Libraries	CUFFTW

6.2.4 Optics

Optics and the setup is the last major part of the system (see Fig. 6.10). In this part there are phase-only SLMs, driver module of the SLMs, a CCD array, beam splitters (half mirrors), beam expanders, LEDs and spatial filters. The light emerging from the LED first passes through a spatial filter. Spatial filter contains an objective lens and a pinhole. The objective lens has $40\times$ magnification factor and the diameter of the pinhole is $200\mu m$. Incoming light is first focused by the objective lens. Pinhole is then placed at the focal point of the objective. With the help of this spatial filter high frequency components including noise is eliminated significantly. In addition, this method increases the spatial coherence of the illuminating light. The experimental results show that, using a pinhole with a diameter between 50 and $500\mu m$ gives satisfactory results. After passing through an objective lens and a pinhole, the light becomes divergent. To collect the light and to have a somewhat uniform plane wave we use beam expanders. Beam expanders can either expand or shrink the beam by adjusting distance between lenses inside of the expander. This setup is the same for all color LEDs (red, green and blue) and the resultant plane

waves illuminate the phase-only SLMs. The light is modulated and reflected back. At the reconstruction distance, holographic reconstructions from all three SLMs are overlapped. Alignments are done by using micro-stages. For this system we again used Holoeye's HEO1080P phase-only spatial light modulators [71]. To record the color holographic reconstruction of the 3D object we used a CCD array. Characteristics of LEDs are shown in Table 6.2.

Table 6.2: **Characteristics of LEDs**

Part Number	Color	Emission Angle*	Wavelength
EDER-1LA3	Red	120°	620 - 630 nm.
EDET-1LA2	Green	150°	515 - 535 nm.
EDEB-1LA5	Blue	150°	455 - 475 nm.

*Emission Angle is the full angle where the intensity of light falls to the half of the on-axis intensity. (©2009 Edison Opto Corporation. Reprinted with permission)

6.2.5 Results

Table 6.3 shows the performance analysis of the system for a size of two-megapixel holographic fringe patterns. Results show that when three GPU boards are used in the system, 3D objects that contain 10000 object points can be displayed in real-time. In addition, as the number of GPUs increases, the frame rate also increases proportionally. Therefore, if we add more GPUs we can increase the frame rate accordingly. Figs. 6.11 and 6.12 show a 3D model and the computer reconstruction from the hologram computed using ACPAS, respectively. We used Rayleigh-Sommerfeld wave propagation algorithm to obtain the numerical reconstructions from the computer generated holograms. Moreover, we compared the optical reconstructions for laser and LED illumination. Fig. 6.13 shows the results for monochromatic reconstructions (green light). For the laser illumination case, high speckle noise is observed in the optical reconstruction (see Fig. 6.13(a)). Reconstruction seems sharper even though the speckle noise degrades the quality. For the LED illumination case, there is no observable speckle noise in the reconstruction. Although optical reconstructions are slightly blurred, there is no speckle and the quality of

the reconstructions is satisfactory (see Fig. 6.13(b)). In our experiments we used Edixeon 1 Watt point type LEDs by Edison Opto Corporation. Fig. 6.14 shows a 2D photograph of the optical reconstruction taken by a CCD array.

Table 6.3: **Performance analysis of the system for two Megapixel hologram output ("Real-time color holographic video display system," F. Yaraş, H. Kang and L. Onural, in 3DTV Conference: The True Vision - Capture, Transmission and Display of 3D Video, IEEE, 2009. ©2009 IEEE. Reprinted with permission.)**

No of Obj. Points	One GPU	Two GPUs	Three GPUs
1	15.8 fps	31.6 fps	47.5 fps
10	15.7 fps	31.4 fps	47.2 fps
100	15.3 fps	30.7 fps	46.1 fps
1000	13.5 fps	27.0 fps	40.5 fps
10000	6.8 fps	13.6 fps	20.5 fps

In this section, we presented a real-time multiple SLM color holographic display system. It is a promising step for future 3DTV applications. However, we still need to increase the hologram size to have a more comfortable 3D observation experience. For this purpose we present a wide viewing angle multiple SLM holographic display systems in Sec. 6.3 and Sec. 6.4.

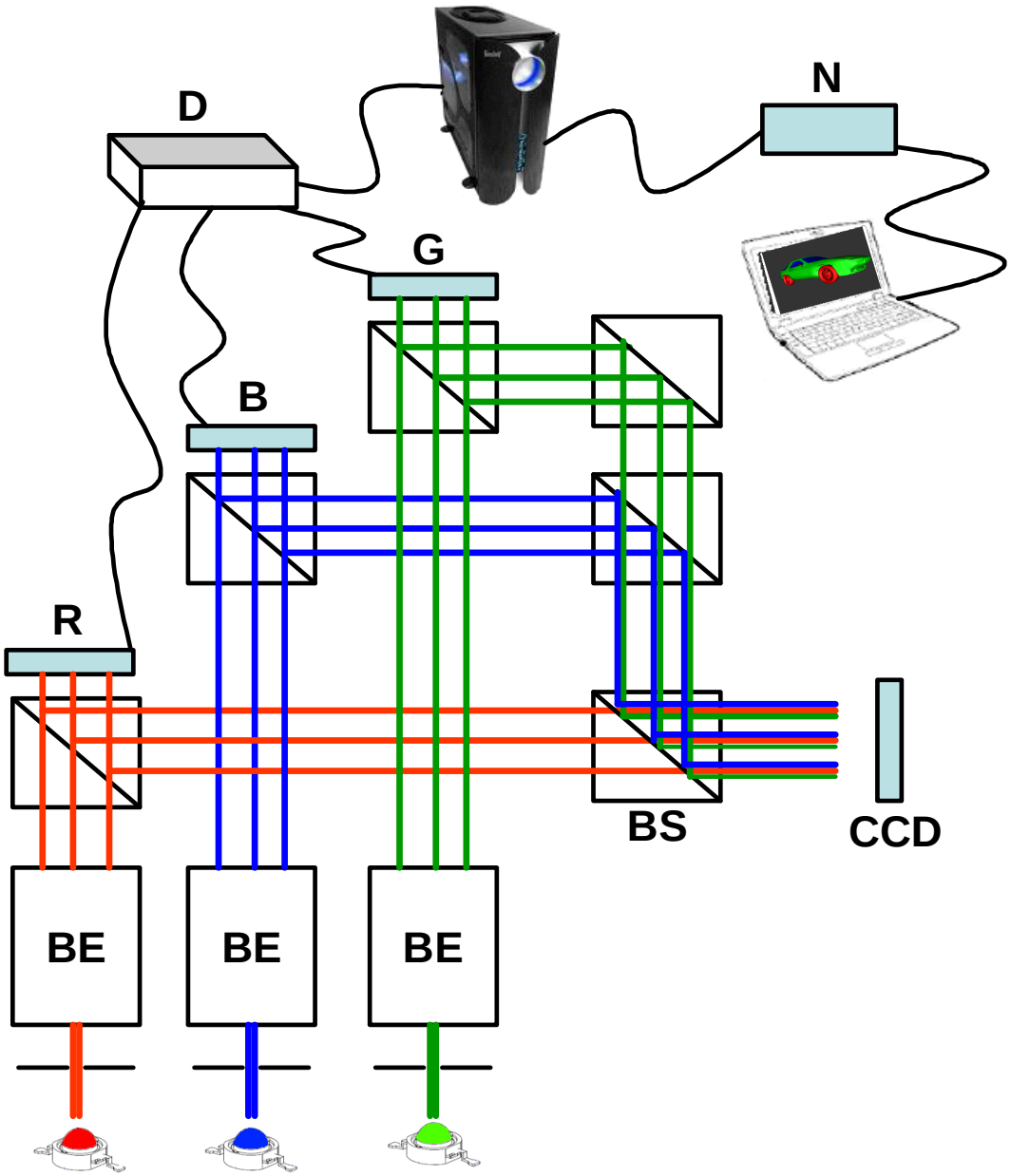

Figure 6.6: Overall setup (BE: Beam expander, R: Red SLM, B: Blue SLM, G: Green SLM, D: Driver unit of SLMs, N: Network, BS: Non-polarized beam splitter.) ("Real-time phase-only color holographic video display system using LED illumination," F. Yaraş, H. Kang and L. Onural, Appl. Opt. 48, H48-H53 (2009). ©2009 OSA. Reprinted with permission.)

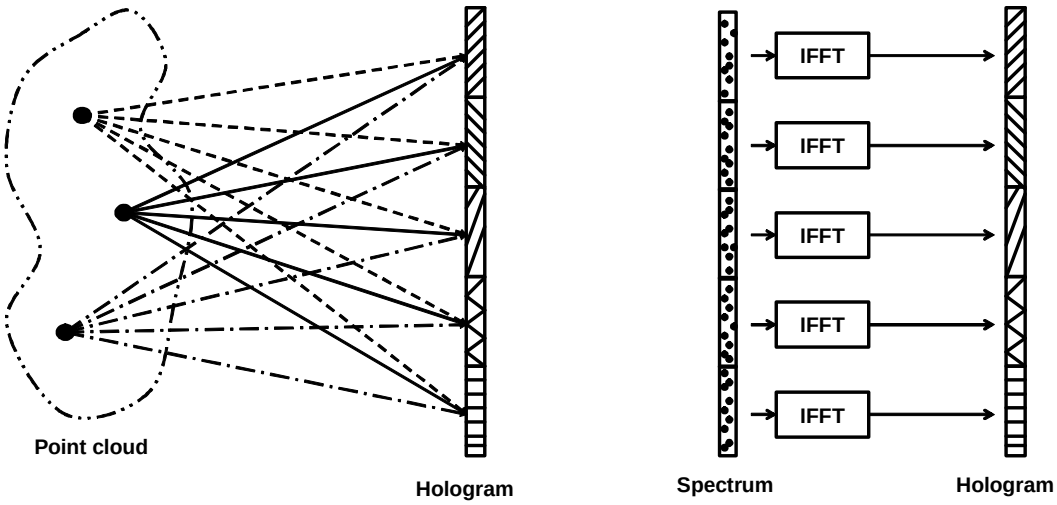

Figure 6.7: Hologram calculation algorithm. ("Real-time phase-only color holographic video display system using LED illumination," F. Yaraş, H. Kang and L. Onural, Appl. Opt. 48, H48-H53 (2009). ©2009 OSA. Reprinted with permission.)

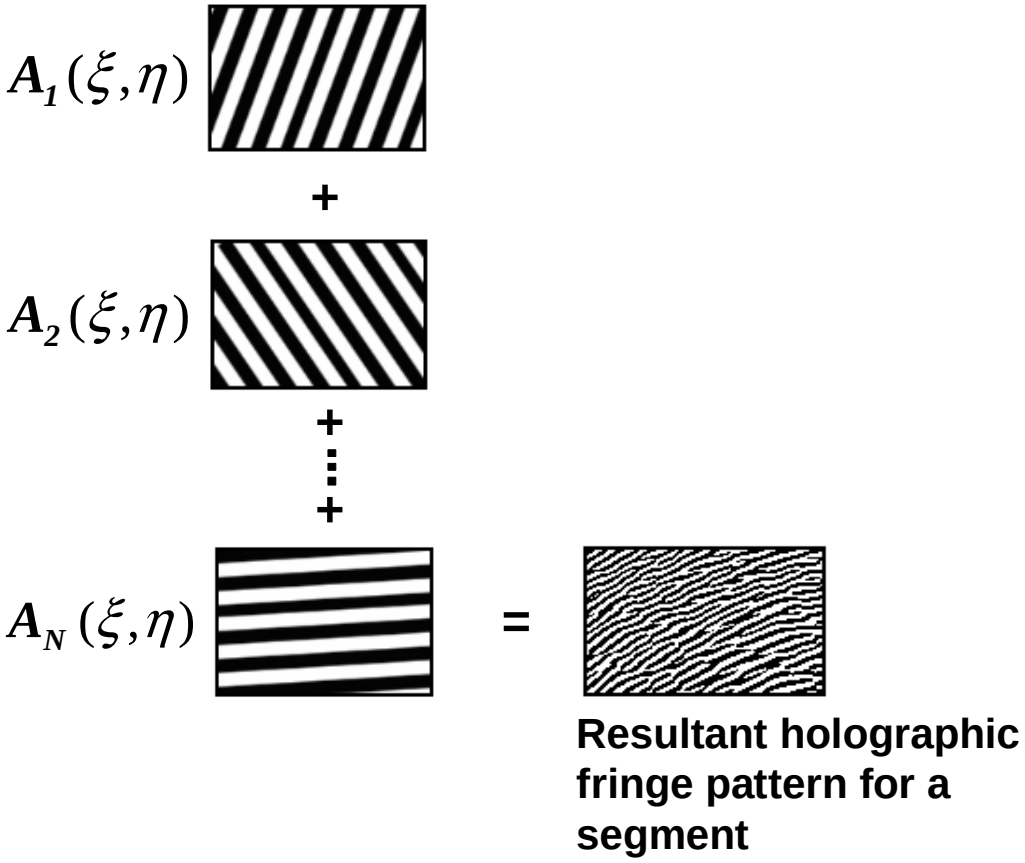

Figure 6.8: Illustration of N-point DFT as a weighted sum of complex sinusoids. ("Real-time phase-only color holographic video display system using LED illumination," F. Yaraş, H. Kang and L. Onural, Appl. Opt. 48, H48-H53 (2009). ©2009 OSA. Reprinted with permission.)

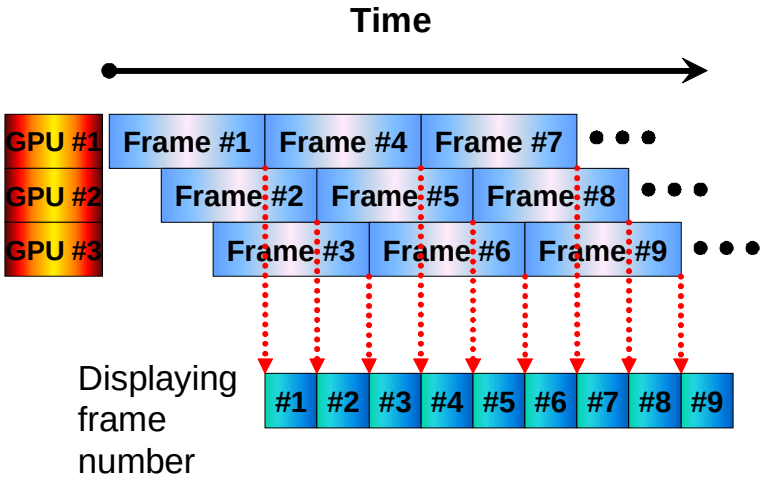

Figure 6.9: Pipelined computation using GPUs ("Real-time color holographic video display system," F. Yaraş, H. Kang and L. Onural, in 3DTV Conference: The True Vision - Capture, Transmission and Display of 3D Video, IEEE, 2009. ©2009 IEEE. Reprinted with permission.)

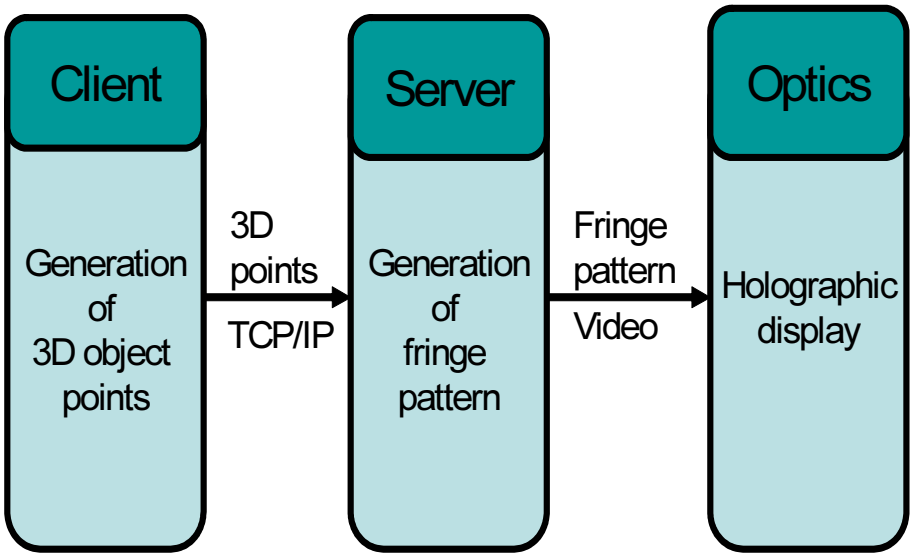

Figure 6.10: The end-to-end system ("Real-time color holographic video display system," F. Yaraş, H. Kang and L. Onural, in 3DTV Conference: The True Vision - Capture, Transmission and Display of 3D Video, IEEE, 2009. ©2009 IEEE. Reprinted with permission.)

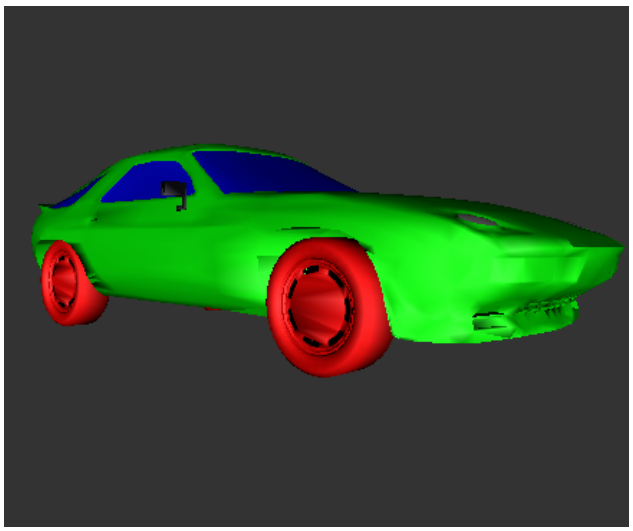

Figure 6.11: A rigid color 3D object ("Real-time phase-only color holographic video display system using LED illumination," F. Yaraş, H. Kang and L. Onural, Appl. Opt. 48, H48-H53 (2009). ©2009 OSA. Reprinted with permission.)

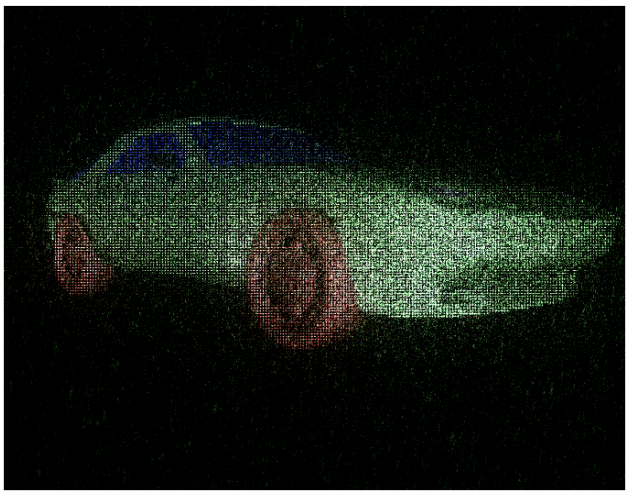

Figure 6.12: Computer reconstruction using the ACPAS algorithm ("Real-time phase-only color holographic video display system using LED illumination," F. Yaraş, H. Kang and L. Onural, Appl. Opt. 48, H48-H53 (2009). ©2009 OSA. Reprinted with permission.)

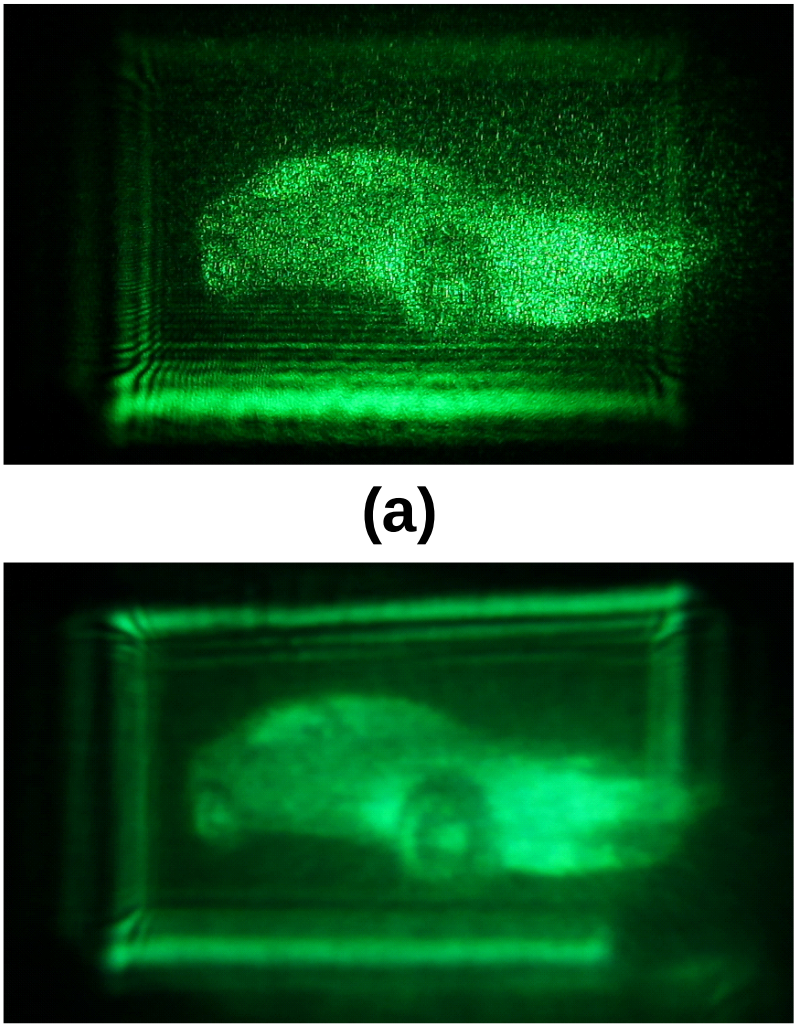

Figure 6.13: Single color reconstruction (a) by green laser (b) by green LED ("Real-time phase-only color holographic video display system using LED illumination," F. Yaraş, H. Kang and L. Onural, Appl. Opt. 48, H48-H53 (2009). ©2009 OSA. Reprinted with permission.)

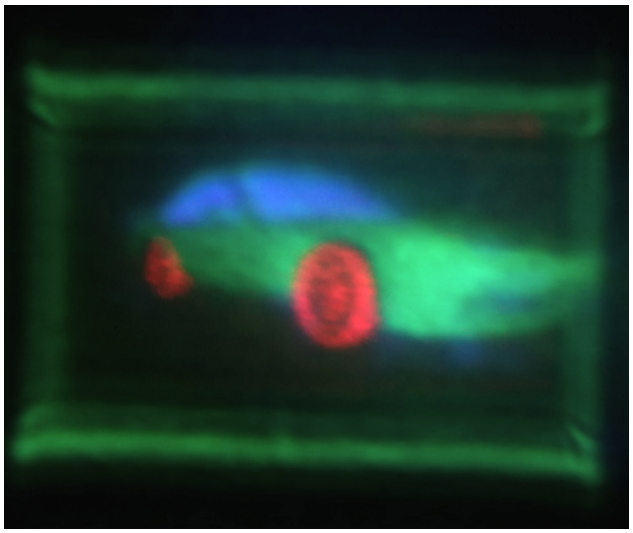

Figure 6.14: Optical reconstruction of a single frame of the 3D object ("Real-time phase-only color holographic video display system using LED illumination," F. Yaraş, H. Kang and L. Onural, Appl. Opt. 48, H48-H53 (2009). ©2009 OSA. Reprinted with permission.)

6.3 Multi-SLM holographic display system with a planar configuration

As mentioned in Chapter 4, if the hologram size is increased, the 3D viewing comfort will also be enhanced. In order to increase the hologram size, we need larger size spatial light modulators. However, commercially available spatial light modulators have limited size due to various physical restrictions. Therefore, we propose a multi-SLM holographic display system. A laboratory prototype is implemented. In this prototype, we used six phase-only SLMs, each having 1920×1080 pixels with a pixel period of $8\mu m$. Those six SLMs are tiled in a three by two setup. With the help this scheme, we can display larger size holograms. All SLMs are aligned by using some optical elements and micro-stages. After the alignment we calculate the computer generated holograms for the larger display. The calculated large hologram is then partitioned into six sub-holograms in order to match with the tiled SLMs. As discussed in the previous sections, driver module of the SLMs directs the sub-holograms to the associated SLMs. SLMs are illuminated by plane waves obtained from LEDs. Therefore, reconstructions can be observed by the naked eye. Since we have a larger hologram size, the field of view is also increased. Thus, the observer can see the optical reconstructions binocularly. Reconstructions are ghost-like 3D images floating in the space.

6.3.1 Advantages of using multiple SLMs

The spatial frequency that can be supported by the spatial light modulators is limited because of their pixelated structures. If we denote the maximum spatial frequency of the hologram as f_{max}, the local maximum diffraction angle for Shannon type recovery (low-pass filtering) can be calculated as:

$$\theta_{max} = \sin^{-1}(\lambda f_{max}), \tag{6.6}$$

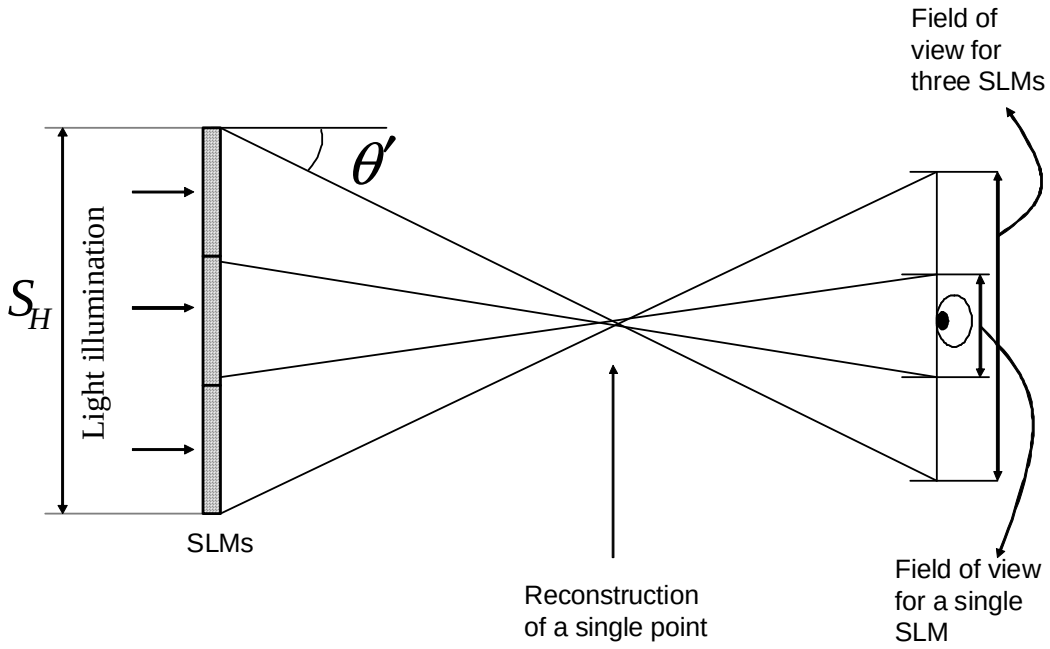

Figure 6.15: Increase in the field of view when multiple SLMs are used ("Multi-SLM holographic display system with planar configuration," F. Yaraş, H. Kang and L. Onural, in 3DTV Conference: The True Vision - Capture, Transmission and Display of 3D Video, IEEE, 2010. ©2010 IEEE. Reprinted with permission.)

where;

$$f_{max} = \frac{1}{2\Delta_p}. \tag{6.7}$$

Here Δ_p denotes the pixel period of the SLM. The reconstruction of a single point in the reconstruction plane is shown in Fig. 6.15. Here in the figure, the field of view denotes an area on the observation plane. Therefore, within the field of view the entire object can be seen while the full bandwidth of the SLM is utilized. As we move outside of the field of view, either some parts of the reconstruction will not be visible or the bandwidth used for reconstruction decreases. Reduction in bandwidth affects the quality and sharpness of the reconstruction. As the figure depicts, field of view increases when multiple spatial light modulators are used in planar configuration. Please note that the full bandwidth of some of the SLMs are not utilized in this configuration (i.e. $\theta' < \theta_{max}$ for centered SLMs). As mentioned in Chapter 4, we need larger hologram sizes to support higher diffraction angles for moving observers. For small size holograms, binocular vision may not be possible and this leads to an insufficient parallax for the holographic reconstructions. Such small size

holograms are inevitable if we use a single spatial light modulator. However if we use multiple SLMs, we can increase the holograms size; thus, the field of view. In addition, since hologram size is increased, we can reconstruct larger size objects compared to the single SLM case (see Fig. 6.16). If we use N spatial light modulators side by side, the space for the holographic reconstruction can be calculated as:

$$S_R = N \times S_{SLM} + 2D_R \tan(\theta_{max}), \tag{6.8}$$

where D_R is the distance between the SLMs and the reconstruction, and S_{SLM} is the size of a single SLM. It is shown that each addition SLM increases the available space for the reconstruction.

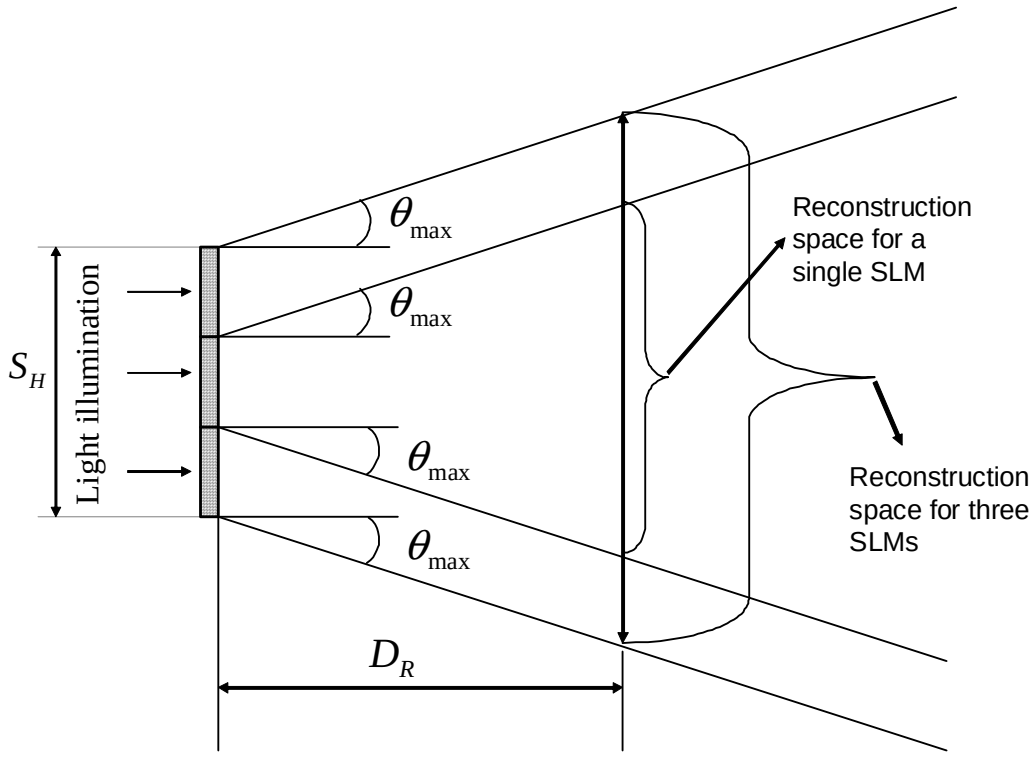

Figure 6.16: Increase in the reconstruction space when multiple SLMs are used ("Multi-SLM holographic display system with planar configuration," F. Yaraş, H. Kang and L. Onural, in 3DTV Conference: The True Vision - Capture, Transmission and Display of 3D Video, IEEE, 2010. ©2010 IEEE. Reprinted with permission.)

Another advantage of multiple SLM configurations is related to the quality of the reconstructions. When multiple SLMs are used, quality of the reconstructions significantly increases. Fig. 6.17 illustrates the effect of using multiple SLMs on the quality of the

reconstruction. The number of pixels that contributes to the reconstruction of a single point in Fig. 6.17b is significantly larger than that of the one in Fig. 6.17a. In the figures, the zone whose corners are the point P and the two ends of the display denotes the field where all the pixels can contribute to the reconstruction. We use the point P as a reference point for the size of the reconstructions. Since both objects in Fig. 6.17 (a) and (b) are equally distant from the point P and the apical angles at the point P are the same, we assure that the reconstruction size of both objects are the same. Although the size of the reconstructed objects are the same, the number of pixels contributed to the reconstruction is different. As in Chapter 4, we can also discuss the reconstruction quality in terms of *space-bandwidth product (SBP)*. Here the bandwidth is limited by the maximum band supported by the SLM. In other words full band is used for the reconstructions. Therefore, the limiting factor of the quality of the reconstruction is the number of pixels that are used for the reconstructions. Therefore, if we use more SLMs, we can obtain higher quality holographic reconstructions. There is also a trade off between the number of pixels used for reconstruction and the field of view. If we sacrifice from the quality a little, we can increase the field of view (see Fig. 6.22).

Yet another advantage of multiple SLM configurations is ability to reconstruct 3D objects larger than the SLM size [54]. Such methods are discussed in Section 5. Those reconstructions can be totally visible if we use a diffuser or a screen at the reconstruction plane. However, if we try to look at the reconstructions directly by the naked eye, we can only see a part of it (see Fig. 6.18). The reconstructions can only be seen totally if the reconstruction is in the viewable area. One possible way to increase the reconstruction size is therefore to increase the hologram size (see Fig. 6.19).

6.3.2 The Gap Problem

Although tiling the SLMs side by side is advantageous, it may not be possible due to some physical difficulties. As shown in Fig. 5.3, there is a metallic mount around the spatial light modulators. Therefore, if we put them side by side, the mount yields gaps in the field of view. The ideal system depicted in Fig. 6.15 may be no longer feasible and

it may turn out to be as in Fig. 6.20. To solve this problem we propose a method that uses a beam splitter (half-mirror) to fill the gap between two SLMs by an image of the third one (see Fig. 6.21). For other multiple SLM designs and prototypes we use similar approaches to solve this gap problem. The usage of the beam splitters to eliminate the gap between SLMs in the holographic display systems reported in [59, 146, 147].

6.3.3 Setup and Hologram Generation

For our laboratory prototype, we used six phase-only spatial light modulators manufactured by HoloEye [71]. The top view of the setup is shown in Fig. 6.23(a). As in the previous experiments, we used a spatial filter to filter out the noise in the illuminating beam. After the spatial filter, the divergent beam collimated by lenses to obtain a uniform plane wave illumination. Here we use a LED as the light source. The plane wave illumination is directed to the SLMs with the help of optics, such as half-mirrors and mirrors. We calculate the large hologram by using the Rayleigh-Sommerfeld wave propagation algorithm [10]. The number of pixels in the large hologram is 5760×2160 (the same size with the display, see Fig. 6.23(b)). Then we partition the hologram into sub-holograms with a size of 1920×1080 pixels each. Upper row and the lower row are constructed by different beam-splitters, separately. Then the resultant two rows are combined by the third beam-splitter.

6.3.4 Experimental Results

We used a square pyramid as a 3D model for our experiments. The model is shown in Fig. 6.24. The optical reconstruction obtained from the developed system is shown in Fig. 6.25. The photographs are taken by a Canon 5D Mark-II camera. The reconstruction distance is $0.5m$. Fig. 6.25 (a), (b) and (c) show the left, front and right view of the reconstructed 3D object, respectively. As depicted by the figures, the field of view increases when the hologram size increases, as expected. Thus, if use more SLMs, we

can improve the 3D perception. We conclude that even with three SLMs along the horizontal direction, the field of view is increased, significantly. Results motivated us to further increase the field of view by increasing the number of SLMs and also try different configurations. Therefore this leads us to next step which is the circularly configured phase-only SLMs.

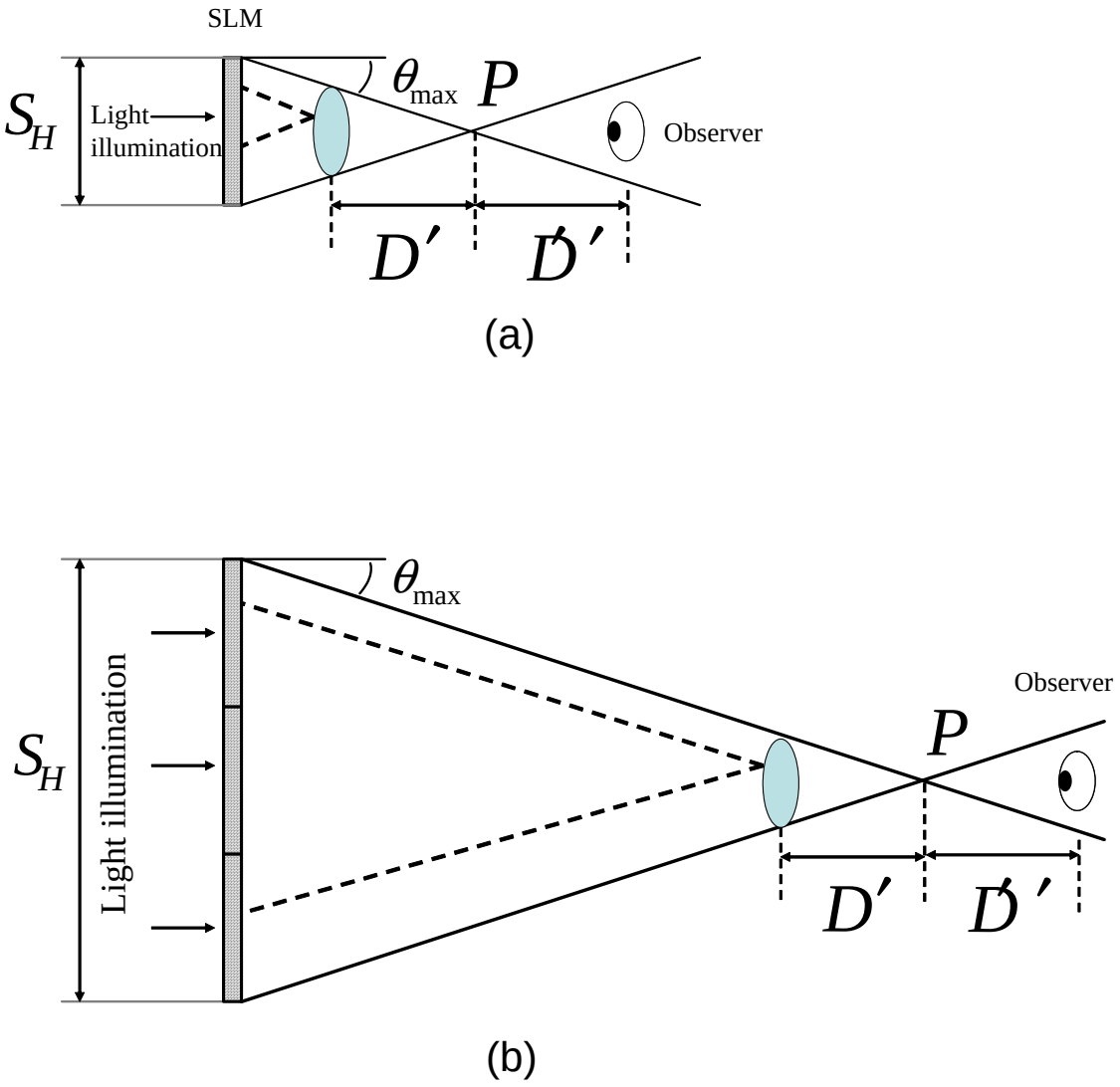

Figure 6.17: Increase in the quality when multiple SLMs are used. Only those SLM pixels within the dotted cone contributed to the image ("Multi-SLM holographic display system with planar configuration," F. Yaraş, H. Kang and L. Onural, in 3DTV Conference: The True Vision - Capture, Transmission and Display of 3D Video, IEEE, 2010. ©2010 IEEE. Reprinted with permission.)

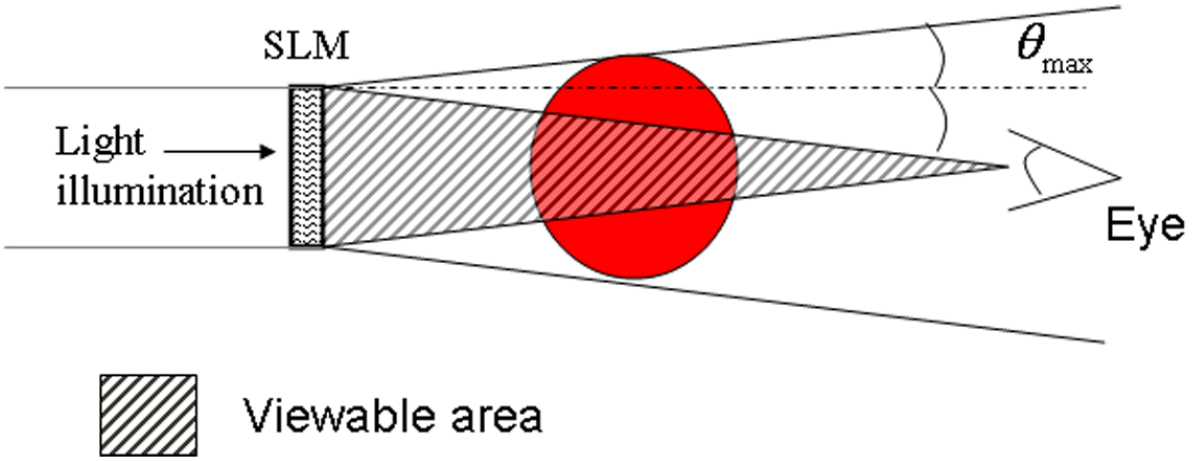

Figure 6.18: Illustration of larger object reconstruction with a single SLM ("Circularly configured multi-SLM holographic display system," F. Yaraş, H. Kang and L. Onural, in 3DTV Conference: The True Vision - Capture, Transmission and Display of 3D Video, IEEE, 2011. ©2011 IEEE. Reprinted with permission.)

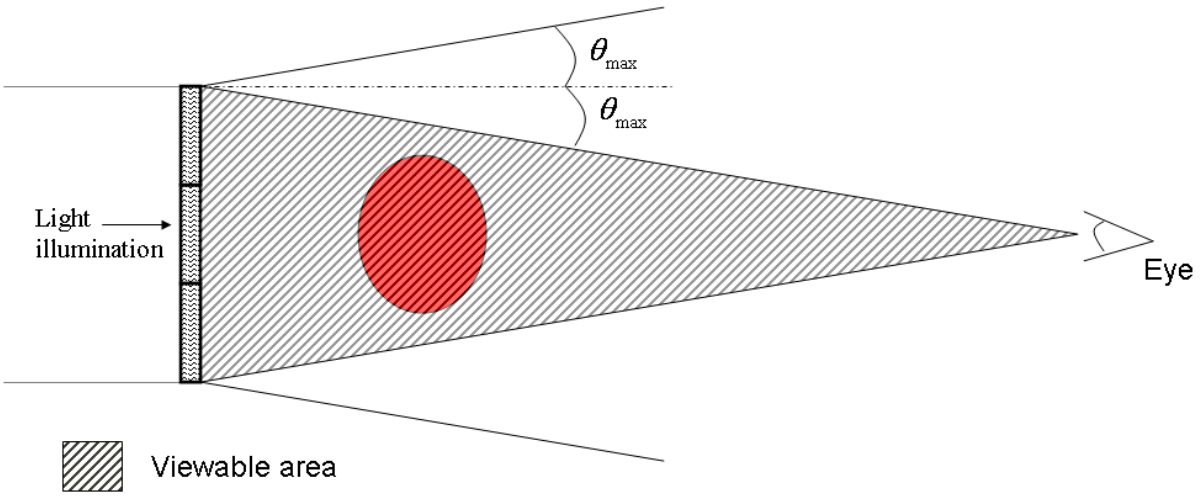

Figure 6.19: Illustration of larger object reconstruction with multiple SLMs ("Circularly configured multi-SLM holographic display system," F. Yaraş, H. Kang and L. Onural, in 3DTV Conference: The True Vision - Capture, Transmission and Display of 3D Video, IEEE, 2011. ©2011 IEEE. Reprinted with permission.)

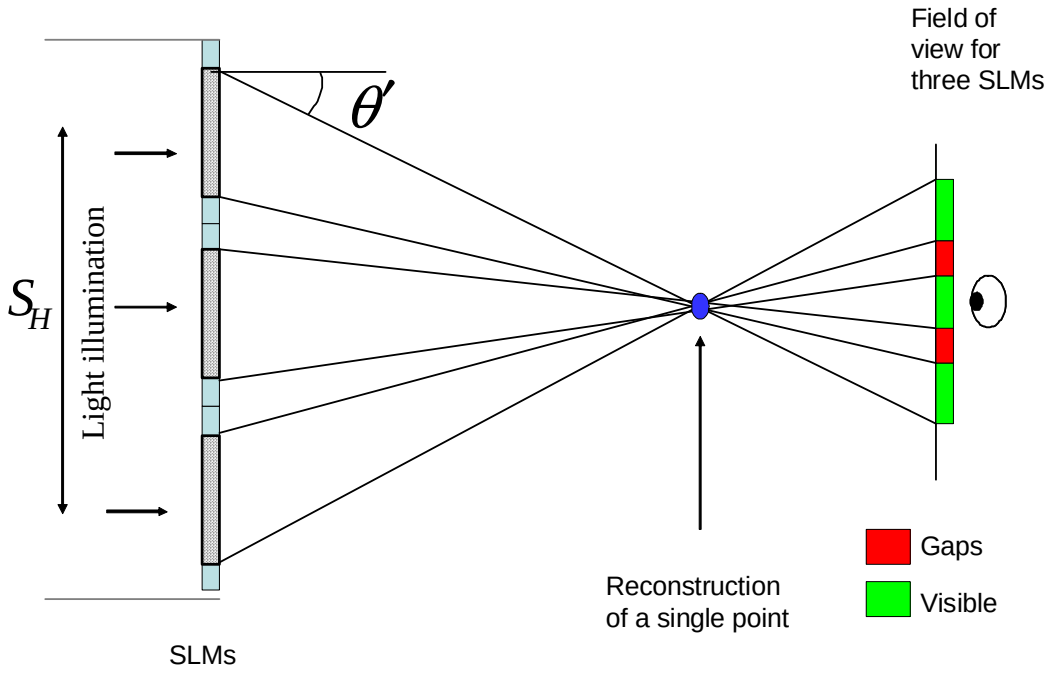

Figure 6.20: Discontinuous field of view due the mount of the SLM.

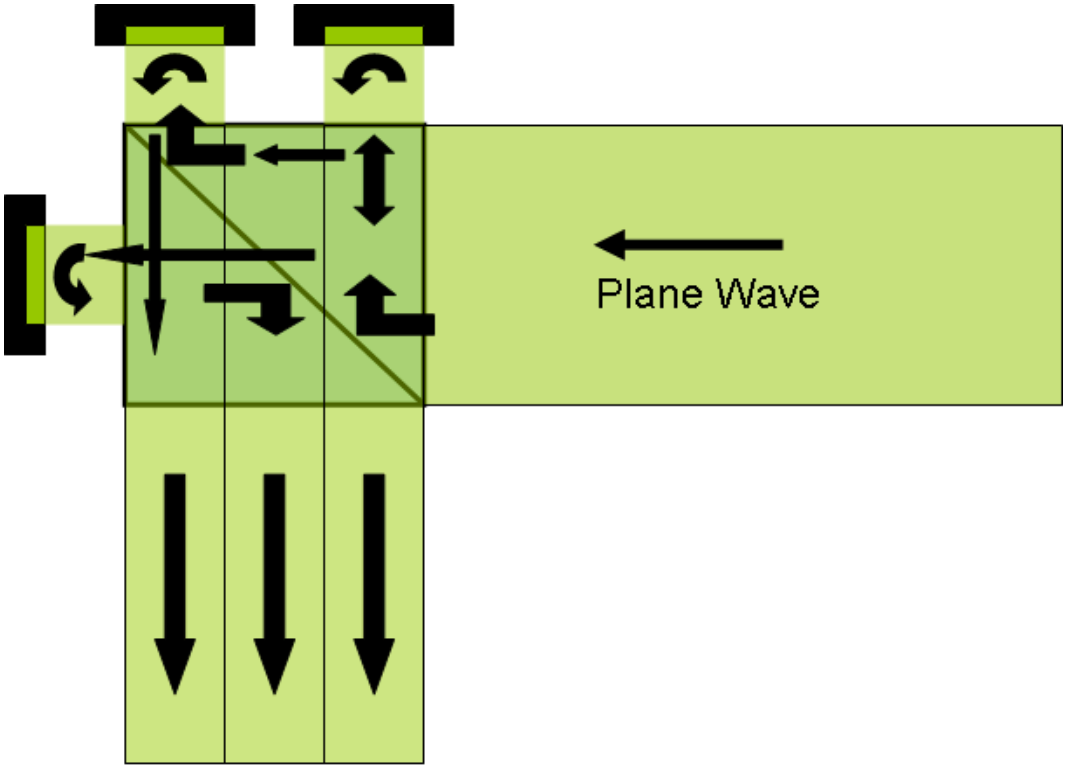

Figure 6.21: Removing the gaps by using a beam-splitter ("Circularly configured multi-SLM holographic display system," F. Yaraş, H. Kang and L. Onural, in 3DTV Conference: The True Vision - Capture, Transmission and Display of 3D Video, IEEE, 2011. ©2011 IEEE. Reprinted with permission.)

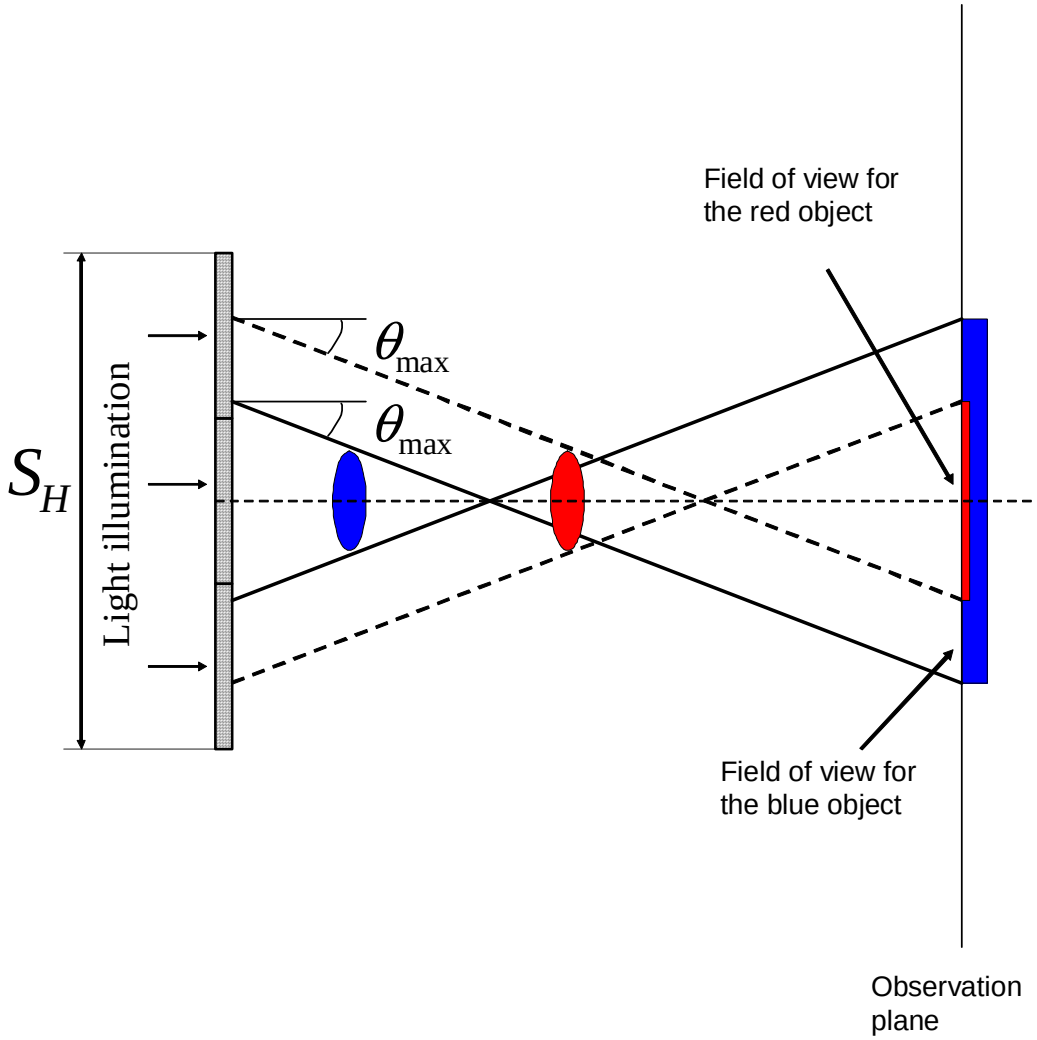

Figure 6.22: Field of view increases when object gets closer to the SLM ("Multi-SLM holographic display system with planar configuration," F. Yaraş, H. Kang and L. Onural, in 3DTV Conference: The True Vision - Capture, Transmission and Display of 3D Video, IEEE, 2010. ©2010 IEEE. Reprinted with permission.)

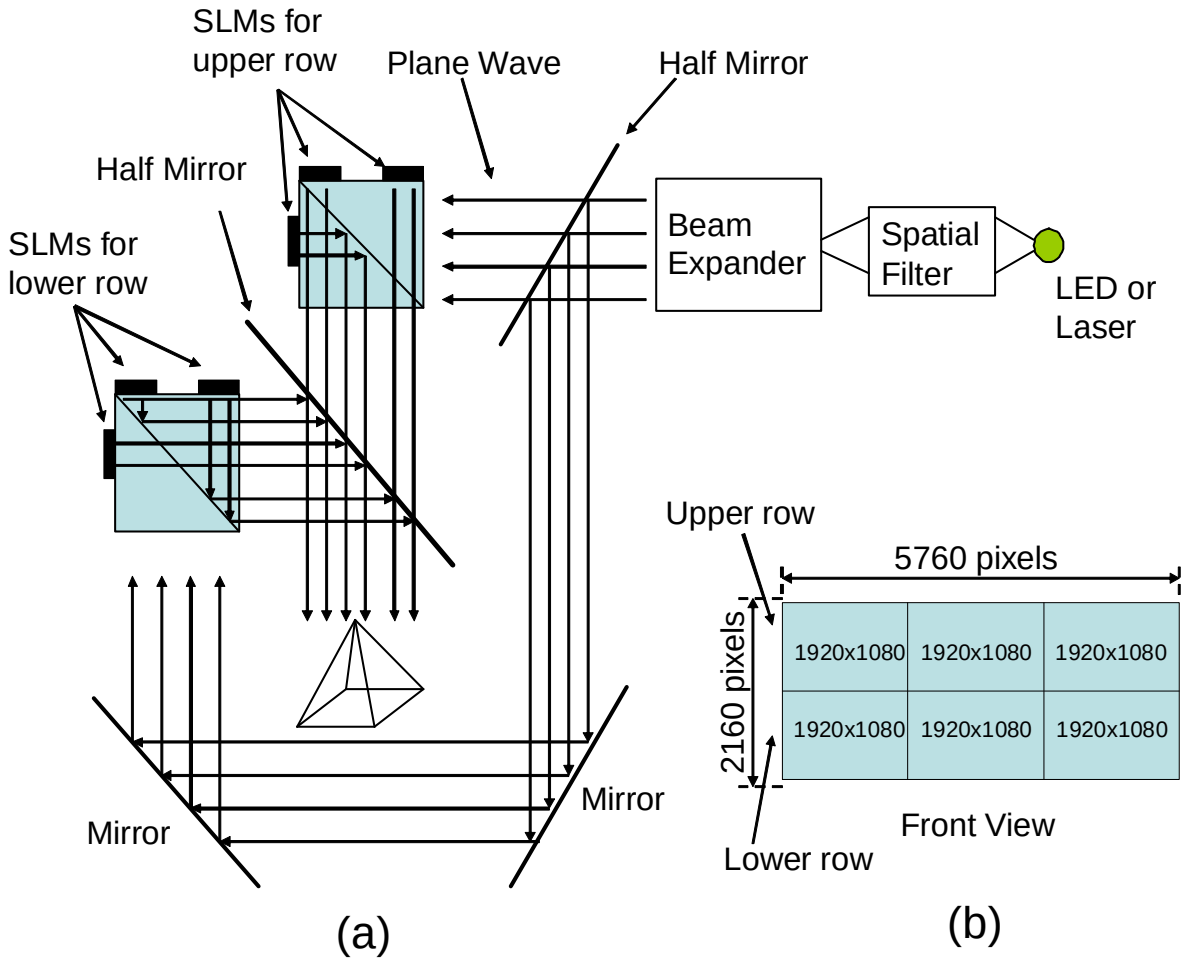

Figure 6.23: (a) Top view of the setup, (b) front view of the tiled SLMs ("Multi-SLM holographic display system with planar configuration," F. Yaraş, H. Kang and L. Onural, in 3DTV Conference: The True Vision - Capture, Transmission and Display of 3D Video, IEEE, 2010. ©2010 IEEE. Reprinted with permission.)

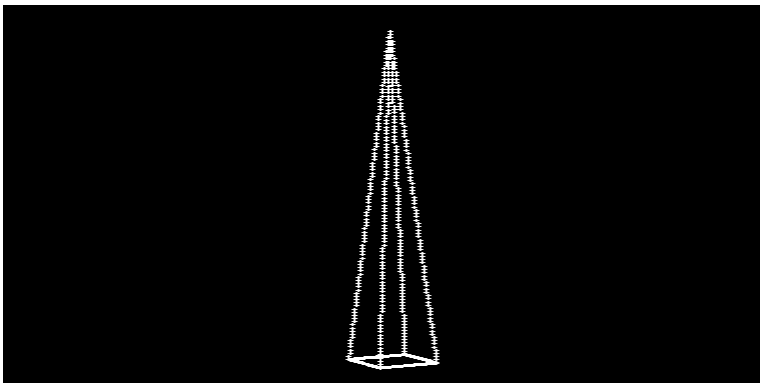

Figure 6.24: Rigid 3D model of a square pyramid ("Multi-SLM holographic display system with planar configuration," F. Yaraş, H. Kang and L. Onural, in 3DTV Conference: The True Vision - Capture, Transmission and Display of 3D Video, IEEE, 2010. ©2010 IEEE. Reprinted with permission.)

Figure 6.25: Optical reconstructions: (a) left, (b) front and (c) right view ("Multi-SLM holographic display system with planar configuration," F. Yaraş, H. Kang and L. Onural, in 3DTV Conference: The True Vision - Capture, Transmission and Display of 3D Video, IEEE, 2010. ©2010 IEEE. Reprinted with permission.)

6.4 Circular Holographic Video Display System

In the previous section, we demonstrate the advantages of using multiple SLMs in the planar configuration. The results motivated us to build better holographic video display configurations. As discussed in Chapter 4, in order to reduce the bandwidth requirements a circular configuration is needed. Some parts of this section is based on our publications [138] and [137].

6.4.1 Field of View in Circular Holographic Displays

Field of view is an important feature for all types of displays. Larger field of view values bring more freedom to the location of the observers. This is also true for commercially available 2D LCD displays (e.g. PC monitors and TVs). However those kind of displays use diffused light sources at the back of the LCD panels; therefore, they have a wide field of view. For the holographic displays, diffused light sources may not be suitable, since they randomize the phase information; and therefore, the output light is spread to all directions equally. As a result, there would not be any directional variation. Since the directional information is crucial for 3D visualization, such commercial systems can not be used in 3D display systems. Therefore, we need to use somewhat coherent light sources in holographic display systems. We used either laser or LED illumination in our holographic display prototypes. Temporal coherence of the LEDs and their efficiency has been already discussed in previous sections and in our publications [56]. The field of view is restricted by the size and the pixel period of the SLMs. For a single SLM, the relation between the field of view, the size and the diffraction angle is depicted in Fig. 6.26a. In this figure, the field of view denotes an area on the observation plane. Note that if observer is inside the field of view, the entire object can be seen while the full bandwidth of the SLM is used. If the observer moves outside of the borders of the field of view, some parts of the reconstruction may not be seen. In addition since the bandwidth is not used fully, the quality and therefore the sharpness of the reconstructions may degrade. As discussed in the previous section, since the field of view for a single SLM is not enough for comfortable

3D perception, one alternative is to use multiple SLMs in planar configuration. Although such configuration has advantages over the single SLM case, it may be inadequate in some circumstances. For example, as depicted in Fig. 6.26b, if the full bandwidth of only the middle SLM is used for the reconstruction, then there is no contribution from other SLMs to the reconstruction. Therefore we propose a circular configuration of SLMs to increase the field of view in holographic display systems, see Fig. 6.26c. As shown in the figure, the field of view is increased significantly. As a consequence of this configuration, the observer can move and rotate around the reconstructions and this will yield a better 3D perception. Meanwhile, for the illustration purposes, in the figures we discard the effect of the mount of the SLMs. The gap problem that results from the mount will be discussed in the Section 6.4.2.

6.4.2 Some Laboratory Prototypes

In the first prototype, we used several beam-splitters (half-mirrors) to combine six phase-only spatial light modulators in a circular configuration. Fig. 6.27 shows the schematic of the setup. Here in this setup, we use cube beam-splitters to solve the gap problem. As a consequence of this method three SLMs are tiled side by side. (Fig. 6.21 shows how a beam-splitter is used to combine three SLMs without any gap between them.) Although Fig. 6.21 demonstrates an example of a planar configuration, we can use the same idea for a circular configuration, as well. All we have to do is to rotate the SLMs appropriately. After we have two sets of SLMs (three SLMs for each set), they are combined by a large half-mirror. The resultant display size becomes 11520×1080 pixels and the increase in the field of view illustrated in Fig. 6.27. The observer can move and rotate around the reconstruction within the limits of the resultant field of view.

In this system, each SLMs is rotated by 1° with respect to the next SLM. SLMs can support rotations up to 3°. Alignments and adjustments are crucial while assembling the setup. Fine adjustments may be needed for a better 3D perception. Therefore it is better first to mount SLMs onto micro-stages. Heights of the SLMs from the optic table should be the same and the vertical edges of the SLMs should be parallel to the

surface of the optical table. In addition, direction of the normal vectors of the SLM surfaces should be the same. Centers of the SLMs should be on the same circle and there should not be any gap between the SLMs. After all adjustments are done carefully, the alignment is checked by holographic reconstruction of a single point object. An optimum distance should be calculated. First find the intersection point of all normal vectors of the SLMs. The optimum distance is the distance between the middle point of the surface of an SLM and the intersection point. After we find the optimum distance, we should calculate a hologram of a point and the reconstruction distance should be equal to the optimum distance. If all adjustments are correct, reconstructions from all SLMs (from hologram of a single point) should overlap at the same location in space, i.e. at the optimum distance. If they do not overlap properly, subsequent fine adjustments should be done. The optimum distance in this prototype is $400mm$. The front view of the holographic display is shown in Fig. 6.28. The continuous array of six phase-only spatial light modulators can be seen in Fig. 6.27. The total number of pixels of the resultant system is 11520×1080. Fig. 6.29 shows a photograph of the top view of the setup. In the figure, we can see two beam-splitters and a large half-mirror.

For this prototype, we used two different computer generated 3D model. One of them is a wire-frame cube shaped object (see Fig. 6.30). The model is a point cloud. The computer generated holograms are calculated by using the Rayleigh-Sommerfeld light propagation algorithm [10]. Each point in the point cloud first is propagated to the hologram plane and then the resultant 2D complex fields are superposed. Then we discard the amplitude (since our SLMs are phase-only) and save the phase values as a bitmap grayscale image by mapping the range $[-\pi : \pi]$ to $[0 : 255]$. We perform this procedure for all SLMs just by rotating the 3D object by the corresponding rotation angle. When we rotate the object, we can use the Rayleigh-Sommerfeld light propagation algorithm for parallel planes. Otherwise, one should use the propagation algorithms for tilted planes [29,30,148]. Since our SLMs are rotated by 1° with respect to the next SLM, the rotation angles for are chosen as: -2.5°, -1.5°, -0.5°, $+0.5^\circ$, $+1.5^\circ$ and $+2.5^\circ$.

An optical reconstruction of 3D wire-frame model of a cube is shown in Fig. 6.31.

The pictures in (a), (b) and (c) are taken from left, center and right, respectively. Here in this figure, reconstructions are captured when laser illumination is used. However, to avoid eye hazard, LED illumination is also used as an alternative source and such reconstructions are observed by naked eye. With the help of the resultant wide field of view, reconstructions are observed binocularly. Reconstruction distance is approximately $400mm$. Results show that the total field of view is significantly increased compared to the single SLM case. Although the total field of view of this prototype is about 6°, it can be increased up to 18° since we do not use all the available rotation support of the SLMs (i.e 3° for each SLM).

In another optical reconstruction we used a 3D wire-frame of a pyramid shaped object (see Fig. 6.24). In this experiment, we also constructed a physical wire-frame pyramid. The size and the shape of the physical pyramid and the optical reconstruction are the same. Then we place the physical model just next to the optical reconstruction and at the same distance to the display. Fig. 6.32 shows the optical reconstructions from left, front and right views. The purpose of the physical wire-frame object is to show that the parallax of the holographic display system is correct.

Yet in another circularly configured multi-SLM laboratory prototype we used nine phase-only spatial light modulators. As in the previous prototypes, the gap problem also exists in this setup (see Fig. 6.33). We again solved this problem by using a single beam-splitter (half-mirror) instead of using several of them. This brings an advantage while performing fine adjustments since each additional optical component brings complexity to the system. The schematic of the laboratory prototype is shown in Fig. 6.34. In addition, a cone mirror is used in the illumination part of the system. The design of the illumination part with a cone mirror and its analysis is performed together with Dr. Hoonjong Kang [138]. The cone mirror helps us to direct the illuminating light coming from the light source to 360°. Therefore, all SLMs are illuminated by using only a single light source. However, due to the shape of the cone mirror an astigmatic illumination is formed, i.e. the radius of curvatures of the illuminating light in vertical and horizontal axes are not equal. Fig. 6.35b shows the cross-section of the illuminating light in vertical

and horizontal axes. However the astigmatism of the illuminating wave is canceled out at the hologram generation step by simply multiplying the hologram by the conjugate of the astigmatic wave. Photographs of the laboratory prototype are shown in Fig. 6.36. The alignment of the SLMs and beam splitter are shown in Fig. 6.36a. Fig. 6.36b and Fig. 6.36c show the side view of the setup and the cone mirror, respectively. A photograph taken in a different angle is shown in Fig. 6.36d. As shown in Fig. 6.35a, the SLMs are tilted in vertical direction to position the reconstructed object slightly above the setup. Otherwise reconstructions may be blocked by the components. As discussed in Section 4.4, degradation in reconstruction quality can be neglected up to 20° of tilting.

In this prototype, we use a video of a computer generated model of a horse. A picture of the model is shown in Fig. 6.37. The model consists of a point cloud, like the other 3D models that we used before. However, in this case we use a sequence of 24 frames of video of the model. We know the 3D point cloud data for each frame. We calculate nine holograms for each frame. Those nine holograms correspond to nine phase-only SLMs. The angle between two SLMs is 3° along the horizontal direction. There are three SLM modules in the prototype (see Fig. 6.34). Each module has three phase-only SLMs and they are connected to the driver modules through color channels. The driver modules and their working principles are discussed in previous sections. For each frame, the calculated holograms (nine phase-holograms) are first mapped from $[-\pi : \pi]$ to $[0 : 255]$. Then they are saved as a single bitmap image where each pixel is represented as an 8-bit integer. As shown in Fig. 6.38, those holograms are grouped for the driver modules according to the depicted setup scheme. Then finally, all bitmap images are saved into a single RGB image whose size is $(3 \times M)$ by N where $(M, N) = (1920, 1080)$ is the single SLM size. Then the overall procedure is repeated for all frames of the video. The hologram calculation procedure is explained in the next paragraph. Please note that the hologram calculation procedure is derived together with Dr. Hoonjong Kang [138].

We use the point cloud data of the computer generated 3D model. We denote each point in the point cloud by a complex amplitude and it is defined as $O(x, y, z) = o(x, y, z) \exp(j\theta_o(x, y, z))$, where $o(x, y, z)$ and $\theta_o(x, y, z)$ denote the magnitude and the

phase of the object wave at the source, respectively. Since we use an astigmatic diverging beam to illuminate the SLMs, thus holograms, we need a correction term to cancel out the effect while computing the holograms. Since the illumination waves can be expressed as a separable function, we can define horizontal and vertical correction terms independently. For the horizontal direction, center of the illuminating wave is the center of the cone mirror, due to radial reflection (see Fig. 6.35). The distance between the center of the cone mirror and the SLM is denoted as D_l. In the horizontal direction, the illuminating wave $P(\xi)$, is approximately given as,

$$P(\xi) = \exp\left(jk\frac{\xi^2}{2D_l}\right) \quad . \tag{6.9}$$

Here we assume a paraxial approximation and since the SLMs are small the approximation is valid. For the vertical direction, the cone mirror behaves like a planar mirror. Thus, center of the incoming light is not effected. However the size of the cone mirror is smaller than height of the SLM. If we use a plane wave illumination for the vertical direction, illuminating wave might not cover whole SLM. Therefore we need a divergent illuminating beam also in vertical direction. The center of the vertical illuminating wave is $D_p + D_l$ (see Fig. 6.35). Therefore, the vertical illuminating wave, $P(\eta)$, is given by:

$$P(\eta) = \exp\left(jk\frac{(\eta + S_H/2)^2}{2(D_p + D_l)}\right) \quad , \tag{6.10}$$

where, D_p is the distance between the center of the vertical illumination wave and the cone mirror, and S_H is the height of the SLM. In addition, there exists a strong undiffracted beam at the reconstructions. We separate the reconstruction from the undiffracted beam by using off-axis holography. Additional carrier frequency along the vertical direction is applied and it is given by:

$$P_t(\eta) = \exp\left(jk\eta\sin(\theta_t)\right) \quad , \tag{6.11}$$

where, $\sin(\theta_t)$ is the angle between the reconstructed beam and the undiffracted beam. Thus, the overall correction term becomes:

$$P(\xi,\eta) = \exp\left(jk\frac{\xi^2}{2D_l}\right)\exp\left(jk\frac{(\eta + S_H/2)^2}{2(D_p + D_l)} + jk\eta\sin(\theta_t)\right) \quad . \tag{6.12}$$

As in the previous experiments, we use the Rayleigh-Sommerfeld light propagation algorithm [10]. The resultant complex field for the point cloud data for larger distances, which means evanescent waves do not exist, yields:

$$S(\xi,\eta) = \sum_{p=1}^{N} O(x_p, y_p, z_p) \frac{\exp(jkr_p)}{r_p} \quad , \tag{6.13}$$

where, p is the index of the points, k is the wavenumber ($k = 2\pi/\lambda$, where λ is the wavelength), N is the number of points in the point cloud of the three-dimensional computer graphic model. Here r_p denotes the distance between p^{th} point and the hologram plane and defined as:

$$r_p = [(\xi - x_p)^2 + (\eta - y_p)^2 + z_p^2]^{1/2} \quad . \tag{6.14}$$

The resultant complex field on the hologram plane (ξ, η plane) after multiplying by the correction term becomes:

$$G(\xi,\eta) = P(\xi,\eta) \sum_{p=1}^{N} O(x_p, y_p, z_p) \frac{\exp(jkr_p)}{r_p} \quad . \tag{6.15}$$

Moreover, the pixelated complex field on the hologram plane is calculated by:

$$g(m,n) \triangleq G\left(\big(m - \frac{(M+1)}{2}\big)\Delta_m, \big(n - \frac{(N+1)}{2}\big)\Delta_n \right) \quad , \tag{6.16}$$

where, $m \in [1, 1920]$ and $n \in [1, 1080]$, Δ_m and Δ_n are pixel periods and M and N are number of columns and rows of the pixelated complex field. For our prototype $M = 1920$ and $N = 1080$.

Fig. 6.39 shows the optical reconstruction for a single frame for different viewing angles. The distance between the SLM and the center of the cone mirror, D_l, is $0.3m$. The distance between the SLM and the center of the illuminating wave, $D_p + D_l$, is $0.55m$. The reconstruction distance is about $0.35m$. The size of the reconstruction is about $1cm$. For the illustration purposes, we use laser illumination and the wavelength of the green laser is $532nm$. As an alternative, we use LED illumination and observers can see the reconstructions by naked eye. The total number of pixels in the resultant holographic video display system is 17280×1080. Total field of view is about 24° and observer can move and rotate around the holographic reconstructions, i.e. a ghost-like 3D object floating in space.

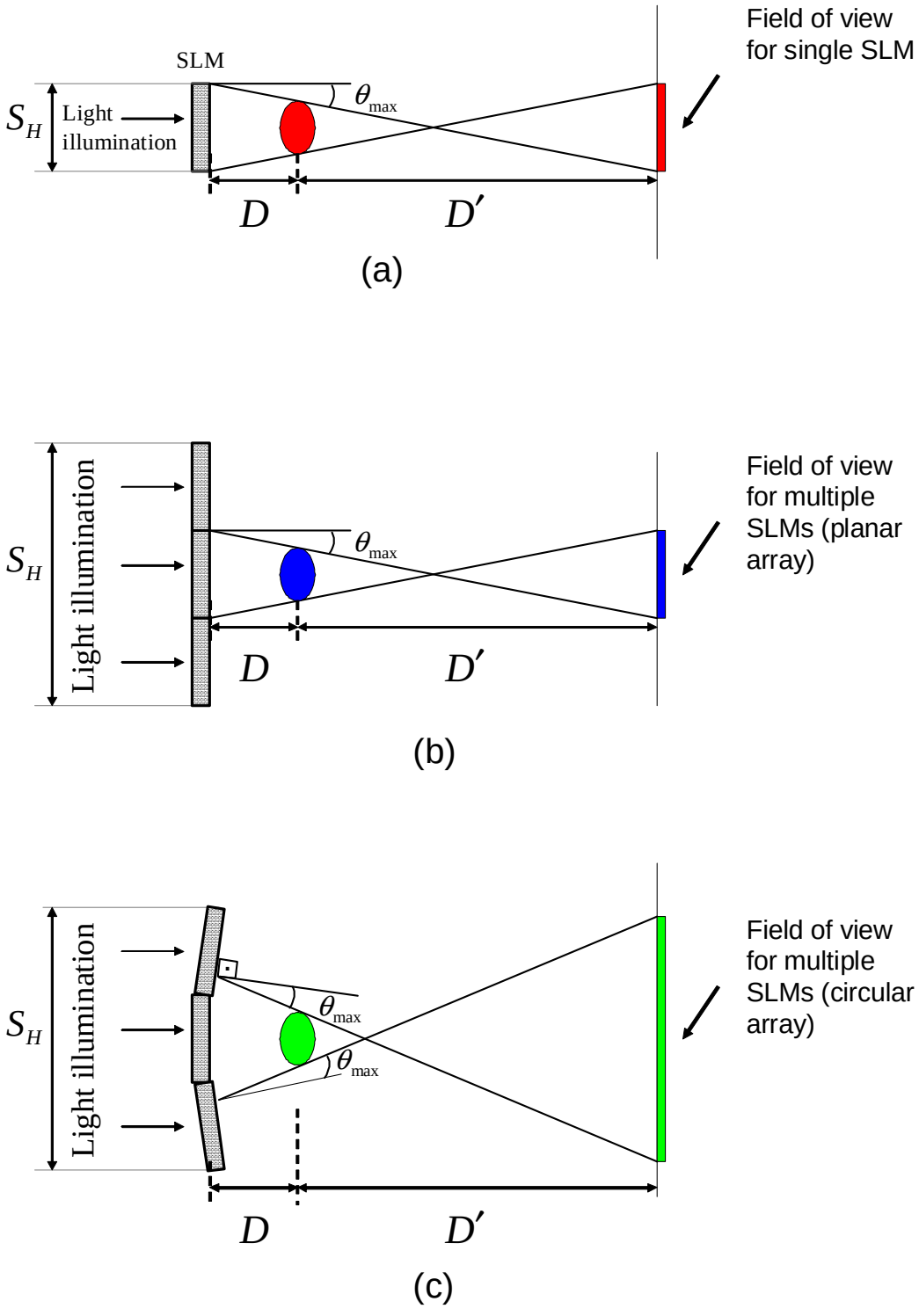

Figure 6.26: Field of view for (a) single SLM, (b) multiple SLMs in planar configuration, (c) multiple SLMs in circular configuration. ("Circular Holographic Video Display System," F. Yaraş, H. Kang and L. Onural, Optics Express vol. 19, no. 10, pp.9147-9156, 2011. ©2011 OSA. Reprinted with permission.)

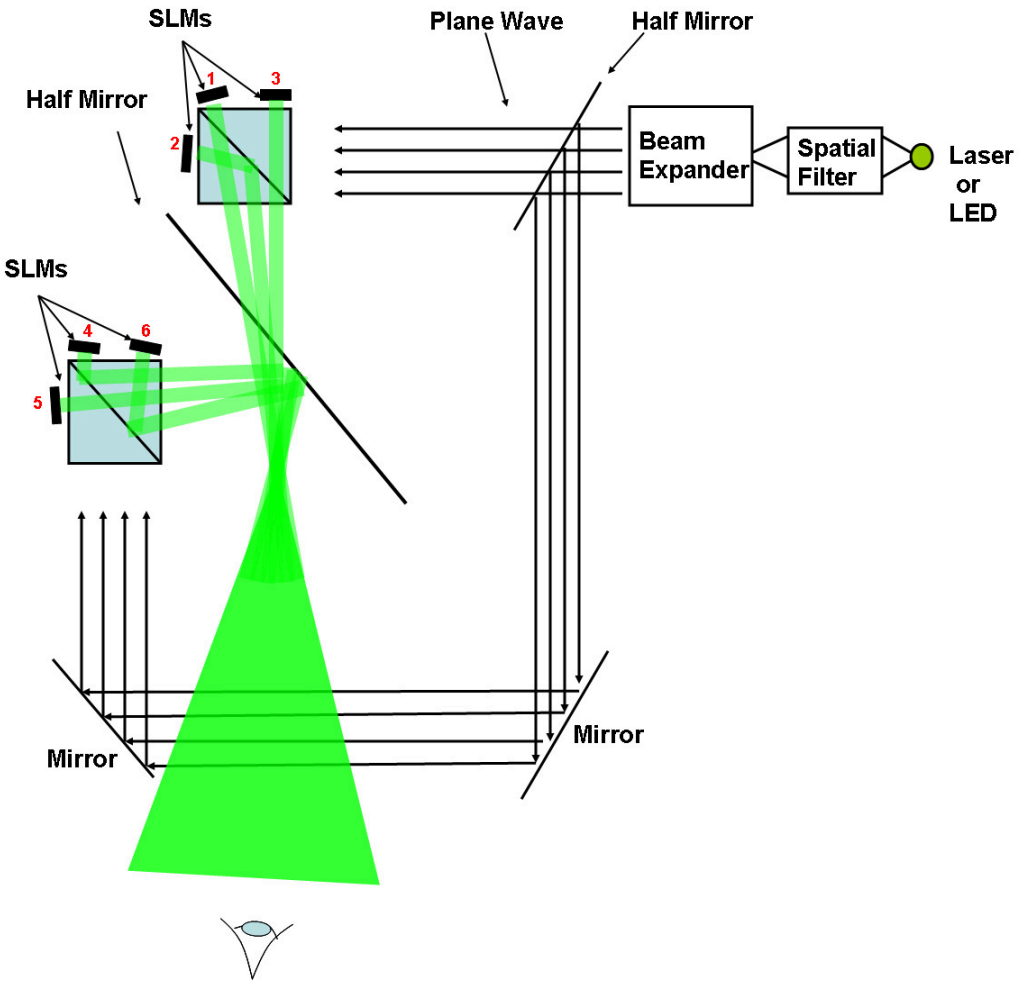

Figure 6.27: Schematic of the setup ("Circularly configured multi-SLM holographic display system," F. Yaraş, H. Kang and L. Onural, in 3DTV Conference: The True Vision - Capture, Transmission and Display of 3D Video, IEEE, 2011. ©2011 IEEE. Reprinted with permission.)

Figure 6.28: Front view of the display ("Circularly configured multi-SLM holographic display system," F. Yaraş, H. Kang and L. Onural, in 3DTV Conference: The True Vision - Capture, Transmission and Display of 3D Video, IEEE, 2011. ©2011 IEEE. Reprinted with permission.)

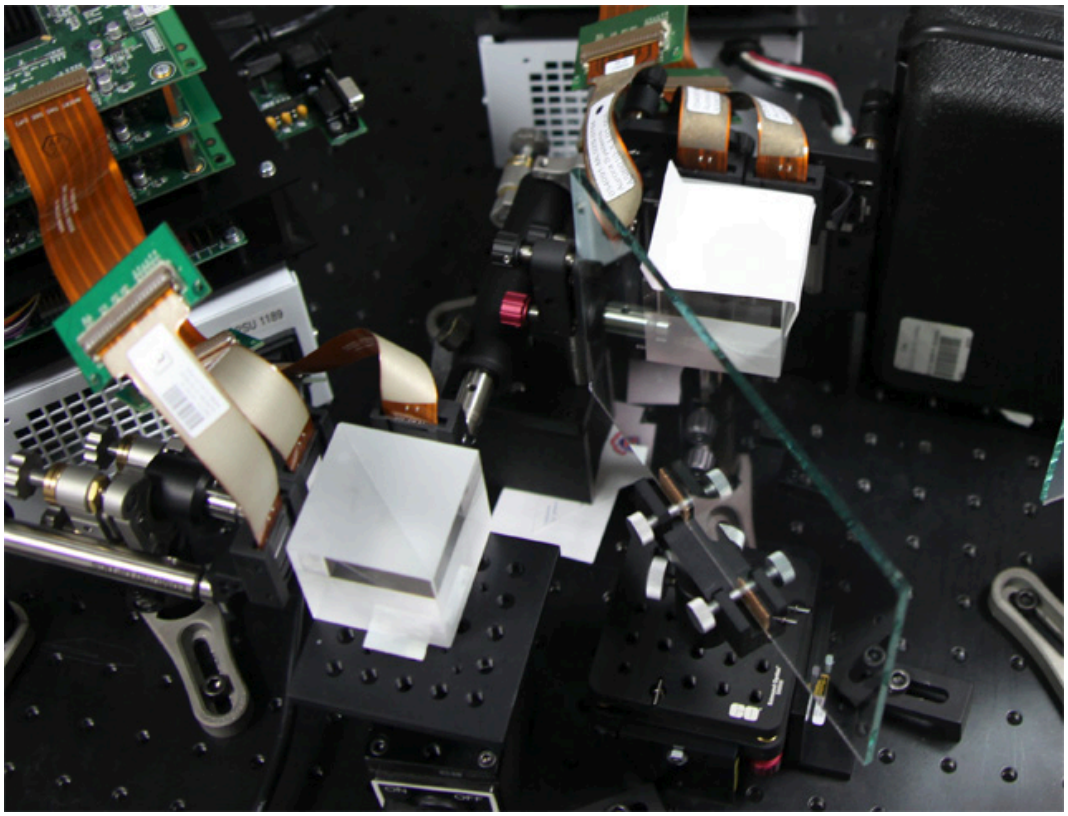

Figure 6.29: Top view of the display ("Circularly configured multi-SLM holographic display system," F. Yaraş, H. Kang and L. Onural, in 3DTV Conference: The True Vision - Capture, Transmission and Display of 3D Video, IEEE, 2011. ©2011 IEEE. Reprinted with permission.)

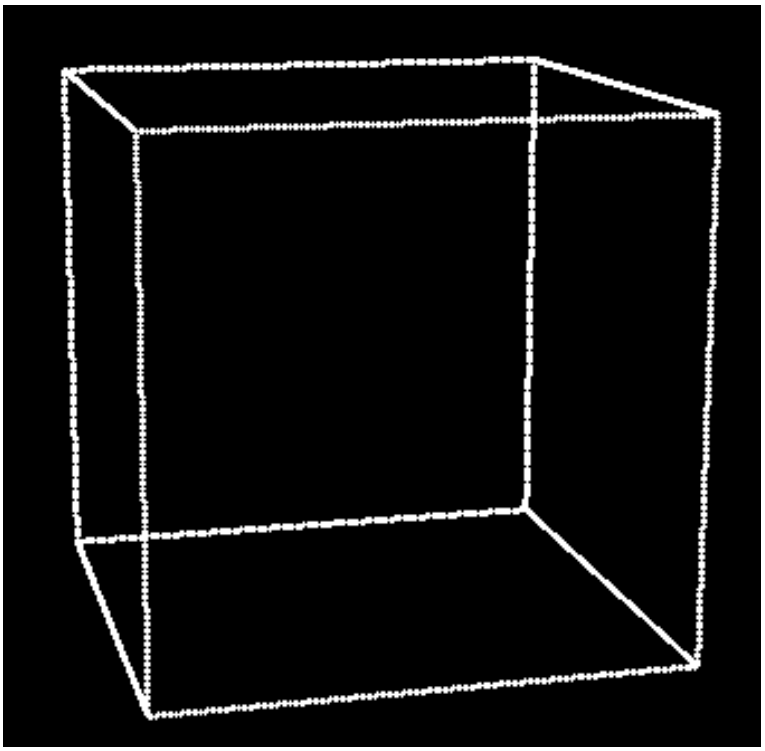

Figure 6.30: Computer generated wire-frame 3D model of a cube ("Circularly configured multi-SLM holographic display system," F. Yaraş, H. Kang and L. Onural, in 3DTV Conference: The True Vision - Capture, Transmission and Display of 3D Video, IEEE, 2011. ©2011 IEEE. Reprinted with permission.)

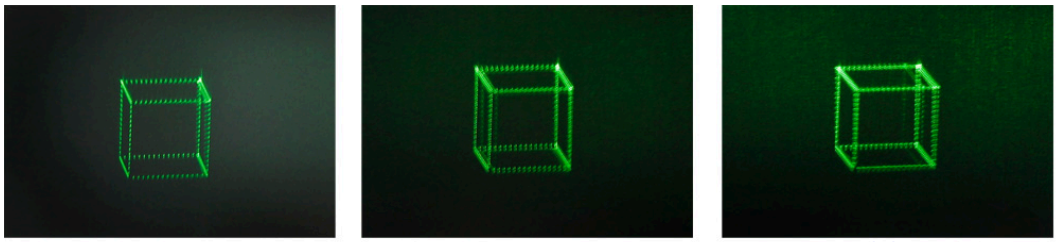

Figure 6.31: Optical reconstruction of 3D wire-frame model of a cube. (a) Left, (b) center, and (c) right views ("Circularly configured multi-SLM holographic display system," F. Yaraş, H. Kang and L. Onural, in 3DTV Conference: The True Vision - Capture, Transmission and Display of 3D Video, IEEE, 2011. ©2011 IEEE. Reprinted with permission.)

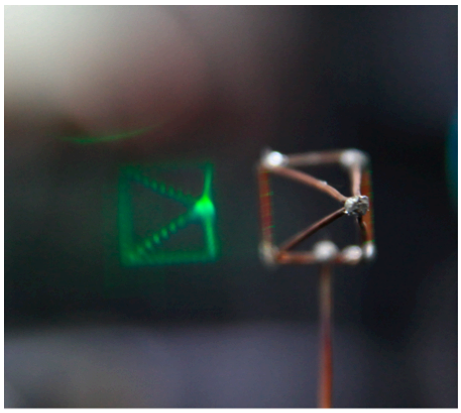

(a)

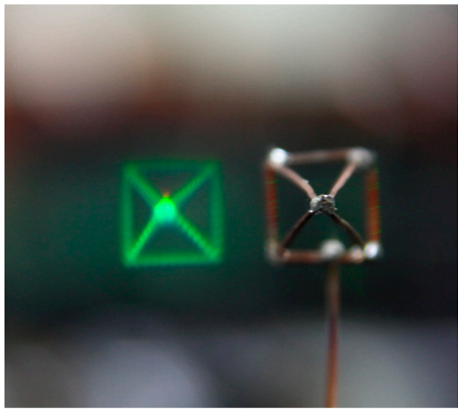

(b)

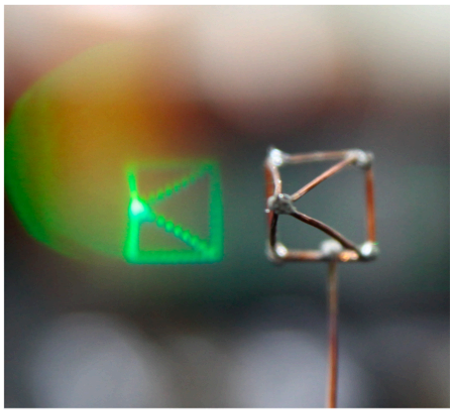

(c)

Figure 6.32: Optical reconstructions from a curved array of SLMs: (a) left, (b) front and (c) right view ("Digital holographic Three-dimensional video displays," L. Onural, F. Yaraş and H. Kang, Proceedings of the IEEE , vol.99, no.4, pp.576-589, April 2011. ©2011 IEEE. Reprinted with permission.)

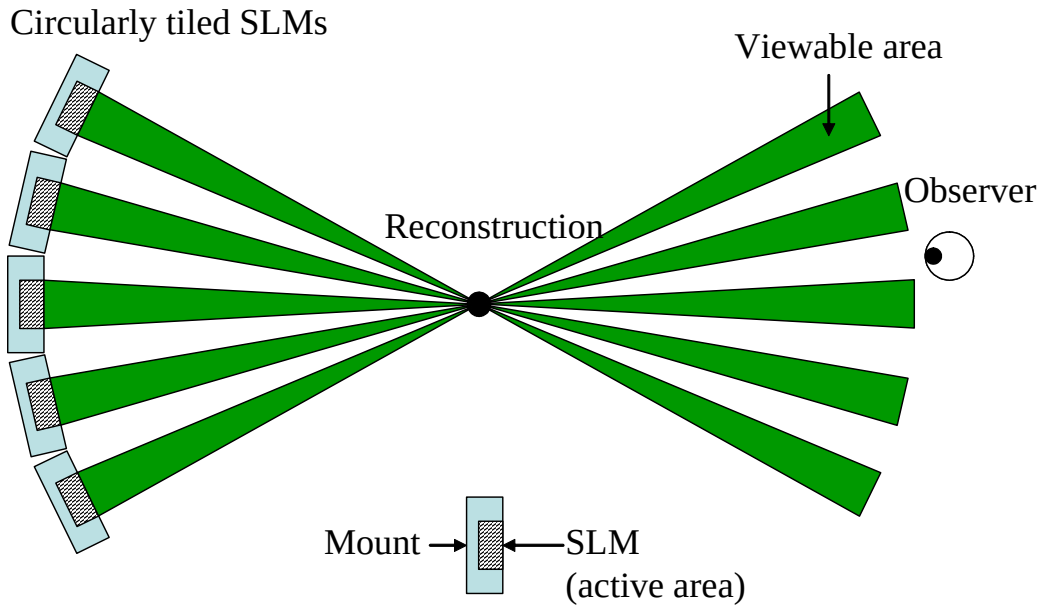

Figure 6.33: Discontinuous field of view due the frame of the SLMs. ("Circular Holographic Video Display System," F. Yaraş, H. Kang and L. Onural, Optics Express vol. 19, no. 10, pp.9147-9156, 2011. ©2011 OSA. Reprinted with permission.)

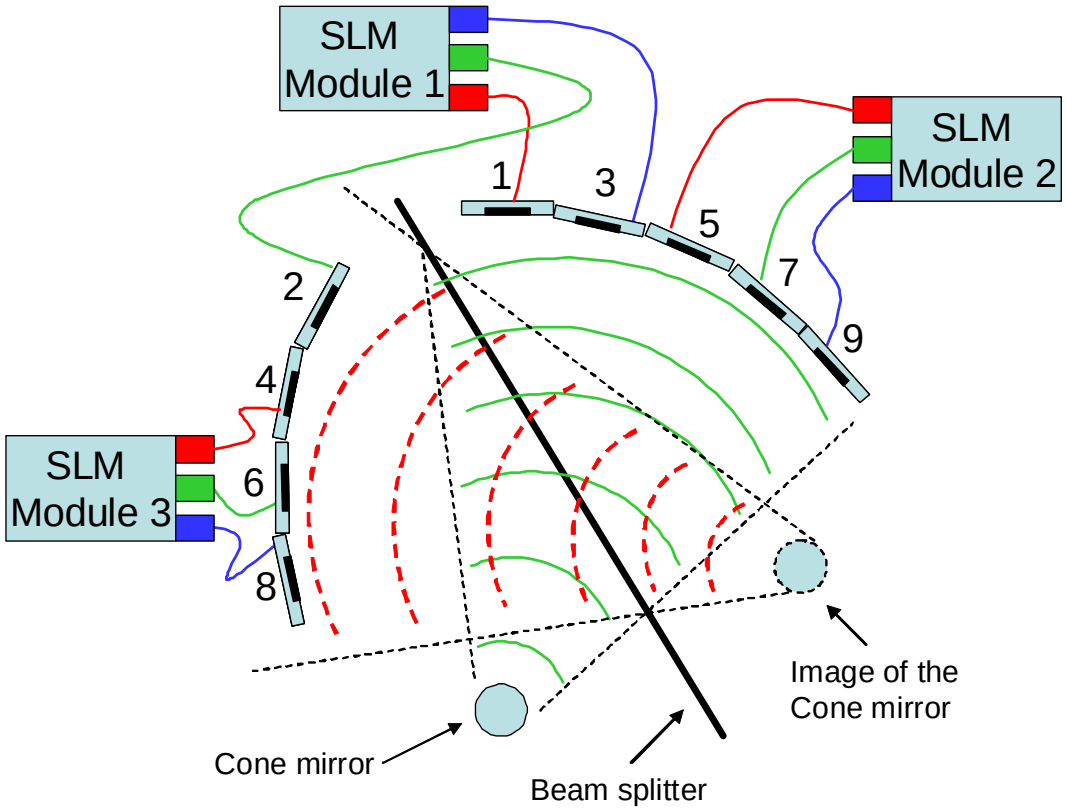

Figure 6.34: Top view of the laboratory prototype ("Circular Holographic Video Display System," F. Yaraş, H. Kang and L. Onural, Optics Express vol. 19, no. 10, pp.9147-9156, 2011. ©2011 OSA. Reprinted with permission.)

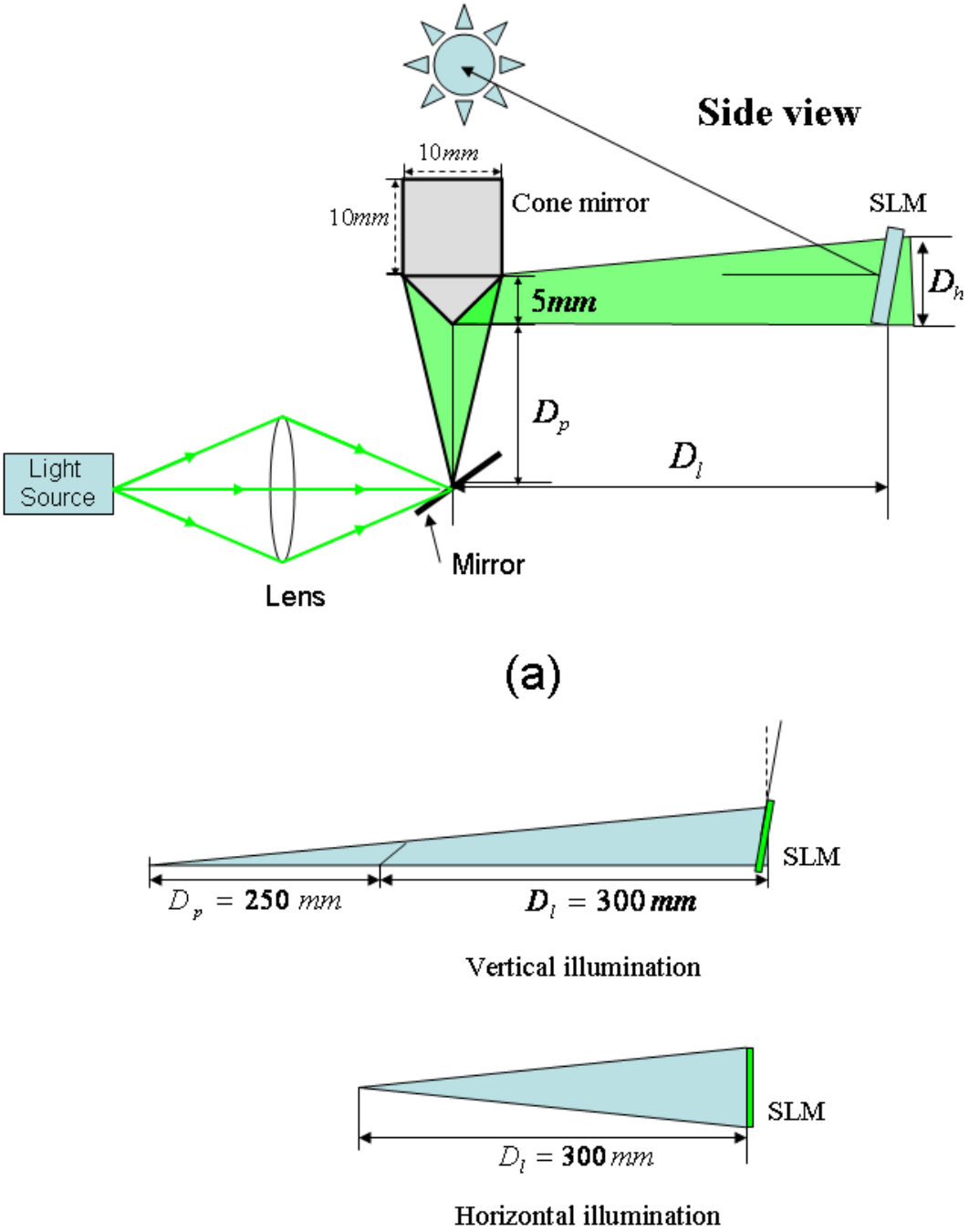

Figure 6.35: (a) Side view of the experimental setup. (b) Vertical and horizontal illumination ("Circular Holographic Video Display System," F. Yaraş, H. Kang and L. Onural, Optics Express vol. 19, no. 10, pp.9147-9156, 2011. ©2011 OSA. Reprinted with permission.)

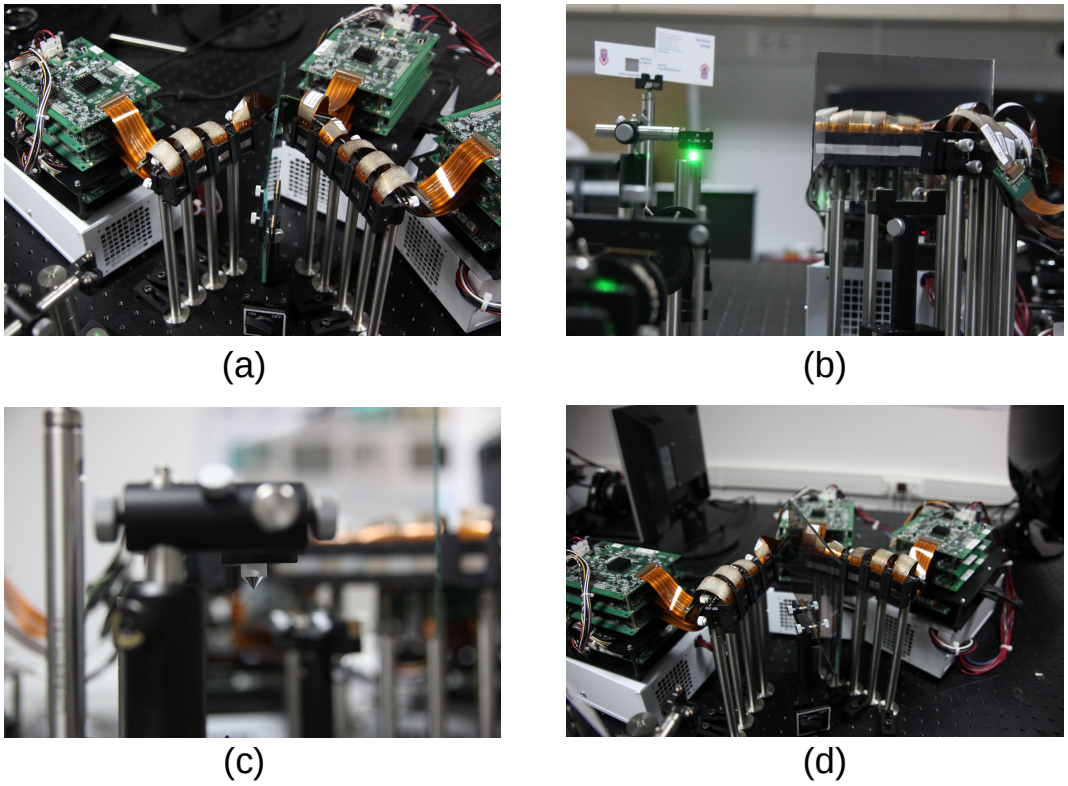

Figure 6.36: Pictures of (a) SLMs and SLM Modules, (b) side view of the setup, (c) cone mirror and (d) SLMs and beam splitter ("Circular Holographic Video Display System," F. Yaraş, H. Kang and L. Onural, Optics Express vol. 19, no. 10, pp.9147-9156, 2011. ©2011 OSA. Reprinted with permission.)

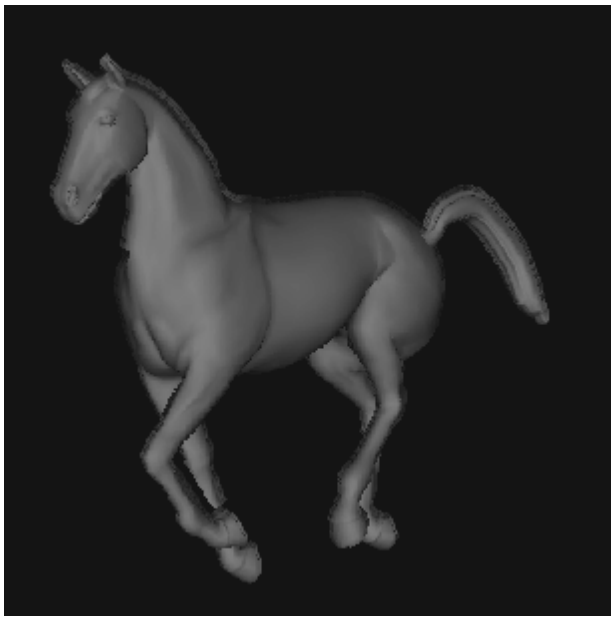

Figure 6.37: Single frame of the video of the 3D horse model ("Circular Holographic Video Display System," F. Yaraş, H. Kang and L. Onural, Optics Express vol. 19, no. 10, pp.9147-9156, 2011. ©2011 OSA. Reprinted with permission.)

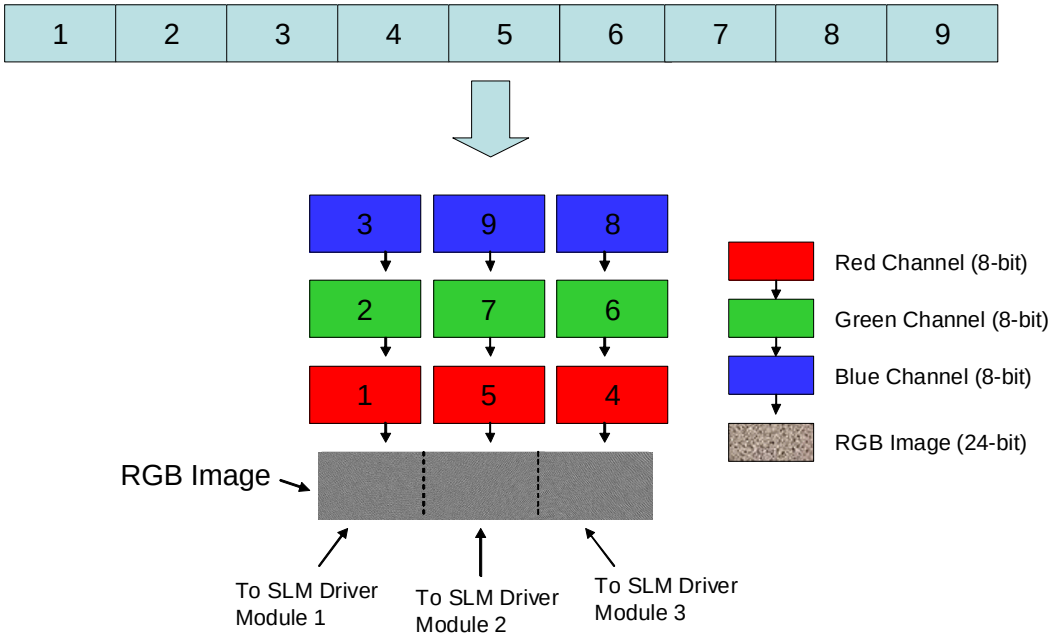

Figure 6.38: Writing nine holograms on a single bitmap image ("Circular Holographic Video Display System," F. Yaraş, H. Kang and L. Onural, Optics Express vol. 19, no. 10, pp.9147-9156, 2011. ©2011 OSA. Reprinted with permission.)

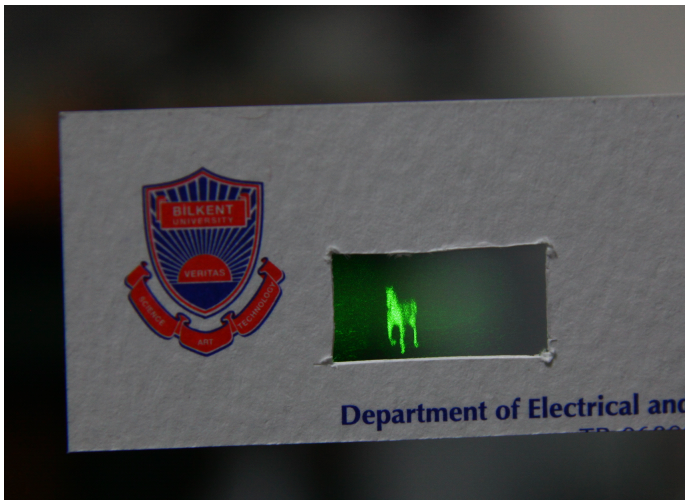

(a)

Figure 6.39 (Continues from next page)

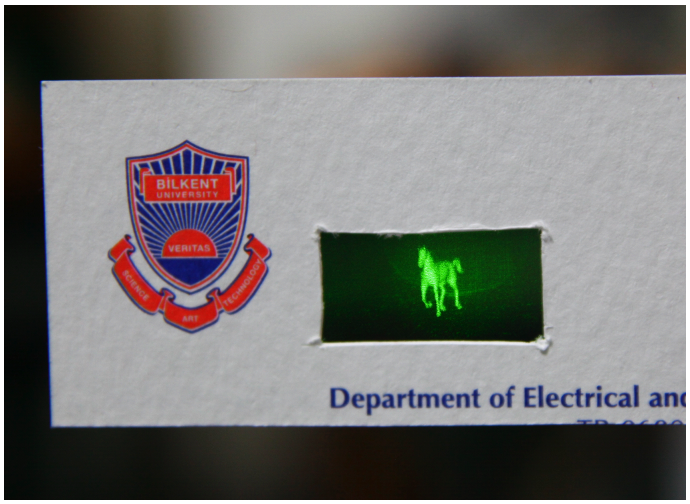

(b)

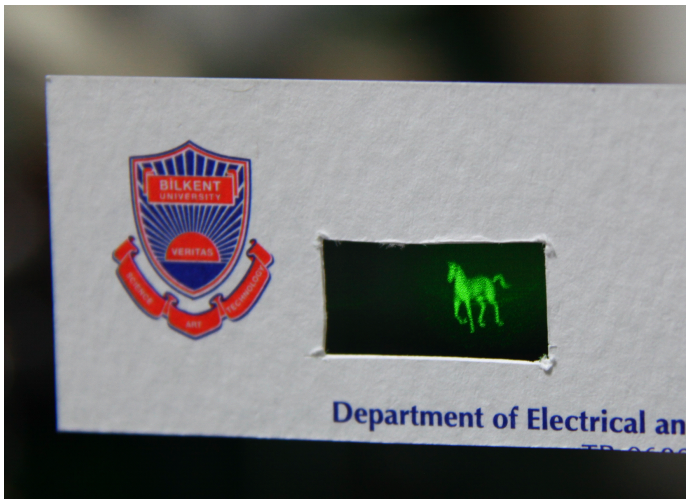

(c)

Figure 6.39: (Continues from previous page) Optical reconstructions for a single frame for (a) 0 degree, (b) 12 degrees and (c) 24 degrees. (The business card with the rectangular aperture is placed both as a size reference and to block distracting optical component views.) ("Circular Holographic Video Display System," F. Yaraş, H. Kang and L. Onural, Optics Express vol. 19, no. 10, pp.9147-9156, 2011. ©2011 OSA. Reprinted with permission.)

Chapter 7

Conclusions

The commercially available spatial light modulators are not adequate for future 3DTV applications. Their small size restricts the comfortable 3D perception in holographic reconstructions. However, due to various physical restrictions size of the SLMs can not be increased indefinitely. Therefore, the size problem should be solved to have a better holographic displays. For this reason, first a quality assessment is needed for holographic reconstructions. For the quality assessment of the holographic displays the space-bandwidth product (SBP) is a good metric. Higher SBP provides higher reconstruction quality. The limitations on the bandwidth and the size of the holographic displays are investigated. The bandwidth restriction results in an equivalent propagation angle restriction of the plane waves that are emerging from the hologram. Higher bandwidth means higher propagation angles of the plane waves. Since high propagation angles carry the high frequency contents of the reconstructions, they affect the "sharpness" of the reconstructed object. Such a bandwidth restriction is equivalent to low-pass filtering the reconstructed image. If we assume that the pixel periods of the SLMs are not the limiting factor for the bandwidth of the hologram and thus the high propagation angles, then the human visual system restricts the bandwidth. Minimum hologram size for a stationary observer is calculated based on such a restriction. In addition, if the observer is free to move along the lateral direction, the needed hologram size increases accordingly. If the display system should support also the rotational motion of the human observer,

the bandwidth and the size of the hologram both increase. Therefore, for a comfortable viewing angle, the space-bandwidth product has to be significantly larger than that of the stationary observer case. Alternatively, large space-bandwidth product may be relieved by using circularly configured multiple SLM holographic display systems.

To implement such systems, several holographic display systems are investigated. A real-time color holographic display system prototype is implemented and tested. It is shown that the point based 3D representation can be transmitted over internet and this method is suitable for real-time holographic fringe pattern generation. Therefore we conclude that it is feasible to drive a holographic display system remotely by storing the 3D information elsewhere. Moreover we show that the multi-GPU computation method can be used in real-time holographic display systems. By using multiple GPUs we increase the frame rate, proportionally. It is observed that LEDs can be used in color holographic video display systems. Although the spectrum of LEDs is wider compared to lasers, the quality of the optical reconstructions is satisfactory. In addition, optical reconstructions can be observed by the naked eye without any eye hazard. Yet in another laboratory prototype, six phase-only spatial light modulators are used and they are tiled in a three by two planar configuration. All alignments are feasible and we are able to generate larger holographic reconstructions. We conclude that even with three SLMs along the horizontal direction, the field of view increases significantly. However, planar holographic displays require more space-bandwidth product to satisfy motion and rotations; the necessity of using a circular configuration of discrete SLM patches is obvious. Therefore this leads us to move to the circular configuration of the phase-only SLMs.

In a circularly configured holographic display prototype, we used six phase-only spatial light modulators that are aligned side by side to obtain a 11520×1080 pixel wide circular holographic display system. All alignments are accomplished by the help of high precision stages. System works either with a laser or a LED illumination. Optical reconstructions show that increase in the viewing angle is significant compared to the single SLM case. Yet in another laboratory prototype we developed a new design of a circularly holographic video display system. In this design, there are nine phase-only spatial light

modulators and they are tiled side by side by using a large half-mirror. The resultant wide circular holographic display system has 17280×1080 pixels in total. Since both the size of the display and the field of view is increased significantly, the ghost-like 3D reconstructions can be observed within a quite large angle. The freedom to move around the reconstructions with a binocular view yields a more comfortable 3D experience. The expected natural parallax is clearly observable. We conclude that the circular configuration is superior than the previous planar configurations. Experimental results are satisfactory and they indicate that circularly holographic display system works successfully.

Bibliography

[1] F. M. Grimaldi, *Physico-mathesis de lumine, coloribus, et iride (Physicomathematical Studies of Light, Colors, and the Rainbow)*, chapter Propositio I. Lumen propagatur seu diffunditur non solum directe, refracte, ac reflexe, sed etiam alio quodam quarto modo, diffracte." (Proposition 1. Light propagates or spreads not only in a straight line, by refraction, and by reflection, but also by another, certain fourth way: by diffraction.), pp. 1–11, Bologna, 1665.

[2] R. Hooke, *Micrographia*, J. Martyn and J. Allestry, London, 1665.

[3] I. Newton, "A letter of mr. isaac newton, professor of the mathematicks in the university of cambridge; containing his new theory about light and colors," *Philosophical Transactions*, , no. 80, pp. 3075–3087, 1672.

[4] C. Huygens, *Traité de la lumière*, Leyden, 1690.

[5] T. Young, "On the theory of light and colours," *Philosophical Transactions*, , no. 92, pp. 12–48, 1802.

[6] M. Faraday, *Experimental Researches in Electricity*, London, 1839.

[7] J. C. Maxwell, *A Treatise on Electricity and Magnetism*, Oxford, 1873.

[8] A. A. Michelson, ," *Am. J. Sci*, vol. 22, pp. 120–129, 1881.

[9] A. Einstein, ," *Ann. d. Physik*, vol. 17, pp. 891–921, 1905.

[10] J. W. Goodman, *Introduction to Fourier Optics*, McGraw-Hill Companies, Inc., New York, second edition, 1996.

[11] D. Gabor, "A new microscopic principle," *Nature*, vol. 161, pp. 777–778, 1948.

[12] D. Gabor, "Microscopy by reconstructed wavefronts," *Proc. Royal Society A*, vol. 197, pp. 454–487, 1949.

[13] D. Gabor, "Microscopy by reconstructed wavefronts: II," *Proc. Royal Society B*, vol. 64, pp. 449–469, 1951.

[14] G. L. Rogers, "Experiments in diffraction microscopy," *Proc. Roy. Soc. Edinb.*, vol. 63A, pp. 193–221, 1952.

[15] H. M. A. El-Sum and P. Kirkpatrick, "Microscopy by reconstructed wavefronts," *Phys. Rev.*, vol. 85, pp. 763, 1952.

[16] A. W. Lohmann, "Optische Einseitenbandübertragung angewandt auf das Gabor-Mikroskop," *Optica Acta*, vol. 3, pp. 97–99, 1956.

[17] E. N. Leith and J. Upatnieks, "Reconstructed wavefronts and communication theory," *JOSA*, vol. 52, pp. 1123–1130, 1962.

[18] E. N. Leith and J. Upatnieks, "Wavefront reconstruction with continuous-tone objects," *Journ Opt Soc Amer*, vol. 53, pp. 1377–1381, 1963.

[19] E. N. Leith and J. Upatnieks, "Wavefront reconstruction with diffused illumination and three-dimensional objects," *JOSA*, vol. 54, pp. 1295–1301, 1964.

[20] Y. N. Denisyuk, "Photographic reconstruction of the optical properties of an object in its own scattered field," *Sov. Phys. Dokl.*, vol. 7, pp. 543, 1962.

[21] J. W. Goodman and R. W. Lawrence, "Digital image formation from electronically detected holograms," *Appl Phys Lett*, vol. 11, pp. 77–79, 1967.

[22] L. P. Yaroslavskii and N. S. Merzlyakov, *Methods of Digital Holography*, Consultants Bureau, New York, 1980.

[23] L. Onural, *Diffraction-Specific Fringe Computation for Electro-Holography*, Ph.D. thesis, Electrical and Computer Engineering, State University of New York at Buffalo, 1985.

[24] L. Onural and P. D. Scott, "Digital decoding of in-line holograms," *Opt. Eng.*, vol. 26, pp. 1124–1132, 1987.

[25] O. Schnars and W. Juptner, "Direct recording of holograms by a CCD target and numerical reconstruction," *Applied Optics*, vol. 33, pp. 179–181, 1994.

[26] T. Kreis, *Handbook of Holographic Interferometry: Optical and Digital Methods*, John Wiley, 2005.

[27] M. Born and E. Wolf, *Principles of Optics: Electromagnetic Theory of Propagation, Interference and Diffraction of Light (7th Edition)*, Cambridge University Press, October 1999.

[28] L. Onural, "Exact analysis of the effects of sampling of the scalar diffraction field," *J. Optical Soc. of America A*, vol. 24, no. 2, pp. 359–367, 2007.

[29] Levent Onural, "Exact solution for scalar diffraction between tilted and translated planes using impulse functions over a surface," *J. Opt. Soc. Am. A*, vol. 28, no. 3, pp. 290–295, Mar. 2011.

[30] G. B. Esmer, *Calculation of scalar optical diffraction field from its distributed samples over the space*, Ph.D. thesis, Bilkent University Dept. of Electrical and Electronics Engineering, Ankara TR, 2010.

[31] G. C. Sherman, "Application of the convolution theorem to Rayleigh's integral formulas," *J Opt Soc Am*, vol. 57, pp. 546–547, 1967.

[32] K. Bauchert, S. Serati, and A. Furman, "Advances in liquid crystal spatial light modulators," in *Optical Pattern Recognition XIII, Proc. of SPIE*, 2002.

[33] Y. Frauel, T. J. Naughton, O. Matoba, E. Tajahueerce, and B. Javidi, "Three-dimensional imaging and processing using computational holographic imaging," vol. 94, no. 3, 2006.

[34] A. Michalkiewicz, M. Kujawinska, T. Kozackia, X. Wangb, and P. J. Bosb, "Holographic three-dimensional displays with liquid crystal on silicon spatial light modulator," in *Interferometry XII: Techniques and Analysis*, 2004, Proc. of SPIE, pp. 85–94.

[35] T. Ito, T. Shimobaba, H. Godo, and M. Horiuchi, "Holographic reconstruction with a $10-\mu m$ pixel-pitch reflective liquid-crystal display by use of a light-emitting diode reference light," *Optics Letters*, vol. 27, no. 16, pp. 1406–1408, 2002.

[36] N. Ohmura, H. Kang, T. Yamaguchi, and H. Yoshikawa, "A method to increase the hologram viewing angle by the beam reconfiguration," in *Practical Holography XXII: Materials and Aplications, Proc. of SPIE*, 2008, vol. 6912, p. 69120O.

[37] K. Takano, N. Minami, and K. Sato, "A simple method of color electro-holographic display system using a white light source and three LCD panels," in *IEEE International Conference on Multimedia and Expo*, 2001, pp. 105–108.

[38] K. Takano and K. Sato, "Color electro-holographic display using a single white light source and a focal adjustment method," *Opt. Eng.*, vol. 41, no. 10, pp. 2427–2433, 2002.

[39] K. Takano, N. Minami, and K. Sato, "Practical method for color electro-holographic display system using a metal halide lamp and three LCD panels," in *Practical Holography XVI and Holographic Materials VIII, Proc. of SPIE*, 2002, vol. 4659, pp. 61–68.

[40] K. Sato and K. Takano, "New type electro-holographic display system using LCDs," in *Three-Dimensional TV, Video, and Display, Proc. of SPIE*, 2002, vol. 4864, pp. 114–121.

[41] K. Takano and K. Sato, "Full-color electroholographic three-dimensional display system employing light emitting diodes in virtual image reconstruction," *Opt. Eng.*, vol. 46, no. 9, pp. 095801, 2007.

[42] K. Sato and K. Takano, "Consideration about HMD-type holography 3D-TV," in *Three-Dimensional TV, Video, and Display III, Proc. of SPIE*, 2004, vol. 5599, pp. 123–134.

[43] R. Tudela, I. Labastida, E. Marti-Badosa, S. Vallmitjana, I. Juvells, and A. Carnicer, "A simple method for displaying fresnel holograms on liquid crystal panels," *Optics Communications*, vol. 214, pp. 107–114, 2002.

[44] R. Tudela, E. Martin-Badosa, I. Labastida, S. Vallmitjana, I. Juvells, and A. Carnicer, "Full complex fresnel holograms displayed on liquid crystal devices," *Journal of Optics A: Pure Applied Optics*, vol. 5, pp. 189–194, 2003.

[45] R. Tudela, E. Martin-Badosa, I. Labastida, S. Vallmitjana, and A. Carnicer, "Wavefront reconstruction by adding modulation capabilities of two liquid crystal devices," *Optical Engineering*, vol. 43 (11), pp. 2650–2657, November 2004.

[46] T. Ito and K. Okano, "Color electroholography by three colored reference lights simultaneously incident upon one hologram panel," *Opt. Express.*, vol. 12, no. 18, pp. 4320–4325, 2004.

[47] K. Sato, A. Sugita, M. Morimoto, and K. Fujii, "Reconstruction of full-color images with a RGB time-sharing holographic display system," in *Display Devices and Systems, Proc. of SPIE*, 2006, vol. 6030, pp. 603004–1–603004–6.

[48] K. Sato, A. Sugita, M. Morimoto, and K. Fujii, "Reconstruction of color images of high quality by a holographic display," in *Practical Holography XX: Materials and Applications, Proc. of SPIE*, 2006, vol. 6136, pp. 61360V–1–61360V–9.

[49] A. Sugita, K. Sato, M. Morimoto, and K. Fujii, "Full-color holographic display and recording of 3D images," in *Practical Holography XIX: Materials and Applications, Proc. of SPIE*, 2005, vol. 5742, pp. 130–139.

[50] T. Yamaguchi and H. Yoshikawa, "Real time calculation for holographic video display," in *Practical Holography XX: Materials and Aplications, Proc. of SPIE*, 2006, vol. 6136, pp. 61360T–01–61360T–10.

[51] T. Yamaguchi, G. Okabe, and H. Yoshikawa, "Full-color image-plane holographic video display," in *Practical Holography XXI: Materials and Aplications, Proc. of SPIE*, 2007, vol. 6488, p. 64880Q.

[52] S.C. Kim, J.W. Moon, and E.S. Kim D.W. Lee, K.C. Son, "Holographic full-color 3D display system using color-LCoS spatial light modulator," in *Practical Holography XIX: Materials and Applications, Proc. of SPIE*, 2005, vol. 5742, pp. 223–233.

[53] J.W. Moon, D.W. Lee, S.C. Kim, and E.S. Kim, "Color LCoS-based full-color electro-holographic 3D display system," in *Cockpit and Future Displays for Defense and Security, Proc. of SPIE*, 2005, vol. 5801, pp. 294–303.

[54] F. Yaraş, M. Kovachev, R. Ilieva, M. Agour, and L. Onural, "Holographic reconstructions using phase-only spatial light modulators," in *3DTV Conference: The True Vision - Capture, Transmission and Display of 3D Video, IEEE*, 2008.

[55] F. Yaras and L. Onural, "Color holographic reconstruction using multiple SLMs and LED illumination," in *Proc. SPIE.*, 2009, vol. 7237, p. 72370O.

[56] F. Yaraş, H. Kang, and L. Onural, "Real-time phase-only color holographic video display system using led illumination," *Appl. Opt.*, vol. 48, no. 34, pp. H48–H53, 2009.

[57] F. Yaraş, H. Kang, and L. Onural, "Real-time multiple SLM color holographic display using multiple GPU acceleration," in *Digital Holography and Three-Dimensional Imaging*. 2009, p. DWA4, Optical Society of America.

[58] F. Yaraş, H. Kang, and L. Onural, "Real-time color holographic video display system," in *3DTV Conference: The True Vision - Capture, Transmission and Display of 3D Video, IEEE*, 2009.

[59] F. Yaraş, H. Kang, and L. Onural, "Multi-SLM holographic display system with planar configuration," in *3DTV Conference: The True Vision - Capture, Transmission and Display of 3D Video, IEEE*, 2010.

[60] T. Mishina, F. Okano, and I. Yuyama, "Time-alternating method based on single-sideband holography with half-zone-plate processing for the enlargement of viewing zones," *Appl. Opt.*, vol. 38-17, pp. 3703–3713, 1999.

[61] F. Okano T. Mishina, M. Okui, "Viewing-zone enlargement method for sampled hologram that uses high-order diffraction," *Appl. Opt.*, vol. 41-8, pp. 1489–1499, 2002.

[62] K. Choi, J. Kim, Y. Lim, and B. Lee, "Full parallax viewing-angle enhanced computer-generated holographic 3D display system using integral lens array," *Opt. Express*, vol. 13, no. 26, pp. 10494–10502, 2005.

[63] J. Hahn, H. Kim, Y. Lim, G. Park, and B. Lee, "Wide viewing angle dynamic holographic stereogram with a curved array of spatial light modulators," *Opt. Express*, vol. 16, no. 16, pp. 12372–12386, 2008.

[64] M. Stanley, M. A. G. Smith, A. P. Smith, P. J. Watson, S. D. Coomber, C. D. Cameron, C. W. Slinger, and A. D. Wood, "3D electronic holography display system using a 100 mega-pixel spatial light modulator," in *Optical Design and Engineering*, 2004, vol. 5249 of *Proc. of SPIE*, pp. 297–308.

[65] C. Kohler, X. Schwab, and W. Osten, "Optimally tuned spatial light modulators for digital holography," *Appl. Optics*, vol. 45, no. 5, pp. 960–967, 2006.

[66] E. G. van Putten, I. M. Vellekoop, and A. P. Mosk, "Spatial amplitude and phase modulation using commercial twisted nematic LCDs," *Appl. Optics*, vol. 47, no. 12, pp. 2076–2081, 2008.

[67] J. Otón, P. Ambs, M. S. Millán, and E. Pérez-Cabré, "Multipoint phase calibration for improved compensation of inherent wavefront distortion in parallel aligned liquid crystal on silicon displays," *Appl. Optics*, vol. 46, no. 23, pp. 5667–5679, 2007.

[68] F. Reinitzer, "Beitrge zur kenntniss des cholesterins," *Wiener Monatschr, Fr Chem.,*, vol. 9, pp. 421–441, 1888.

[69] J. A. Neff, R. A. Athale, and S. H. Lee, "Two-dimensional spatial light modulators: a tutorial," *Proceedings of the IEEE*, vol. 78, no. 5, pp. 826–855, May 1990.

[70] H. Dai, K. X. Y. Liu, X. Wang, and J. Liu, "Characteristics of LCoS phase-only spatial light modulator and its applications," *Optics Communications*, vol. 238, no. 4-6, pp. 269–276, 2004.

[71] S. Osten, S. Krger, and A. Steinhoff, "Spatial light modulators based on reflective micro-displays," *Technishes Messen*, vol. 73, pp. 149–156, 2006.

[72] S. T. Tang, F. H. Yu, J. Chen, M. Wong, H. C. Huang, and H. S. Kwok, "Reflective twisted nematic liquid crystal displays. i. retardation compensation," *Journal of Applied Physics*, vol. 81, no. 9, pp. 5924–5929, 1997.

[73] O. Trushkevych, N. Collings, W. A. Crossland, and T. D. Wilkinson, "Resolution in optically addressed spatial light modulators based on dye-doped liquid crystals," *Appl. Opt.*, vol. 45, no. 35, pp. 8889–8892, 2006.

[74] J. B. Sampsell, "Digital micromirror device and its application to projection displays," 1994, vol. 12, pp. 3242–3246, AVS.

[75] J. S. Kollin, S. A. Benton, and M. L. Jepsen, "Real-time display of 3-D computed holograms by scanning the image of an acousto-optic modulator," in *Proc. SPIE, Holographic Optics II: Principles and Applications*, 1989, vol. 1136, pp. 178–185.

[76] J. S. Kollin, S. A. Benton, and M. L. Jepsen, "Real-time display of 3-d computed holograms by scanning the image of an acousto-optic modulator," in *Proc. SPIE, Holographic Optics II: Principles and Applications*, G. M. Morris, Ed., 1989, vol. 1136, pp. 178–185.

[77] P. S.-Hilaire, S. A. Benton, M. Lucente, and P. M. Hubel, "Color images with the MIT holographic video display," in *Proc. SPIE, Practical Holography VI*, S. A. Benton, Ed., 1992, vol. 1667, pp. 73–84.

[78] L. Onural, G. Bozdagi, and A. Atalar, "New high-resolution display device for holographic three-dimensional video: Principles and simulations," *Opt Eng*, vol. 33, pp. 835–844, 1994.

[79] M. Lucente P. St.-Hilaire, S.A. Benton and P.M. Hubel, "Color images with the MIT holographic video display," in *Proc. of SPIE, Practical Holography VI*, 1992.

[80] P. St.-Hilaire, "Scalable optical architectures for electronic holography," in *Ph. D. Thesis, Program in Media Arts and Sciences, MIT*, 1994.

[81] P. St-Hilaire, S. A. Benton, M. Lucente, J. D. Sutter, and W. J. Plesniak, "Advances in holographic video," in *Proc. of SPIE, Practical Holography VII*, 1993.

[82] P. St.-Hillaire, M. Lucente, J.D. Sutter, R. Pappu, C.J.Sparrell, and S. Benton, "Scaling up the MIT holographic video system," in *Proc. of the Fifth Inter. Symposium on Display Holography*, 1995.

[83] M. L. Jepsen, "Holographic video: design and implementation of a display system," in *M.S. Thesis, Department of Architecture, MIT*, 1989.

[84] Joel S. Kollin, "Design and information considerations for holographic television," in *M.S. Thesis, Department of Architecture, MIT*, 1988.

[85] M. Lucente and T. Galyean, "Rendering interactive holographic images," in *Proc. of SIGGRAPH '95*, 1995, pp. 387–394.

[86] J. Underkoffler, "Towards accurate computation of optically reconstructed holograms," in *M.S. Thesis, Program in Media Arts and Sciences, MIT*, 1991.

[87] D. E. Smalley, Q. Y. J. Smithwick, and Jr. V. M. Bove, "Holographic video display based on guided-wave acousto-optic devices," 2007, vol. 6488, p. 64880L, SPIE.

[88] S. Reichelt, R. Haussler, N. Leister, G. Futterer, and A. Schwerdtner, "Large holographic 3D displays for tomorrows TV and monitors - solutions, challenges, and prospects," *IEEE Lasers and Electro-Optics Society, 2008. LEOS 2008. 21st Annual Meeting of the*, pp. 194–195, 2008.

[89] R. Häussler, A. Schwerdtner, and N. Leister, "Large holographic displays as an alternative to stereoscopic displays," 2008, vol. 6803, p. 68030M, SPIE.

[90] S. Reichelt, H. Sahm, N. Leister, and A. Schwerdtner, "Capabilities of diffractive optical elements for real-time holographic displays," 2008, vol. 6912 of *Proc. of SPIE*, p. 69120P.

[91] A. Schwerdtner, R. Häussler, and N. Leister, "Large holographic displays for real-time applications," 2008, vol. 6912 of *SPIE*, p. 69120T.

[92] N. Leister, A. Schwerdtner, G. Fütterer, S. Buschbeck, J.-C. Olaya, and S. Flon, "Full-color interactive holographic projection system for large 3D scene reconstruction," 2008, vol. 6911, p. 69110V, SPIE.

[93] M. Stanley, P. Conway, S. Coomber, J. Jones, D. Scattergood, C. Slinger, B. Bannister, C. Brown, W. Crossland, and A. Travis, "A novel electro-optic modulator system for the production of dynamic images from giga-pixel computer generated holograms," in *Proc. SPIE, Practical Holography XIV and Holographic Materials VI*, 2000, vol. 3956, pp. 13–22.

[94] C. Slinger, C. Cameron, and M.Stanley, "Computer-generated holography as a generic display technology," *Computer*, vol. 38, no. 8, pp. 46–53, 2005.

[95] T. Shimobaba, S. Hishinuma, and T. Ito, "Special-purpose computer for holography HORN-4 with recurrence algorithm," *Computer Physics Communications*, vol. 148, no. 2, pp. 160 – 170, 2002.

[96] T. Yabe, T. Ito, and M. Okazaki, "Holography machine HORN-1 for computer-aided retrieval of virtual three-dimensional image," *Japanese journal of applied physics. Pt. 2, Letters*, vol. 32, no. 9, pp. L1359–L1361, 1993.

[97] Y. Ichihashi, T. Ito, H. Nakayama, N. Masuda, A. Shiraki, and T. Shimobaba, "Development of special-purpose computer HORN-6 for holography," *3D Image Conference 2008*, 2008.

[98] T. Ito, N. Masuda, K. Yoshimura, A. Shiraki, T. Shimobaba, and T. Sugie, "Special-purpose computer HORN-5 for a real-time electroholography," *Opt. Express*, vol. 13, no. 6, pp. 1923–1932, 2005.

[99] T. Shimobaba, N. Masuda, T. Sugie, S. Hosono, S. Tsukui, and T. Ito, "Special-purpose computer for holography HORN-3 with pld technology," *Computer Physics Communications*, vol. 130, July 2000.

[100] T. Ito, T. Yabe, M. Okazaki, and M. Yanagi, "Special-purpose computer HORN-1 for reconstruction of virtual image in three dimensions," *Comp. Phys. Commun.*, vol. 82, pp. 104–110, 1994.

[101] T. Yabe T. Ito, H. Eldeib and T. Kunugi, "Special-purpose computer for holography HORN-2," *Comp. Phys. Commun.*, vol. 93, pp. 13–20, 1996.

[102] T. Hamano and H. Yoshikawa, "Image-type CGH by means of e-beam printing," in *Practical Holography XII*. 1998, vol. 3293, pp. 2–14, SPIE.

[103] T. Yamaguchi, G. Okabe, and H. Yoshikawa, "Real-time image plane full-color and full-parallax holographic video display system," *Optical Engineering*, vol. 46, no. 12, pp. 125801, 2007.

[104] T. Yatagai, "Stereoscopic approach to 3-D display using computer-generated holograms," *Appl. Opt.*, vol. 15, no. 11, pp. 2722–2729, 1976.

[105] H. Kang, T. Yamaguchi, and H. Yoshikawa, "Accurate phase-added stereogram to improve the coherent stereogram," *Appl. Opt.*, vol. 47, no. 19, pp. D44–D54, 2008.

[106] H. Kang, T. Fujii, T. Yamaguchi, and H. Yoshikawa, "Compensated phase-added stereogram for real-time holographic display," *Opt. Eng.*, vol. 46, no. 9, pp. 095802, 2007.

[107] H. Yoshikawa J. Tamai, "Faster computation of subsampled coherent stereogram (in japanese)," in *The Journal of the Institute of Television Engineers of Japan*, 1996, vol. 50, pp. 1612–1615.

[108] M. Yamaguchi, H. Hoshino, T. Honda, and N. Ohyama, "Phase-added stereogram: calculation of hologram using computer graphics technique," in *Practical Holography VII: Imaging and Materials*. 1993, vol. 1914, pp. 25–31, SPIE.

[109] H. Yoshikawa and H. Kameyama, "Integral holography," in *Practical Holography IX*. 1995, vol. 2406, pp. 226–234, SPIE.

[110] H. Kang, "Quality improvements of the coherent holographic stereogram for natural 3D display and its applications," in *PhD. Thesis, Nihon University*, 2008.

[111] H. Kang, F. Yaraş, and L. Onural, "Graphics processing unit accelerated computation of digital holograms," *Appl. Opt.*, vol. 48, no. 34, pp. H137–H143, 2009.

[112] H. Kang, F. Yaraş, L. Onural, and H. Yoshikawa, "Real-time fringe pattern generation with high quality," in *Digital Holography and Three-Dimensional Imaging*. 2009, p. DTuB7, Optical Society of America.

[113] H. Kang, F. Yaraş, and L. Onural, "Quality comparison and acceleration for digital hologram generation method based on segmentation," in *3DTV Conference: The True Vision - Capture, Transmission and Display of 3D Video, IEEE*, 2009.

[114] "http://www.televisionbroadcast.com/article/79134," .

[115] Levent Onural, Fahri Yaraş, and Hoonjong Kang, "Digital holographic three-dimensional video displays," *Proc. of the IEEE*, vol. 99, no. 4, pp. 576–589, 2011.

[116] R. L. De Valois and K. K. De Valois, *Spatial Vision*, Oxford Science Publications, 1990.

[117] M. F. Deering, "The limits of human vision," in *2nd International Immersive Projection Technology Workshop*, 1998.

[118] D. A. Atchison and G. Smith, *Optics of the human eye*, Elsevier Health Sciences, 2000.

[119] L. Onural, A. Gotchev, H. M. Ozaktas, and E. Stoykova, "A survey of signal processing problems and tools in holographic three-dimensional television," *Circuits and Systems for Video Technology, IEEE Transactions on*, vol. 17, no. 11, pp. 1631–1646, 2007.

[120] R. Gonzalez and R. Woods, *Digital Image Processing*, pp. 518–519, Addison-Wesley Publishing Company, 1992.

[121] T. M. Kreis, "Frequency analysis of digital holography," *Optical Engineering*, vol. 41, no. 4, pp. 771–778, April 2002.

[122] L. Onural, "Sampling of the diffraction field," *Appl Opt*, vol. 39, pp. 5929–5935, 2000.

[123] F. Gori, "Fresnel transform and sampling theorem," *Opt Commun*, vol. 39, pp. 293–297, 1981.

[124] B. E. A. Saleh and M. C. Teich, *Fundamentals of Photonics*, Wiley, New York, 1991.

[125] G. A. Mills and I. Yamaguchi, "Effects of quantization in phase-shifting digital holography," *Appl. Opt.*, vol. 44, no. 7, pp. 1216–1225, 2005.

[126] L. I. Goldfischer, "Autocorrelation function and power spectral density of laser-produced speckle patterns," *J. Opt. Soc. Am.*, vol. 55, no. 3, pp. 247–252, 1965.

[127] H. J. Gerritsen, W. J. Hannan, and E. G. Ramberg, "Elimination of speckle noise in holograms with redundancy," *Appl. Opt.*, vol. 7, no. 11, pp. 2301–2311, 1968.

[128] Jr. Mark E. Myers and Andrew M. Wims, "Elimination of speckle noise in laser light scattering photometry," *Appl. Opt.*, vol. 11, no. 4, pp. 947–949, 1972.

[129] M. Matsumura, "Speckle noise reduction by random phase shifters," *Appl. Opt.*, vol. 14, no. 3, pp. 660–665, 1975.

[130] J. Amako, H. Miura, and T. Sonehara, "Speckle-noise reduction on kinoform reconstruction using a phase-only spatial light modulator," *Appl. Opt.*, vol. 34, no. 17, pp. 3165–3171, 1995.

[131] J. M. Huntley and L. Benckert, "Speckle interferometry: noise reduction by correlation fringe averaging," *Appl. Opt.*, vol. 31, no. 14, pp. 2412–2414, 1992.

[132] Y. Barkana and M. Belkin, "Laser eye injuries," *Survey of Ophthalmology*, vol. 44, no. 6, pp. 459 – 478, 2000.

[133] S.-C. Kim H. Kang, N. Ohmura and E.-S. Kim, "Method to enlarge the hologram viewing window using a mirror module," *Optical Engineering*, vol. 48, no. 7, pp. 075801, 2009.

[134] H. Zhang, J. Zhang, and L. Wu, "Evaluation of phase-only liquid crystal spatial light modulator for phase modulation performance using a twymangreen interferometer," *Meas. Sci. Technol.*, vol. 18, no. 6, pp. 1724–1728, 2007.

[135] R. W. Gerchberg and W. O. Saxton, "A practical algorithm for the determination of the phase from image and diffraction plane pictures," *Optik*, vol. 35, pp. 706–713, 1972.

[136] G. Liu and P. D. Scott, "Phase retrieval and twin-image elimination for in-line fresnel holograms," *J. Opt. Soc. Am.*, vol. 4, pp. 159, 1987.

[137] F. Yaraş, H. Kang, and L. Onural, "Circularly configured multi-SLM holographic display system," in *3DTV Conference: The True Vision - Capture, Transmission and Display of 3D Video, IEEE*, 2011.

[138] F. Yaraş, H. Kang, and L. Onural, "Circular holographic video display system," *Opt. Express*, vol. 19, no. 10, pp. 9147–9156, 2011.

[139] L.P. Lesem, P.M. Hirsch, and J.A Jordan Jr., "The kinoform: a new wave front reconstruction device," *IBM J. Res. Dev.*, vol. 13, pp. 150155, 1969.

[140] K. Taima, H. Ueda, H. Okamoto, T. Kubota, Y. Nakamura, H. Nishida, H. Takahashi, and E. Shimizu, "New approach to the interactive holographic display system," in *Proc. SPIE.*, 1994, vol. 2176, pp. 23–29.

[141] J. A. Watlington, M. E. Lucente, C. J. Sparrell, Jr. V. M. Bove, and I. Tamitani, "Hardware architecture for rapid generation of electro-holographic fringe patterns," in *Practical Holography IX*, Stephen A. Benton, Ed., 1995, vol. 2406 of *Proc. SPIE*, pp. 172–183.

[142] H. Yoshikawa and T. Yamaguchi, "Fast hologram calculation for holographic video display," in *Proc. SPIE.*, 2006, vol. 6027, pp. 561–566.

[143] M. Janda, I. Hanak, and L. Onural, "Hologram synthesis for photorealistic reconstruction," *JOSA A*, vol. 25, no. 12, pp. 3083–3096, 2008.

[144] N. Masuda, T. Ito, T. Tanaka, A. Shiraki, and T. Sugie, "Computer generated holography using a graphics processing unit," *Opt. Express*, vol. 14, no. 2, pp. 603–608, 2006.

[145] L. Ahrenberg, P. Benzie, M. Magnor, and J. Watson, "Computer generated holography using parallel commodity graphics hardware," *Optics Express*, vol. 14, no. 17, pp. 7656–7641, 2006.

[146] N. Fukaya, K. Maeno, O. Nishikawa, K. Matumoto, K. Sato, and T. Honda, "Expansion of the image size and viewing zone in holographic display using liquid crystal devices," in *Proc. SPIE*, 1995, vol. 2406, pp. 283–289.

[147] K. Maeno, N. Fukaya, O. Nishikawa, and T. Honda, "Electroholographic display using 15-megapixel LCD," in *Proc. SPIE, Practical Holography X*, 1996, vol. 2652, pp. 15–23.

[148] G. B. Esmer, "Computation of holographic patterns between tilted planes," M.S. thesis, Bilkent University Dept. of Electrical and Electronics Engineering, Ankara TR, 2004.